Experimental Investigation into the Effect of Aerodynamic Add-ons on the Aerodynamic Characteristics of the Flying V

J. J. D. van Uitert

Delft University of Technology

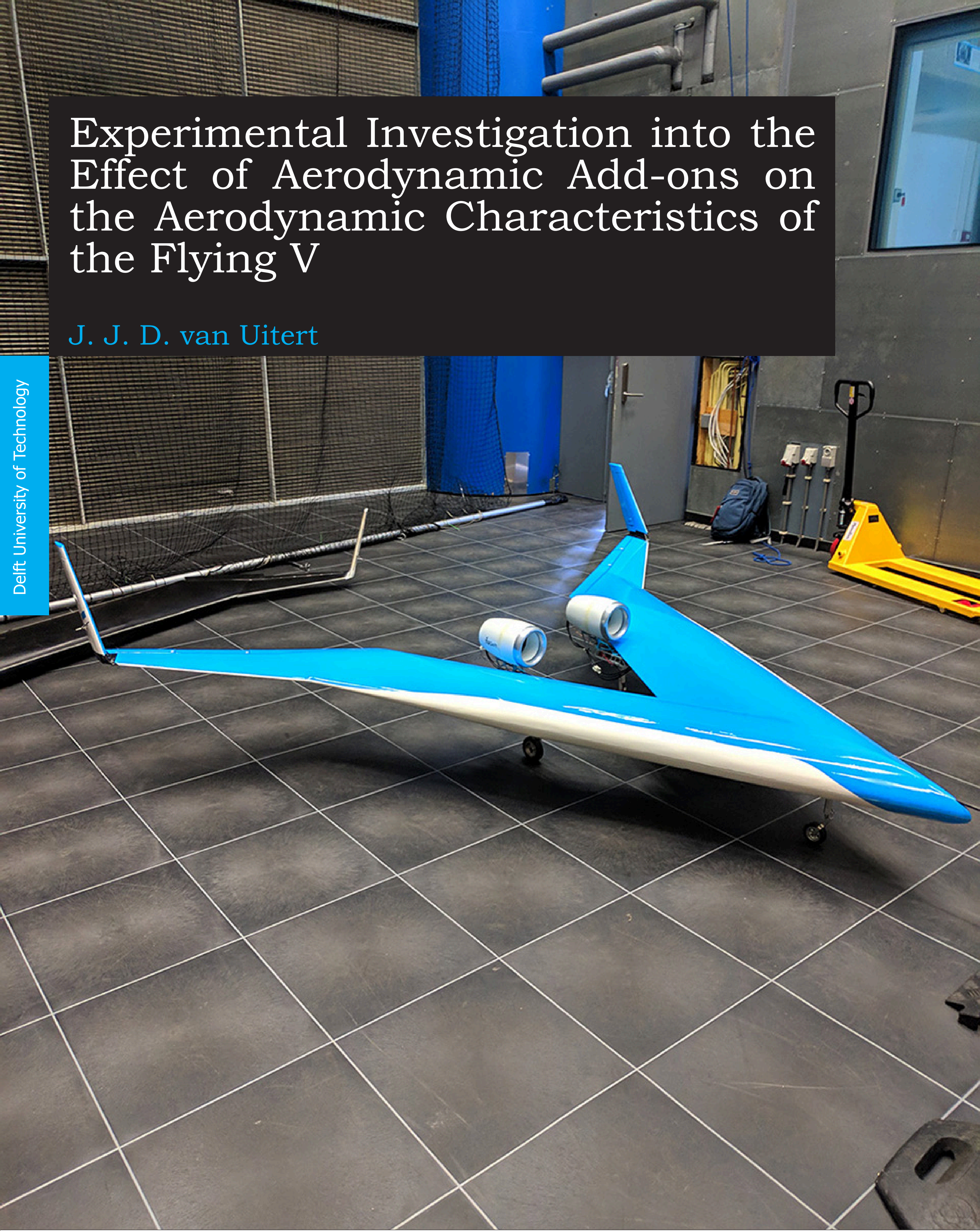

TU Delft Delft University of Technology

Challenge the future

Experimental Investigation into the Effect of Aerodynamic Add-ons on the Aerodynamic Characteristics of the Flying V

by

J. J. D. van Uitert

in partial fulfillment of the requirements for the degree of

Master of Science
in Aerospace Engineering

at the Delft University of Technology,
to be defended publicly on Monday January 18, 2021 at 10:00 AM.

Student number:	4228537		
Project duration:	September 9, 2019 – January 18, 2021		
Thesis committee:	Prof. L. L. M. Veldhuis,	TU Delft	
	Ir. W. A. Timmer,	TU Delft	
	Dr. ir. R. Vos,	TU Delft,	supervisor

An electronic version of this thesis is available at http://repository.tudelft.nl/.

TU Delft

Summary

This research has been performed with the purpose of understanding the cause of the unstable pitch break experienced by the Flying V at a lift coefficient of $C_L = 0.95$. Without understanding and possibly elimination of the pitch break, the flying V's usable maximum lift coefficient is lower and the pitching moment behavior and gust response unpredictable. Three possible solutions are investigated empirically, with the ultimate goal of eliminating the unstable pitch break. First, the application of a trip strip to the suction and pressure side of the wing is investigated. Second and third, the implementation of vortilons and fences is investigated. The experiments are performed in the TU Delft's Open Jet Facility using a 4.6% scaled half-span model of the Flying V. The wind tunnel experiments are evaluated using force and moment data and flow visualization using tufts. The application of trip strips results in an increase in pitching moment coefficient up to a lift coefficient of $C_L = 0.65$ and introduces the unstable pitch break at $C_L = 0.80$ compared to $C_L = 0.95$ for the clean wing. Flow visualizations showed an improvement in the flow over the outboard wing when the trip strips were applied. Combining both observations, it is recommended to apply the trip strips on the outboard wing of the Flying V scaled flight testing model only. Vortilons have shown to have no effect on the unstable pitch break. The combination of a vortilon and the trip strips could decrease the pitching moment coefficient of the flying V up to a lift coefficient of $C_L = 0.70$, depending on the spanwise location of the vortilon. Placing a fence could result in a favorable pitching moment coefficient characteristic, depending on its spanwise location and size. A fence placed at the spanwise location of the leading edge kink results in a decrease of pitching moment coefficient between a lift coefficient of $C_L = 0.30$ and 1.1. Furthermore, a fence located at the leading edge kink and spanning the entire suction surface chord postponed the unstable pitch break experienced by the Flying V. Therefore, it is recommended to install that fence on the Flying V scaled flight testing model.

Acknowledgements

This thesis marks the end of an interesting and challenging but joyful time at the Delft University of Technology. After my BSc. in Mechanical Engineering I continued in Aerospace Engineering and with this thesis before me, I can say I am really happy that I made that switch. I have learned a lot during this research and thanks to many I have learned even more.

I want to thank my supervisor Roelof Vos first and foremost for his enthusiastic attitude during all of our encounters. He provided me with critics that motivated me to push on and empowered me to believe in my own ideas and designs. Despite being incredibly busy finishing the Flying V scaled flight testing model, Malcolm Brown, Alberto Ruiz Garcia and Daniel Atherstone always found the time to help out with questions about the wind tunnel model, technical challenges during the wind tunnel experiments and discussions about the results I got. Thank you guys! My time in the wind tunnel would have been incredibly more painful if it wasn't for Sjoerd van Empelen and Nelson Johnson. We all know the challenges during the wind tunnel experiments and I want to thank you very much for all the time you guys spent there with me. Last but definitely not least, I want to thank Reynard de Vries and Biagio della Corte to lend their expertise on PIV right in between their own wind tunnel experiments. I have learned a lot from you, thank you!

I would like to thank my family and friends for the unconditional support during this research and the rest of my time at the TU Delft. A shout out goes to Wouter en Johan who helped me a lot finalizing this report. I am excited to see what the future has in store for me and look forward to other challenging projects like the Flying V!

Jeroen van Uitert
Delft, January 2021

Contents

Nomenclature

Symbols

b	=	half span of the wind tunnel model	[m]
c	=	chord	[m]
$\bar{c}$	=	mean aerodynamic chord	[m]
C_D	=	drag coefficient	[-]
C_L	=	lift coefficient	[-]
$C_{L_{\text{max}}}$	=	maximum lift coefficient	[-]
C_l	=	rolling moment coefficient	[-]
C_M	=	pitching moment coefficient	[-]
D	=	drag	[N]
d_1	=	suction surface trip strip location	[mm]
d_2	=	pressure surface trip strip location	[mm]
F_x	=	force in x-direction	[N]
F_y	=	force in y-direction	[N]
F_z	=	force in z-direction	[N]
$\vec{F}$	=	force vector	[-]
Fence #a	=	fence with height 0.5t	[-]
Fence #b	=	fence with height 0.25t	[-]
Fence #c	=	suction surface fence length equals chord	[-]
h	=	height	[mm]
L	=	lift	[N]
l	=	rolling moment	[Nm]
M	=	pitching moment	[Nm]
M_x	=	moment around x-axis	[Nm]
M_y	=	moment around y-axis	[Nm]
M_z	=	moment around z-axis	[Nm]
$\vec{M}$	=	moment vector	[-]
Ma	=	Mach number	[-]
n	=	number of samples	[-]
$\boldsymbol{R}$	=	rotation matrix	[-]
q	=	dynamic pressure	[Pa]
$\vec{r}$	=	translation vector	[-]
S	=	surface area	[m^2]
t	=	maximum local airfoil thickness	[mm]
t_{n-1}	=	t-distribution score	[-]
V	=	airspeed	[m/s]
x	=	stream wise coordinate	[m]
x_i	=	sample	[-]
x_l	=	confidence interval lower bound	[-]
x_u	=	confidence interval upper bound	[-]
x_{ref}	=	moment reference position	[m]
y	=	spanwise coordinate	[m]
α	=	angle of attack	[°]
Δ_{max}	=	maximum measurement error	[%]
σ_Δ	=	standard deviation of measurement error	[%]
η	=	spanwise position y/b	[-]
μ	=	sample mean	[-]
σ	=	sample standard deviation	[-]

Subscripts

ref	=	moment reference point
bal	=	balance reference frame
mod	=	model reference frame

List of Figures

List of Tables

1

Introduction

In this thesis the wind tunnel model, wind tunnel setup, aerodynamic add-on design and measurement techniques will be discussed in Chapter 2, validation of the results is presented in Chapter 3, the results of the wind tunnel campaigns can be found in Chapter 4 and the conclusions and recommendations in Chapter 5.

1.1. The Aviation Industry

The aviation industry is growing rapidly with an increase in passengers in Europe of 50% from 2005 - 2017 and an increase in number of flights by 8% in the same period. The amount of passengers as well as the number of flights is expected to keep increasing the coming years. From 2017 to 2040 the number of flights is expected to have been increased by 42%. This results in increased emissions and a higher pressure from the aviation sector on the climate [4]. For instance, the CO_2 emissions increased with 16% between 2005 and 2017 and the NO_x emissions increased with 25% in the same period. Both emissions are expected to increase the coming years. The CO_2 emissions are expected to have been increased by 40% in 2040 compared to 2005 and in the same period the NO_x emissions are expected to have been increased by 45%. Therefore the main focus of research and development should be on making aircraft more efficient in the propulsion and aerodynamic domain. To enable institutions to research these topics, several research projects have been setup. Examples of these initiatives are the Clean Sky and Future Sky projects funded by the European Union under the Horizon2020 umbrella [5–7]. Not only public institutions commit to cleaner aviation, companies like Airbus are working several projects aiming to reduce aviation emissions. Examples of these projects are ZEROe, E-Fan X and Maveric [8–10]. The first two projects focus on hybrid-electric or hydrogen propulsion on existing aircraft and the last focuses on increased aerodynamic efficiency by design. This last category is defined as unconventional aircraft configurations, that consists of all aircraft designs other than the aircraft populating the skies today. Examples of designs are blended wing body aircraft

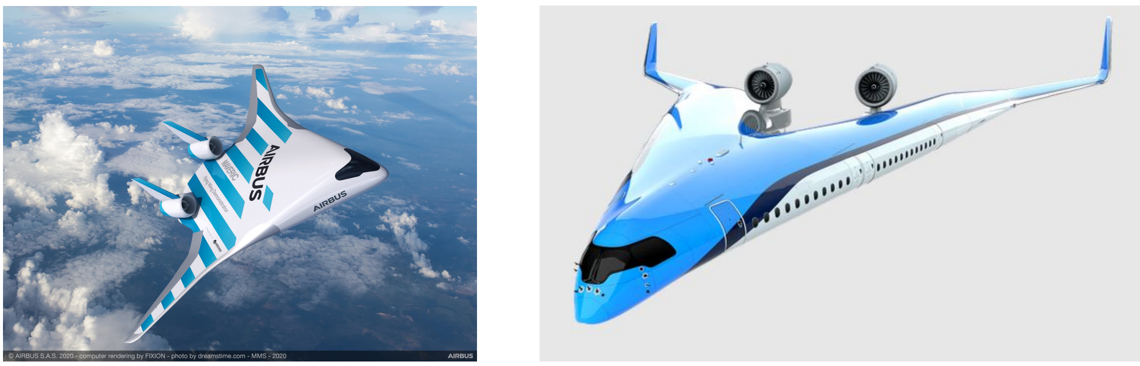

(a) The Airbus Maveric sub-scale flight testing model [10]

(b) The TU Delft's Flying V [11]

Figure 1.1: An example of two unconventional aircraft configurations: a blended wing body (a) and a flying wing (b)

(BWB) and flying wings (FW), see Figure 1.1. The Maveric is an example of such a BWB and the Flying V an example of a FW. These unconventional configurations have a common advantage, they all have the potential to increase the aerodynamic efficiency with up to 20% compared to the conventional configuration and thus reduce the emissions [12].

1.2. The Flying V

The first concept of the Flying V was designed by J. Benad [13], claiming an improved lift over drag ratio (L/D) of 10% and 2% weight reduction for the same mission profile as an even sized commercial aircraft of the latest generation, like the Airbus A350-900. After research at the TU Delft, an initial design optimization was carried out for cruise conditions (Alt = 13km, Ma = 0.85) and an efficiency increase of around 20% seemed possible [14]. In order to be able to investigate the low speed characteristics of the Flying V, a 4.6%-scaled full-span flying model is built for the purpose of scaled flight testing. Before this model is flown, a 4.6%-scaled half-span model was built to gain insight in the low speed longitudinal stability and control characteristics of the Flying V. This model was used in various wind tunnel experiments in the Open Jet Facility of the TU Delft [1–3, 15]. The results of those wind tunnel campaigns indicate an unstable pitch break around 20° angle of attack at an airspeed of $V = 20$ m/s, see Figure 1.2.

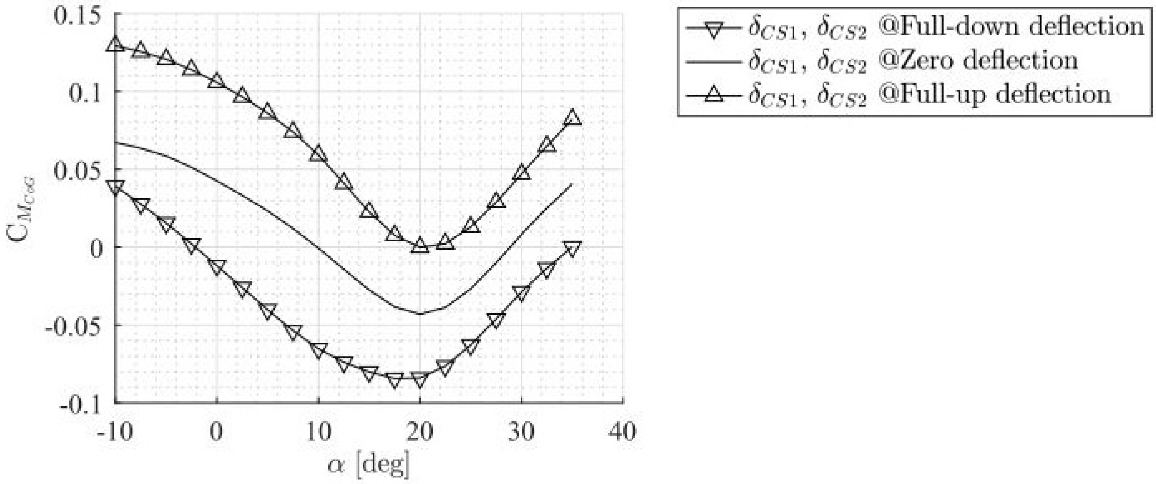

Figure 1.2: Pitching moment coefficient with angle of attack of the strip-on Flying V wind tunnel model, from [1]

Such an unstable pitch break in combination with a gust could have disastrous consequences for the aircraft. Especially since the Flying V needs to take-off and land at relatively high angles of attack due to the lack of high lift devices. Furthermore, the usable maximum lift coefficient ($C_{L_{\text{max}}}$) is limited by the pitching moment coefficient rather than the stall angle of attack of the aircraft. In other words, the unstable pitch break at an angle of attack of $\alpha = 20^\circ$ decreases the usable $C_{L_{\text{max}}}$. It is desired to be able to fly at higher lift coefficients than is currently possible, therefore the current research is carried out.

1.3. Current Research

The goal of this research is to gain insight in the aerodynamics behind the unstable pitch break and to find possible solutions to postpone the pitch break. With the results of wind tunnel campaigns, it is hoped to answer the following question: What is the influence of aerodynamic add-ons on the pitching moment coefficient of the Flying V? For a clear structure, this question is divided in three sub-questions:

- What is the effect of the position of the aerodynamic add-on on the pitching moment and change in pitching moment with angle of attack of the wing?
- What is the effect of the size of an aerodynamic add-on on the pitching moment and change in pitching moment with angle of attack of the wing?

- What is the effect of adding trip strips on the pitching moment and change in pitching moment with angle of attack of the wing?

2
Method

In this section the Open Jet Facility (OJF) of the TU Delft is described, as well as the wind tunnel campaigns, test setup, the Flying V half model and the design of the aerodynamic add-ons. The wind tunnel used for this research is the OJF at the TU Delft. It is a closed circuit open jet wind tunnel with a test chamber of 13 by 8 by 8 meters. The jet of the OJF has an octagonal shape with a dimension of 285 by 285 cm and the airspeed can be increased up to 32 m/s. In order to answer the research questions posed in the previous section, two wind tunnel campaigns are set up: W1 and W2. In W1 a trip strip and various aerodynamic add-ons, fences and pylon vortex generators (vortilons), are added to the wing to investigate their influence on the aerodynamics and the pitching moment. In W2 several redesigns of one of these add-ons are investigated.

2.1. Wind Tunnel Model

The model used in this research is a scaled half-model of the Flying V, see Figure 2.1. This scale is chosen as it is exactly the same as the scaled flight testing (SFT) model (4.6% of the Flying V) and therefore the wind tunnel results can be translated directly to the SFT model. The wind tunnel model is constructed from a fiberglass-foam laminate and spans 1.495 m. It has a root chord of 1.1 m, the inboard leading edge sweep is 64° and the outboard leading edge sweep is 38°. The model was designed by Palermo and a more detailed description of the design can be found in [16].

2.2. Wind Tunnel Setup

The wind tunnel model is installed on a six-component balance, which is mounted on a rotary table. Both the balance and rotary table are placed below the bottom of the wind tunnel jet, shielded by a plate, preventing the jet to influence the measurements. Because a half model is used, a reflection plane is created and the model is floating above that plane, preventing the construction influencing the measurements. Rotation of the model is enabled by circular cutouts in both plates. The construction of aluminum beams between balance and model is shielded from the flow as well and elliptical leading edges are installed on the splitting plate to achieve an as clean as possible flow over the reflection plane. For a complete overview of the setup, see Figure 2.2.

The maximum single load range for the balance is shown in Table 2.1. The measurement accuracy of the balance is shown in Table 2.2.

Component	Range	Component	Range
F_x	± 250 N	M_x	± 550 Nm
F_y	± 600 N	M_y	± 500 Nm
F_z	± 3500 N	M_z	± 125 Nm

Table 2.1: Maximum single loads allowed on the balance

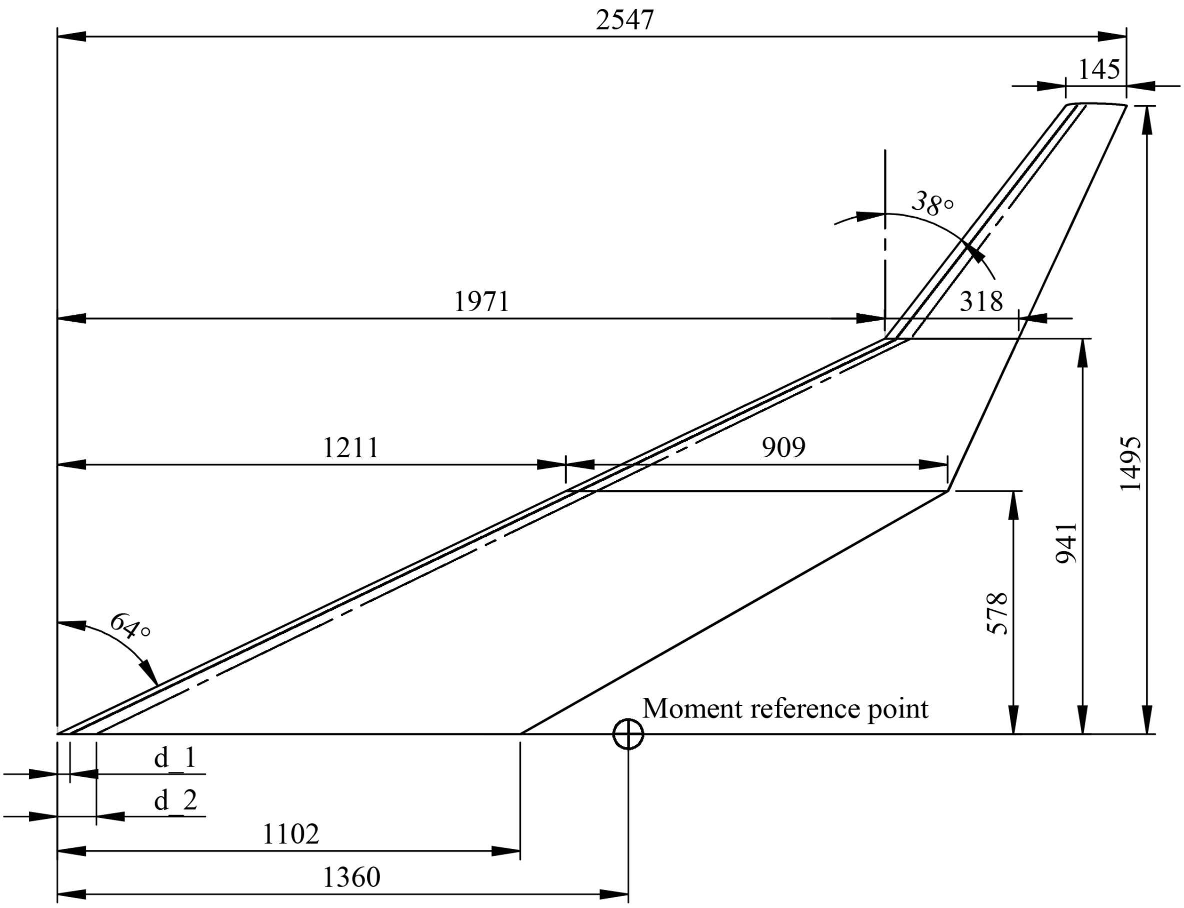

Figure 2.1: Flying V wind tunnel model planform with trip strip locations d_1 and d_2, dimensions in mm

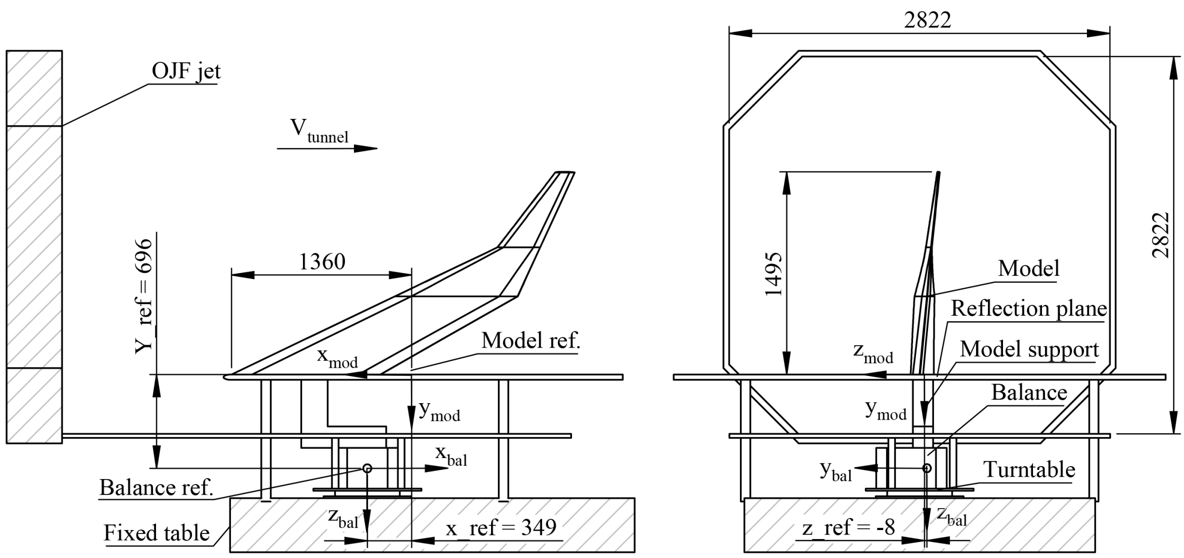

Figure 2.2: Side view (left) and rear view (right) of the Flying V wind tunnel setup (model support cover not shown), dimensions in mm

	ΔF_x	ΔF_y	ΔF_z	ΔM_x	ΔM_y	ΔM_z
Δ_{max}	0.06	0.23	0.16	0.05	0.05	0.25
σ_Δ	0.02	0.05	0.05	0.01	0.01	0.07

Table 2.2: Maximum error, Δ_{max}, and standard deviation of the measurement error, σ_Δ, in [%]

2.3. Aerodynamic Add-on Design

Both fence and vortilon design are based on designs found in previous research. The driving design parameter for fences is the relative height, h, with respect to the local thickness of the wing, t, found to be $h = 0.5t$ [17]. The effectiveness of a fence increases as it protrudes in front of the leading edge and sweeps from the pressure side to the suction side of the wing [18, 19]. The spanwise placement of the fence is based on previous research into aerodynamic add-ons [17, 19], combined with the knowledge about the flow field of the clean wing that is available to date [15, 16]. In the case of the Flying V, the leading edge kink and the trailing edge kink are identified as interesting regions. Two other interesting regions are halfway between root and trailing edge kink and halfway between leading and trailing edge kink respectively [15]. Therefore fences are installed at those spanwise locations, see Figure 2.3. To save weight and keep the increase of wetted surface as small as possible, the fence runs from $x/c = 0.25$ on the pressure side of the wing to $x/c = 0.25$ on the suction side. The thickness of the fences is 4 mm for fence 1 and 2. Fences 3 and 4 are 3 and 2 mm thick. These thicknesses are chosen to ensure sufficient structural stiffness to sustain wind speeds up to 30 m/s. As an example, Fence 1a is shown in Figure 2.4.

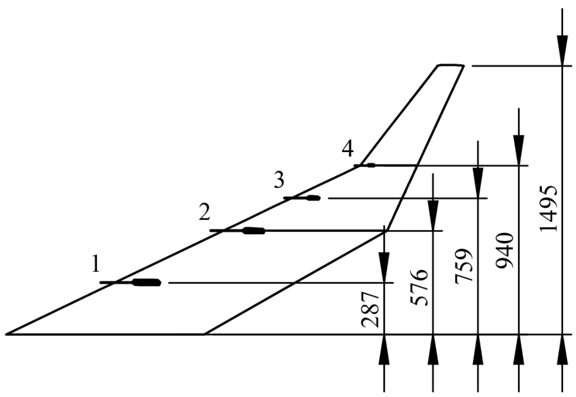

Figure 2.3: Spanwise fence locations on the wind tunnel model, dimensions in mm

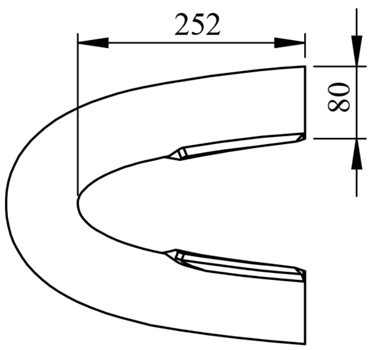

Figure 2.4: Design of fence 1a, for spanwise location 1 where $\eta = 0.19$, dimensions in mm

As will become clear in Chapter 4, spanwise location 4 is found to be the most effective location to install a fence. To be able to answer the sub-questions posed in the introduction, see Chapter 1, four additional fences are designed for spanwise location 4. During the second wind tunnel campaign these designs are installed on the wing and the effect on the wing is measured. The results are shown in Figure 4.10. In previous research it was found that an increase in fence height and area increases the vortex strength of the vortex resulting from the fence [17, 20]. These findings are used in the new designs for a fence at spanwise location 4. Based on this knowledge and the results from the first wind tunnel campaign, it is expected that the highest and longest fence, fence 4ac, will yield the greatest difference in pitching moment coefficient behavior.

The effective spanwise location for the installation of a vortilon cannot be defined based on prior research. Therefore, the most effective spanwise location to install a vortilon has to be found empirically. Vortilons are designed for fourteen locations along the span of the half model, equally spaced starting 100 mm from the root of the wing, see Figure 2.5. The vortilons are triangular shapes, as in the research of Rao[21], with a leading edge sweep of 30° and similar in dimension of those used by Rao, adjusted for the thickness of the Flying V wing along its span, see Figure 2.6 for an example. Like the fences, the thickness of a vortilon is kept as small as possible while ensuring it can sustain the loads at $V = 30$ m/s. Both the fences as well as the vortilons are designed with flanges to create a large enough surface area for the add-ons to stick to the wind tunnel model. The influence of the vortilons and fences on the flow around the wing is expected to be far greater than the influence of the flanges. Double sided tape is used to install the add-ons on the wing, as this allows for easy and fast installation and swapping of the add-ons. All add-ons are 3D printed.

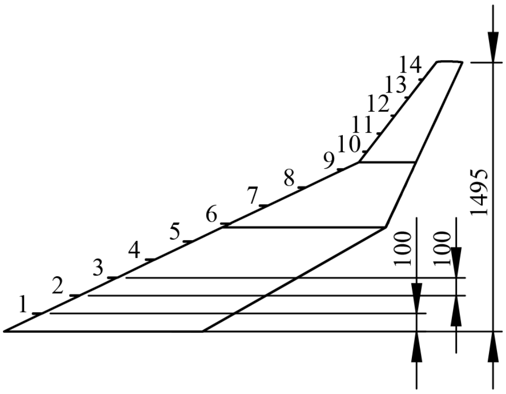

Figure 2.5: Equally spaced spanwise vortilon locations on the wind tunnel model, dimensions in mm

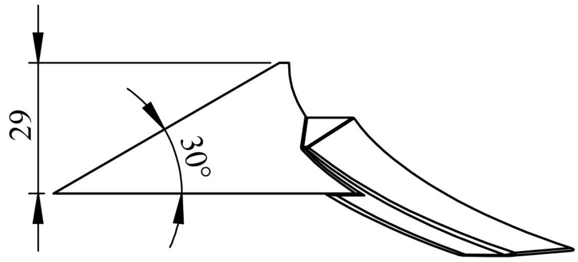

Figure 2.6: Design of vortilon 3, for spanwise location 3 where $\eta = 0.20$, dimensions in mm

2.4. Measurements

The forces and moments acting on the wind tunnel model are measured using a six component balance in the balance reference frame and transformed to the model reference frame. Furthermore, tuft visualizations are used to qualitatively assess the flow around the model. Measurements are taken in a range of angles of attack from $\alpha = -5°$ to $30°$. For $\alpha = 15°$ to $25°$ a step of $1°$ is used. To reduce the number of samples, a coarser $5°$ step in angle of attack is taken in the range of $\alpha = -5°$ to $5°$ and for the rest of the samples a step of $2.5°$ is used. Forces and moments are defined in the wind tunnel model reference frame, mod, see Figure 2.2. Because the forces, F, and moments, M, are measured in the balance reference frame, bal , they need to be converted from the balance reference frame to the model reference frame. The following equations are used:

$$\begin{aligned} \vec{F}_{\text{mod}} &= \mathbf{R}_{\text{bal,mod}} \vec{F}_{\text{bal}} \\ \vec{M}_{\text{mod}} &= \mathbf{R}_{\text{bal,mod}} \vec{M}_{\text{bal}} + \vec{r}_{\text{bal,mod}} \times \mathbf{R}_{\text{bal,mod}} \vec{F}_{\text{bal}} \,. \end{aligned} \tag{2.1}$$

Where $\mathbf{R}_{\text{bal,mod}}$ represents the rotation matrix between the balance and model reference frame. $\vec{r}_{\text{bal,mod}}$ represents the translation from balance to model reference frame origin. Their numeric values are represented by:

$$\mathbf{R}_{\text{bal,mod}} = \begin{bmatrix} -1 & 0 & 0 \\ 0 & 0 & 1 \\ 0 & 1 & 0 \end{bmatrix} \quad \text{and} \quad \vec{r}_{\text{bal,mod}} = [x_{\text{ref}} \quad y_{\text{ref}} \quad z_{\text{ref}}] \tag{2.2}$$

and the values of $\vec{r}_{\text{ref,bal}}$ can be found in Figure 2.2. Using Equations (2.1) and (2.2), the lift force L, drag force D, pitching moment M and rolling moment l can be calculated, see Equation (2.3). The lift and drag force are defined in the wind reference frame, where the pitching and rolling moment are defined in the model reference frame.

$$\begin{aligned} L &= -F_{x_{\text{bal}}} \sin(\alpha) - F_{y_{\text{bal}}} \cos(\alpha) \qquad & M &= M_{z_{\text{bal}}} + F_{x_{\text{bal}}} y_{\text{ref}} - F_{y_{\text{bal}}} x_{\text{ref}} \\ D &= F_{x_{\text{bal}}} \cos(\alpha) - F_{y_{\text{bal}}} \sin(\alpha) \qquad & l &= -M_{x_{\text{bal}}} + F_{y_{\text{bal}}} z_{\text{ref}} + F_{z_{\text{bal}}} y_{\text{ref}} \,. \end{aligned} \tag{2.3}$$

Now that the forces and moments are transformed to the model and wind reference frame, the lift , drag, pitching moment and rolling moment coefficient (C_L,C_D,C_M,C_l) are calculated using the following formulas:

$$C_L = \frac{L}{q\,S} \qquad C_M = \frac{M}{q\,S\,\bar{c}}$$
$$C_D = \frac{D}{q\,S} \qquad C_l = \frac{l}{q\,S\,b}\,, \tag{2.4}$$

where the model surface area S = 0.935 m^2, the mean aerodynamic chord $\bar{c}$ = 0.82 m and the model half span b = 1.495 m.

All measurements are performed three times. Preferably, these measurements would be spread throughout the wind tunnel campaign. However, it was not possible to guarantee an exact match in installed position and orientation of the aerodynamic add-ons when they had been removed from the wing. Therefore the three measurements per case were carried out right after each other. To be able to make a confidence interval interpretation of the measurements, the mean μ and standard deviation σ are calculated

$$\mu = \frac{\sum_1^n x_i}{n} \quad \text{and} \quad \sigma = \sqrt{\frac{\sum_1^n (x_i - \mu)^2}{n-1}}\,, \tag{2.5}$$

where x_i represents the sample and n the number of samples. For all experiments in the research, $n = 3$. The confidence interval can be calculated using the following equation:

$$(x_l, x_u) = \mu \pm t_{n-1}\frac{\sigma}{\sqrt{n}}\,, \tag{2.6}$$

where x_l and x_u are the lower and upper bounds of the confidence interval and $t_{n-1} = 4.30$ for a 95% confidence interval using the t-distribution.

3

Verification & Validation

Validation of the wind tunnel setup is carried out by making three comparisons. First, the short-term repeatability of the clean wing measurements is investigated using the t-distribution, see Equation (2.6) and Figure 3.1. Second, a comparison is made with previous research [1–3], see Figure 3.2. This comparison is done for the wing with trip strips applied to suction and pressure surface (strip-on) and without any of the add-ons. Third, a verification step is carried out, comparing the clean wing results of the first wind tunnel campaign, W1, with the clean wing results of the second wind tunnel campaign, W2, see Figure 3.3.

3.1. Short-Term Repeatability

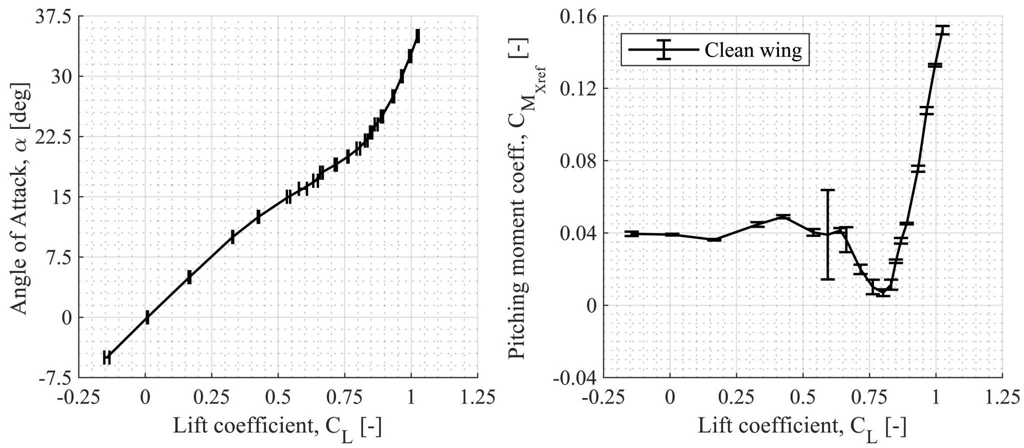

Figure 3.1: 95% confidence interval of the Flying V wing half model wind tunnel setup

The short-term repeatability can be concluded to be good, judging the small error bars displayed in Figure 3.1. The error bars represent the interval wherein 95% of the measurements fall. However, a relatively large error bar is seen in the $C_L - C_M$ plot at a lift coefficient of $C_L = 0.6$ corresponding with an angle of attack of $\alpha = 12.5°$. This could be the result of a highly variable flow field at that lift coefficient resulting in a large difference in instantaneous measurement results. Looking at the oil flow visualizations of Viet [15], it is observed that the surface flow patterns change significantly between $\alpha = 9°$ and $15°$. While at an angle of attack of $9°$ there are no signs of vortex formation, at $\alpha = 15°$ at least three clear surface flow patterns corresponding to a vortex can be seen. The onset of development of two of the three vortices lies between angle of attack of $\alpha = 11°$ and $13°$ and as vortex formation is not a linear process, this could be an explanation for the relatively large error bar at $C_L = 0.6$. Both Palermo and van Empelen[1, 3] observed a similar difference in uncertainty range between 15 and 12.5° angle of attack, respectively, and the other angles measured in their wind tunnel campaigns.

3.2. Comparison with Previous Research

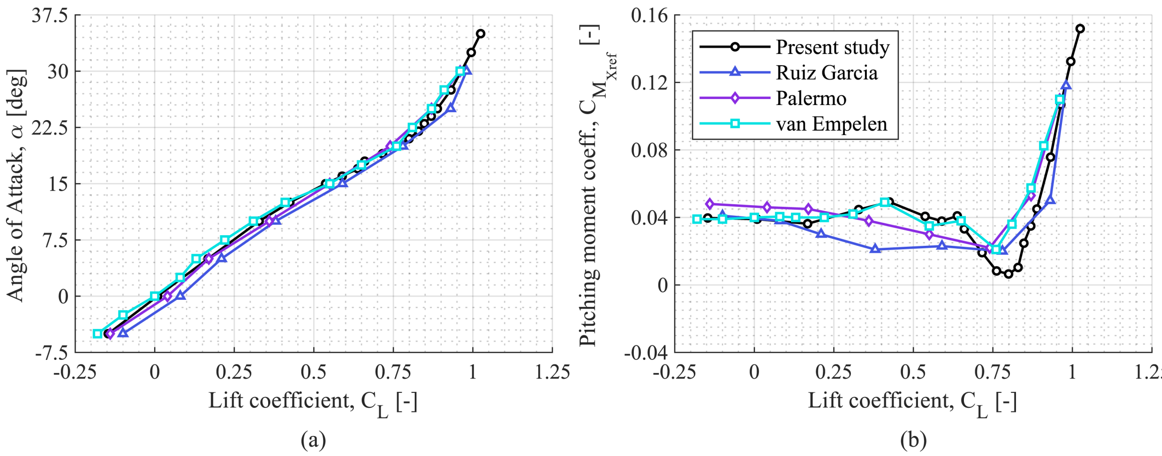

Figure 3.2: Comparison of present and previous reasearch [1–3] of the Flying V half model in strip-on configuration

Comparing the results of the present study with that of previous research[1–3], it is apparent there are some differences. Figure 3.2 shows that up to a lift coefficient of $C_L = 0.7$ the $C_M - C_L$ curve of the present study follows that of van Empelen [3]. For higher lift coefficients, the pitching moment coefficient of the current study declines compared to the lift coefficient measured by van Empelen. The pitching moment coefficient remains lower up to a lift coefficient of $C_L = 1$. Three factors are identified that might result in this difference. First, the wind tunnel setup consist of many parts which are subject of play and that results in a slightly different setup each time it is installed in the wind tunnel. Second, the half-model itself is found to structurally change over the course of the wind tunnel campaigns. It is hard to say at which point in time this occurred exactly, but it can be said with certainty that during the present study the model was in a different state than during previous research. The third factor contributing to the difference in results, is the alignment of the half-model in the wind tunnel. The model is aligned with a laser and the human eye and there is no predefined reference on the wind tunnel setup or model, making it impossible to guarantee the same alignment every campaign.

3.3. Comparison of Campaign W1 and W2

In Figure 3.3 the aerodynamic coefficients of the clean wing measured in the first (W1) and second (W2) wind tunnel campaign are displayed. Looking at the $\alpha - C_L$-graph in Figure 3.3(a), it is observed that up to a lift coefficient of $C_L = 0.6$ the angle of attack of the wing in the second wind tunnel campaign is slightly higher. To express this in a more common way: up to a lift coefficient of $C_L = 0.6$, the clean wing generates slightly less lift in the second campaign than in the first campaign. In the same C_L-region, the slope of the curve is lower for the second campaign than that of the first. This could be an indication of a change in installed yaw angle, effectively changing the sweep of the wing and the gap size between half model and reflection plane. Also, this may indicate a misalignment in angle of attack of $\pm 1°$. For a lift coefficient greater than $C_L = 0.6$, the lift coefficients from the first and second wind tunnel campaign match well.

In Figure 3.3(b) the pitching moment coefficient with lift coefficient is shown. From that figure, several observations can be made. First, for campaign W1, a sudden increase in pitching moment coefficient is seen at $C_L = 0.6$. With increasing lift coefficient a region of erratic behavior appears between $C_L = 0.6$ and 0.7, after which an increase in pitching moment coefficient is observed. At $C_L = 0.8$ the pitching moment coefficient declines suddenly. After this sudden drop, the pitching moment coefficient departs at $C_L = 0.95$ and does not recover. Contrary to the first wind tunnel campaign, the results from campaign W2 do not show a sharp drop in C_M. Instead, starting at a lift coefficient of $C_L = 0.6$ the pitching moment coefficient increases moderately up to $C_L = 1.05$, where it

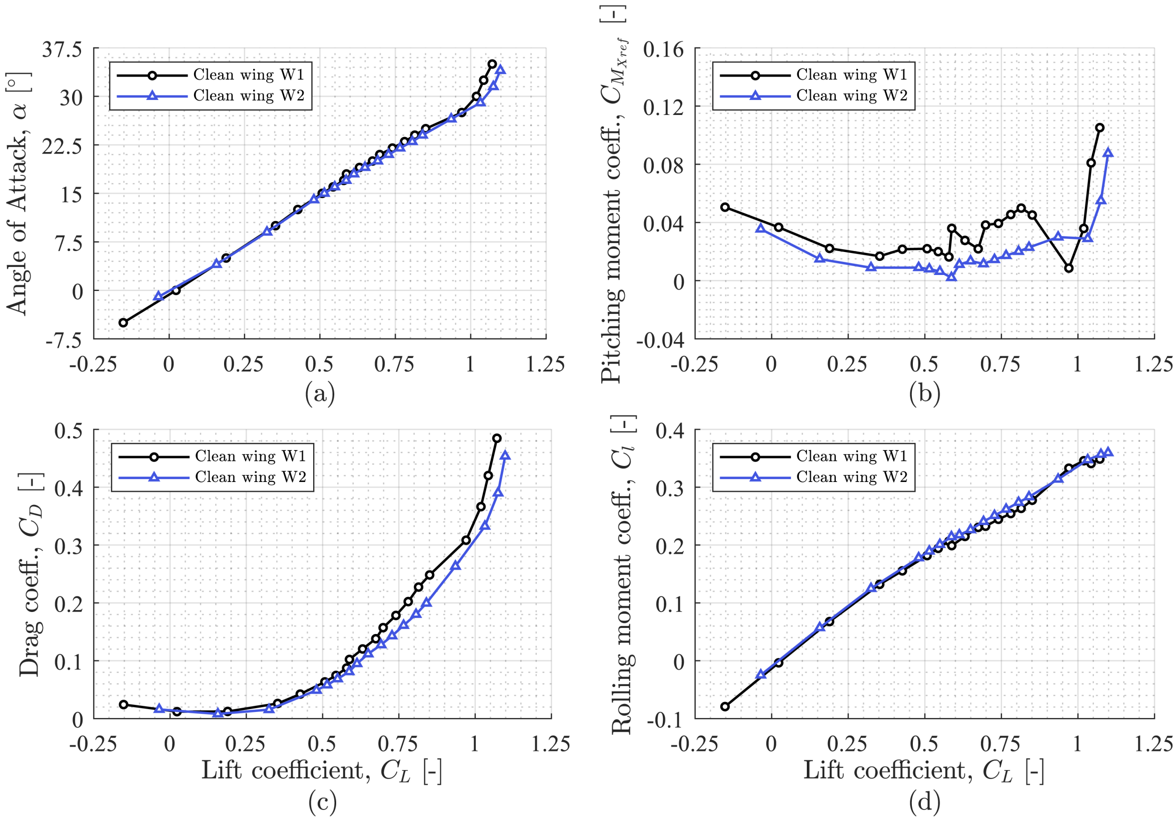

Figure 3.3: Comparison of clean wing results of the first (W1) and second (W2) wind tunnel campaign

departs and does not recover. Overall, the pitching moment coefficient for the clean wing in campaign W2 is lower than that of campaign W1. Three factors are identified that could be the cause of these differences. Firstly, it is suspected that the distance between balance center and moment reference point (x_{ref}) is increased in the order of 20 millimeters. Second, a faulty spar connection in the Flying V wind tunnel model was discovered during the first wind tunnel campaign. And third, the alignment of the setup. Because this is done with a margin of error of $\pm 1°$ and the pitching moment coefficient is very sensitive to angle of attack and thus lift coefficient, this could change the pitching moment characteristic.

Aforementioned factors possibly explaining the differences in lift and rolling moment coefficient also influence the drag coefficient, see Figure 3.3(c).

Inspecting the rolling moment coefficient shown in Figure 3.3(d), it can be concluded that the results of campaign W1 and W2 are a near perfect match. Only around a lift coefficient of $C_L = 0.75$ small differences can be observed. In this region the flow field around the wing is dominated by vortices. The differences in formation and break down of those vortices is suspected to cause this difference in rolling moment coefficient.

4
Results

This chapter presents the results obtained by the wind tunnel experiments and is divided into five sections. Section 4.1 is focused on the difference in aerodynamic coefficients between the flying V in clean and strip-on configuration. The strip-on configuration is shown in Figure 2.1, where the solid line represents the trip strip on the suction surface and the dashed line the trip strip on the pressure surface of the wing. The second section, Section 4.2, presents the influence of the application of a vortilon to the wing's surface. The third section, Section 4.3, presents the influence of the application of a fence to the wing's surface. In Sections 4.4 and 4.5 the effects of vortilons and fences on the Flying V wing in strip-on configuration are discussed. All results presented in this chapter are obtained from wind tunnel measurements with an airspeed of $V = 18.7$ m/s and a moment reference position $x_{\text{ref}} = 1.36$ m from the nose of the aircraft, unless specified differently.

4.1. Trip Strip Effects

In this section the effects of the application of a trip strip to the pressure and suction side of the wing are discussed. The strip-on configuration of the Flying V wind tunnel model is shown in Figure 2.1. The trip strip is applied to the suction as well as the pressure side of the wing and along the entire span, located at a chordwise position of $x/c = 0.05$ for the suction side and $x/c = 0.10$ for the pressure side. Figure 4.1 shows a comparison in drag, pitching moment and rolling moment coefficients with lift coefficient for the clean and strip-on wing. The main focus of this research is the pitching moment characteristic of the flying V wing. Therefore, the results regarding the pitching moment coefficient are discussed first. After the aerodynamic coefficients, flow visualization pictures are presented in Figures 4.2 and 4.3.

In Figure 4.1(b) the pitching moment coefficient characteristics with lift coefficient are shown. From that figure, several observations can be made. First, for the clean wing, a sudden increase in pitching moment coefficient is seen at $C_L = 0.58$. Between $C_L = 0.58$ and 0.7 a region of erratic behavior is observed. At $C_L = 0.81$ the pitching moment coefficient suddenly decreases with increasing lift coefficient, until $C_L = 0.95$. The unstable pitch break experienced by the clean wing is observed at this lift coefficient. For the strip-on case, the overall pitching moment coefficient characteristic is flatter than the characteristic of the clean wing in the lift coefficient region $C_L = -0.15$ to 0.65. Also, for almost the same C_L-region, the absolute pitching moment coefficient value is higher for the strip-on wing than for the clean wing. The sudden drop in pitching moment coefficient followed by a steep unrecoverable increase seen in the results of the clean wing still exists in the results of the strip-on wing. However, this phenomenon is shifted to a lower lift coefficient, now occurring at $C_L = 0.65$. The unstable pitch break experienced by the strip-on wing is observed at $C_L = 0.80$.

Shifting our attention to Figure 4.1(a), the differences between the strip-on and clean wing in lift coefficient with angle of attack become apparent. Looking at the trend of the lift coefficient with angle of attack, it can be observed that up to a lift coefficient of $C_L = 0.5$ the results of the clean wing and wing in strip-on configuration match closely. Between $C_L = 0.5$ and 0.9 the strip-on wing achieves a higher lift coefficient at the same angle of attack compared to that of the clean wing case, after which the clean wing surpasses the strip-on wing and yields a higher lift coefficient from $\alpha = 27.5°$ onward.

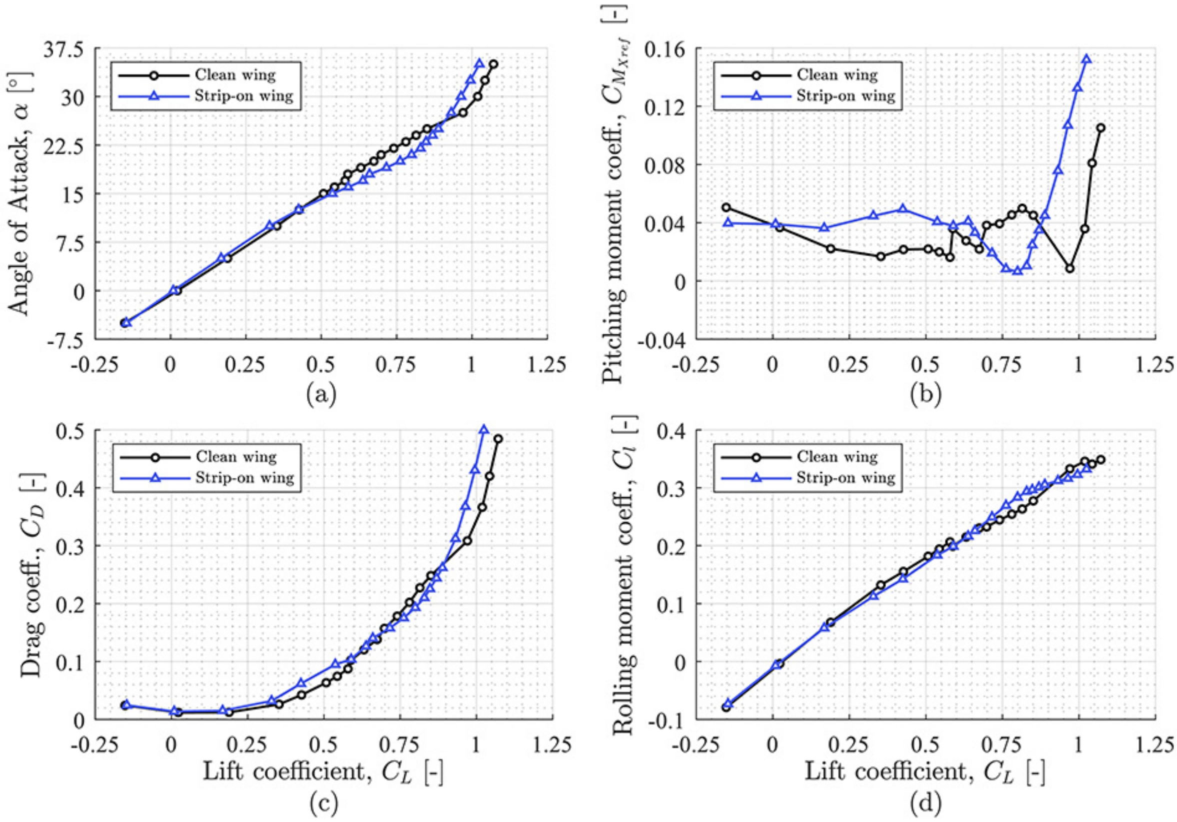

Figure 4.1: Aerodynamic coefficients of the Flying V wing in clean and strip-on configuration

Comparing the drag coefficients of the two cases, see Figure 4.1(c), it is shown that in the region between $C_L = 0$ and 0.7 the strip-on wings' drag coefficient is higher than the drag coefficient of the clean wing. Between $C_L = 0.70$ and 0.88 the clean wings' drag coefficient is higher than that of the strip-on wing. From $C_L = 0.88$ onward, the strip-on wings' drag coefficient is greater again, and the difference between the two increases with increasing lift coefficient.

Looking at Figure 4.1(d), the rolling moment coefficient with lift coefficient is shown. Keeping the lift coefficient trends in mind, it can be observed that the difference in rolling moment coefficient between the clean and strip-on wing is proportional to the differences in lift coefficient.

Based on the observations regarding the pitching moment coefficient in Figure 4.1(b) and rolling moment coefficient in Figure 4.1(d), the following hypothesis is formed. For lift coefficients up to $C_L = 0.60$ the application of trip strips induces a forward and inboard shift in aerodynamic center location. Using the oil flow visualizations from Viet[15], it can be seen that between $C_L = -0.15$ and 0.60 three vortices are formed. It is suspected that the application of the trip strips decreases the lift coefficient at which these vortices are formed. The change in cross-flow, boundary layer thickness and turbulence level caused by the trip strip is suspected to cause this change in vortex formation [22]. The decrease in usable $C_{L_{\max}}$, from $C_L = 0.95$ to 0.80, caused by application of the trip strips is suspected to be the result of an earlier formation of the inboard vortex. The vortex strength increases with increasing lift coefficient and its origin moves towards the leading edge and root of the wing. The increase in strength first yields a decrease in pitching moment coefficient but the movement of this vortex results in a shift of the aerodynamic center towards the leading edge and root of the wing, resulting in an increase in pitching moment coefficient. For the strip-on wing a lower rolling moment coefficient is observed between $C_L = 0.85$ and 1 in Figure 4.1(d). This corroborates the shift in aerodynamic center towards the root of the wing.

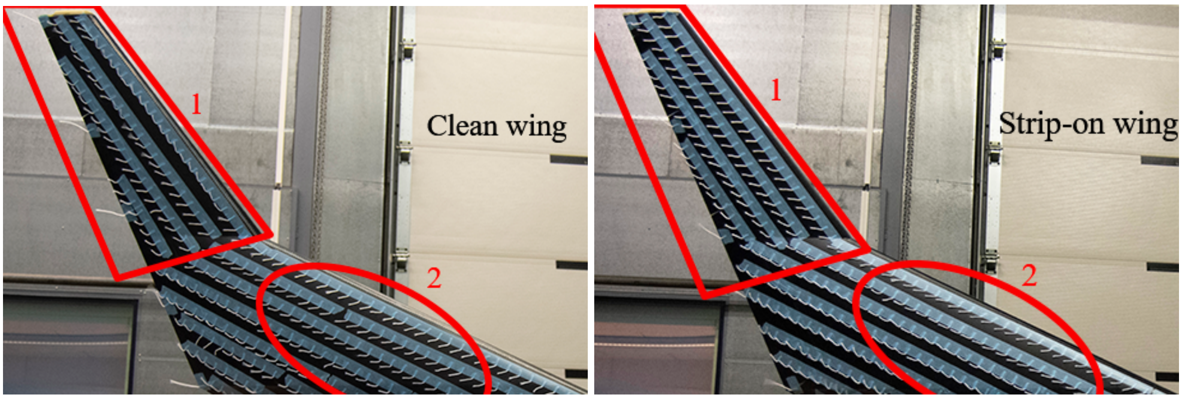

(a) (b)

Figure 4.2: Tuft comparison of clean (a) and strip-on (b) outboard wing at $C_L = 0.33$ and $\alpha = 10^\circ$

In Figure 4.2 a comparison of flow visualizations using tufts is shown for the Flying V half-model in strip-on and clean configuration. Two areas of interest are identified and circled in red. Area 1 on the outboard part of the wing and area 2 on the mid-span part of the wing. Reviewing the flow in area 1, it can be observed that the flow over the strip-on wing seems to be attached to the surface, where the flow over the clean wing seems to be at least partly separated. In area 2 however, it seems the trip strip is making the flow more susceptible to cross-flow compared to the clean wing. Based on these observations, it is thought that it would benefit the Flying V when a trip strip is applied only on the outboard wing and not on the inboard part of the wing.

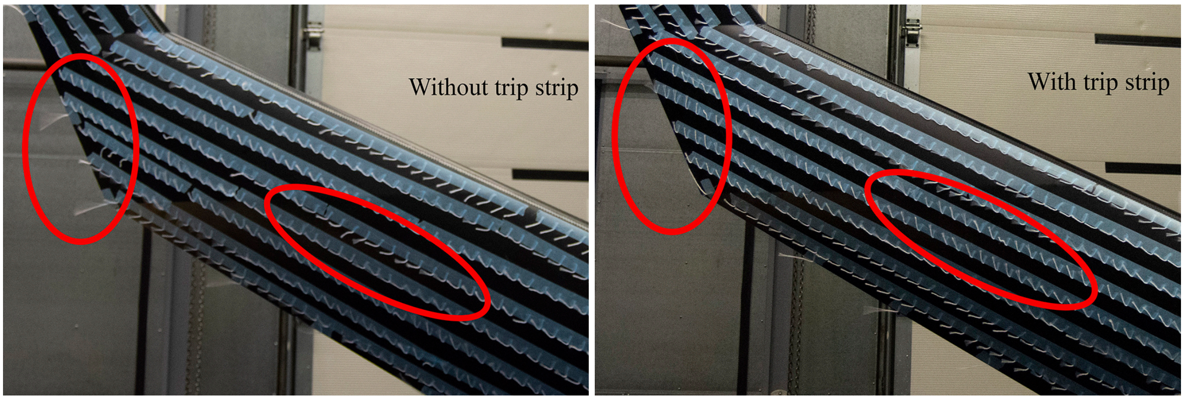

(a) (b)

Figure 4.3: Tuft comparison of clean (a) and strips-on (b) mid section of the wing at $C_L = 0.78$ and 0.76 and $\alpha = 23^\circ$ and 20° respectively

In Figure 4.3, the same wings as in Figure 4.2 are shown, but this time for higher lift coefficients, $C_L = 0.76$ and 0.78, and angles of attack, $\alpha = 20^\circ$ and 23°, respectively. The differences between the two cases is less apparent this time, however two areas are identified where a difference is observed. At the trailing edge of the strip-on wing, the flow seems to have separated from the surface, where for the clean wing evidence of vortex formation is found in the rotation of the two trailing edge tufts. In the area more inboard, mid chord, a clear difference in tuft direction is observed. For the clean wing it seems that the flow velocity on the surface nears zero, where that is not the case for the strip-on wing.

4.2. Vortilon Effects

In this section the effect of the addition of a vortilon to the clean wing of the Flying V will be discussed. The spanwise locations of application are shown in Figure 2.5 and are numbered 1 to 14 from the root to the tip of the wing. The locations are equally spaced along the span of the wing and vortilons are installed one at a time. The design of a vortilon is shown in Figure 2.6. In Figures 4.4 to 4.7 the aerodynamic coefficients of the Flying V with vortilon are shown for each vortilon.

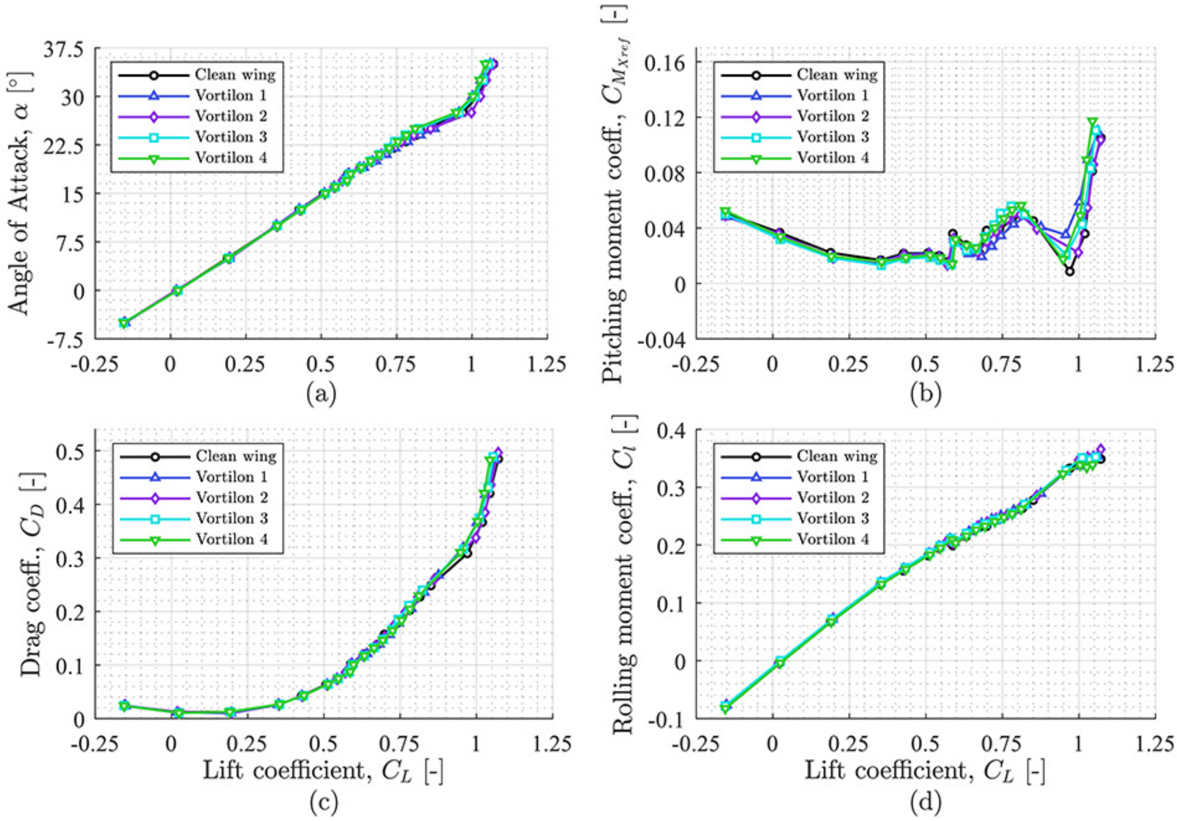

Figure 4.4: Aerodynamic coefficients of the clean Flying V wing with a vortilon at locations 1 to 4, results from W1

In Figure 4.4 the results of several clean wing plus vortilon cases are shown. Looking at Figure 4.4(a) - (d) it can be observed that placing a vortilon at these spanwise locations does not influence the aerodynamic characteristics of the Flying V. The only difference with respect to the clean wing is observed in Figure 4.4(b). At $C_L = 0.95$, where the Flying V experiences the pitch break, the application of a vortilon at spanwise position 1-4 ($\eta = 0.07$ to 0.27) results in an increase in nose-up pitching moment coefficient. The closer to the root the vortilon is placed, the bigger the increase in nose-up pitching moment coefficient.

It is suspected that the size of the vortilons is too small to have an effect on the flow over the wing. Orientation of the vortilon with respect to the flow could also change its effect. Because spanwise locations 1-4 are close to the root of the wing, the increase in pitching moment coefficient is thought to be the result of the formation of a vortex at the vortilon. This shifts the aerodynamic center forward and inboard, resulting in an increased nose-up pitching moment coefficient.

In Figure 4.5 the aerodynamic coefficients of the Flying V with a vortilon at spanwise location 5, 6 and 7 ($\eta = 0.33$ to 0.47) are shown. Looking at Figure 4.5(a), (c) and (d) only minor differences between the vortilon and clean wing cases are observed. All three vortilons presented in this figure result in a slightly lower lift coefficient and a slightly higher drag coefficient for $C_L > 0.95$. In the region of $C_L = 0.55$ to 0.80, the addition of a vortilon reduces the drag coefficient slightly. Shifting our attention to Figure 4.5(b), the differences between clean wing and wing plus vortilon become more apparent. First, the overall pitching moment coefficient characteristic of the three vortilon cases is more nose-down than that of the clean wing up to a lift coefficient of $C_L = 0.80$. Second, the installation of vortilon 5 and 7 eliminates the region of erratic behavior experienced by the clean wing between

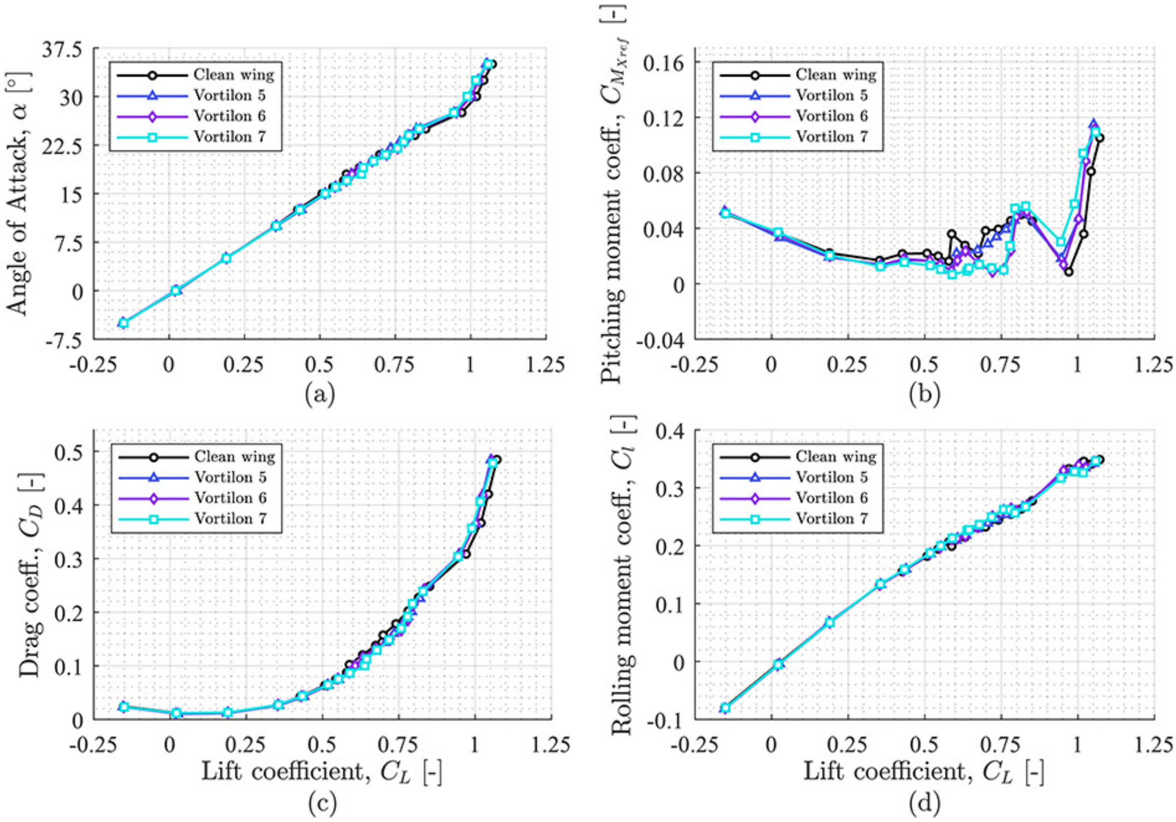

Figure 4.5: Aerodynamic coefficients of the clean Flying V wing with a vortilon at locations 5 to 7, results from W1

$C_L = 0.55$ and 0.70. The installation of vortilon 6 does not eliminate the erratic behavior, however the trend of the pitching moment coefficient curve in the same C_L-region is negative compared to positive for the clean wing. Third, the trend of the pitching moment coefficient curve of vortilon 6 and 7 is generally negative up to $C_L = 0.75$ where that of the clean wing is positive when $C_L > 0.55$. Lastly, the installation of any of the three vortilons increases the pitching moment coefficient at $C_L = 0.95$, where the unstable pitch break occurs.

Based on these wind tunnel measurements, literature[23] and previous research into the Flying V [15], it is suspected that the installation of the vortilons presented in Figure 4.5 lead to the formation of a vortex that interacts with the vortex on the inboard part of the wing. This leads to a outboard and aft shift of the aerodynamic center compared to the clean wing, which increases the nose-down pitching moment. At higher lift coefficients, $C_L > 0.75$, this effect is overcome by the strength of the inboard vortex resulting in an increase in nose-up pitching moment.

In Figure 4.6 the aerodynamic coefficients of the flying V with vortilon 8, 9 and 10 ($\eta = 0.54$ to 0.67) are compared with that of the clean wing. Starting with Figure 4.6(a), it can be seen that the difference in lift coefficient with angle of attack between the clean wing and all three vortilon cases is almost non-existent. The same goes for the drag coefficient and rolling moment coefficient with lift coefficient, shown in Figure 4.6(c) and (d). In Figure 4.6(b) the pitching moment behavior with lift coefficient is shown. The application of vortilon 8 does not influence the behavior of the clean wing, except that it diminishes the region of erratic behavior around $C_L = 0.55$. Focusing on vortilon 9 and 10, two complete different trends can be observed. The application of vortilon 9 results in the same erratic behavior, between $C_L = 0.55$ to 0.70, as the clean wing shows. After that erratic region the pitching moment coefficient of vortilon 9 keeps decreasing up to a lift coefficient of $C_L = 0.75$, where it start to increase again. Vortilon 10 however, does not show the erratic behavior observed in the other cases, but at a lift coefficient of $C_L = 0.65$ the pitching moment starts to increase up to a lift coefficient of $C_L = 0.80$, where it declines before increasing in a steep manner at $C_L = 0.95$. All four cases in this comparison have a usable maximum lift coefficient of $C_{L_{\text{max}}} = 0.95$.

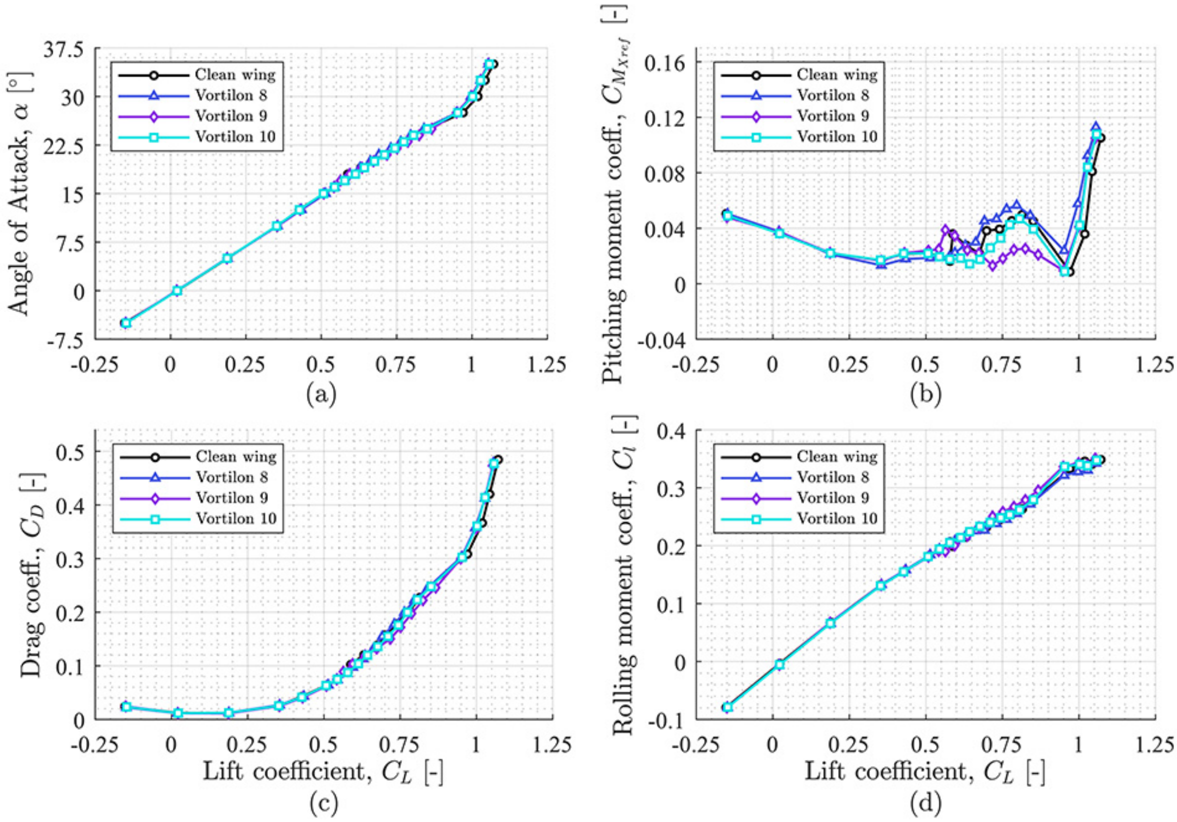

Figure 4.6: Aerodynamic coefficients of the clean Flying V wing with a vortilon at locations 8 to 10, results from W1

It is suspected that the vortex generated by vortilon 10, located outboard of the leading edge kink, interacts with the leading edge kink vortex. This results in the elimination of the region of erratic behavior. Because vortilon 9 is located inboard of the leading edge kink it has the opposite effect on the pitching moment coefficient, compared to vortilon 10, thus increasing the peak in pitching moment coefficient at $C_L = 0.55$. However, based on the observations from Figure 4.6 it is thought that vortilon 9 increases the strength of the leading edge kink vortex, thereby increasing the outboard wings' contribution to the pitching moment coefficient, which is nose-down. Next to the increase in vortex strength, the outboard wing seems to stay effective up to higher lift coefficients when a vortilon is installed at spanwise position 9.

In Figure 4.7 the aerodynamic coefficients of the clean wing are compared with those of the wing and vortilon at locations 11 to 14 ($\eta = 0.74$ to 0.94). As with all previous vortilon results, the application of vortilon 11 - 14 does not lead to significant change in the lift, drag and rolling moment coefficient characteristics (Figure 4.7(a), (c) and (d)). Looking at Figure 4.7(b), some differences between clean wing and wing plus vortilon are observed. Focusing on the region of erratic behavior in pitching moment coefficient of the clean wing between $C_L = 0.55$ and 0.70, it is observed that only the installation of a vortilon at spanwise location 11 eliminates this erratic behavior. Not only the region of erratic behavior is eliminated, a vortilon at location 11 increases the nose-down pitching moment between $C_L = 0.35$ to 0.80 compared to that of the clean wing. For $C_L > 0.80$ the installation of one of these four vortilons does not affect the pitching moment coefficient.

A trend can be observed from the results shown in Figure 4.7(b): the more outboard the vortilon is installed, the less effect is has on the wing. This would be a logical explanation as the vortex resulting from the vortilon covers a smaller part of the wing when it is installed more outboard. The elimination of the region of erratic behavior is thought to be caused by the interaction of the vortilon 11 vortex and leading edge kink vortex. This results in an increased effectiveness of the outboard wing, in turn resulting in an outboard and aft shift of the aerodynamic center. As a result, the nose-down pitching moment is increased by the installation of vortilon 11.

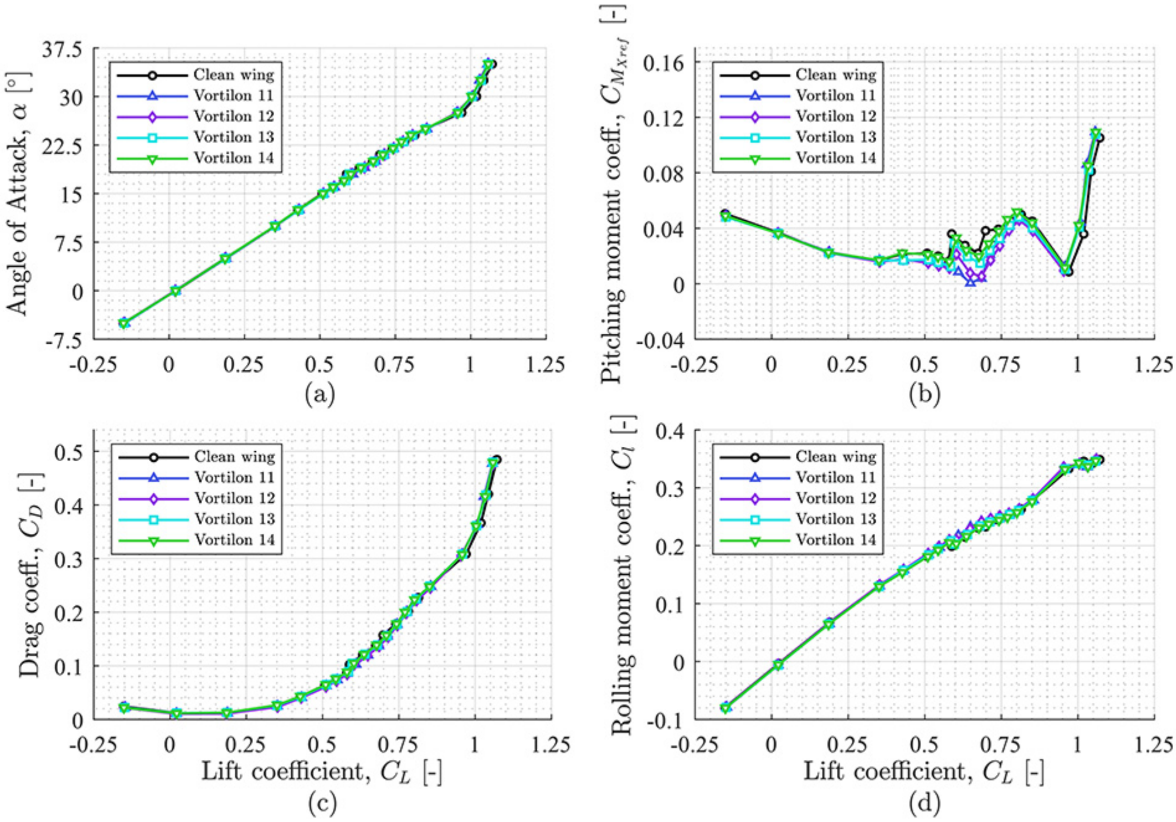

Figure 4.7: Aerodynamic coefficients of the clean Flying V wing with a vortilon at locations 11 to 14, results from W1

4.3. Fence Effects

In this section the effect of the addition of a fence to the wing of the Flying V will be discussed. The different spanwise locations of application are shown in Figure 2.3 and are numbered 1 to 4 from the root to the tip of the wing. The letter behind the number of the spanwise location represents different fence heights and lengths. Fences with a quarter chord length and height of $h = 0.5t$ are named a, with a quarter chord length and height of $h = 0.25t$ are named b, and with length equals local chord are named c. The latter may be used in combination with the first two, as in Figure 4.10. Fences are installed on the wing in clean configuration one at a time. In Figures 4.8 and 4.9 the aerodynamic coefficients of the Flying V with fence are shown.

In Figure 4.8 the aerodynamic characteristics of the Flying V equipped with a fence with height $h = 0.5t$ at spanwise location 1, 2 or 3 ($\eta = 0.19$, 0.40 and 0.51) are shown. Focusing on fence 1a and 2a, it is observed that for a lift coefficient of $C_L > 0.55$ the drag and pitching moment coefficient (Figure 4.8(c) and (b)) are increased compared to those of the clean wing. The unstable pitch break now occurs at $C_L = 0.55$ where the unstable pitch break experienced by the clean wing is observed at $C_L = 0.95$, see Figure 4.8(b). In the same lift coefficient range ($C_L > 0.55$), the installation of these fences results in the need for a greater angle of attack to reach the same lift coefficient as the clean wing, see Figure 4.8(a). Fence 3a shows a lesser influence on the lift and drag coefficient, however the pitching moment coefficient is still increased compared to that of the clean wing. Unlike fence 1a and 2a, which showed a great decrease in usable $C_{L_{\text{max}}}$, the installation of fence 3a results in a slightly lower unstable pitch break lift coefficient, $C_L = 0.90$, compared to the clean wings' $C_L = 0.95$. The rolling moment coefficient, see Figure 4.8(d), does not seem to be affected by the installation of either of the fences.

Fence 1 and 2 increase inboard vortex strength but promote vortex breakdown. This shifts the aerodynamic center inboard and forward which results in an increase in nose-up pitching moment. Because fence 3 is located more outboard, this fence has less influence on the inboard vortex. It still increases the nose-up pitching moment, but follows the trend of the clean wings' pitching moment coefficient quite closely.

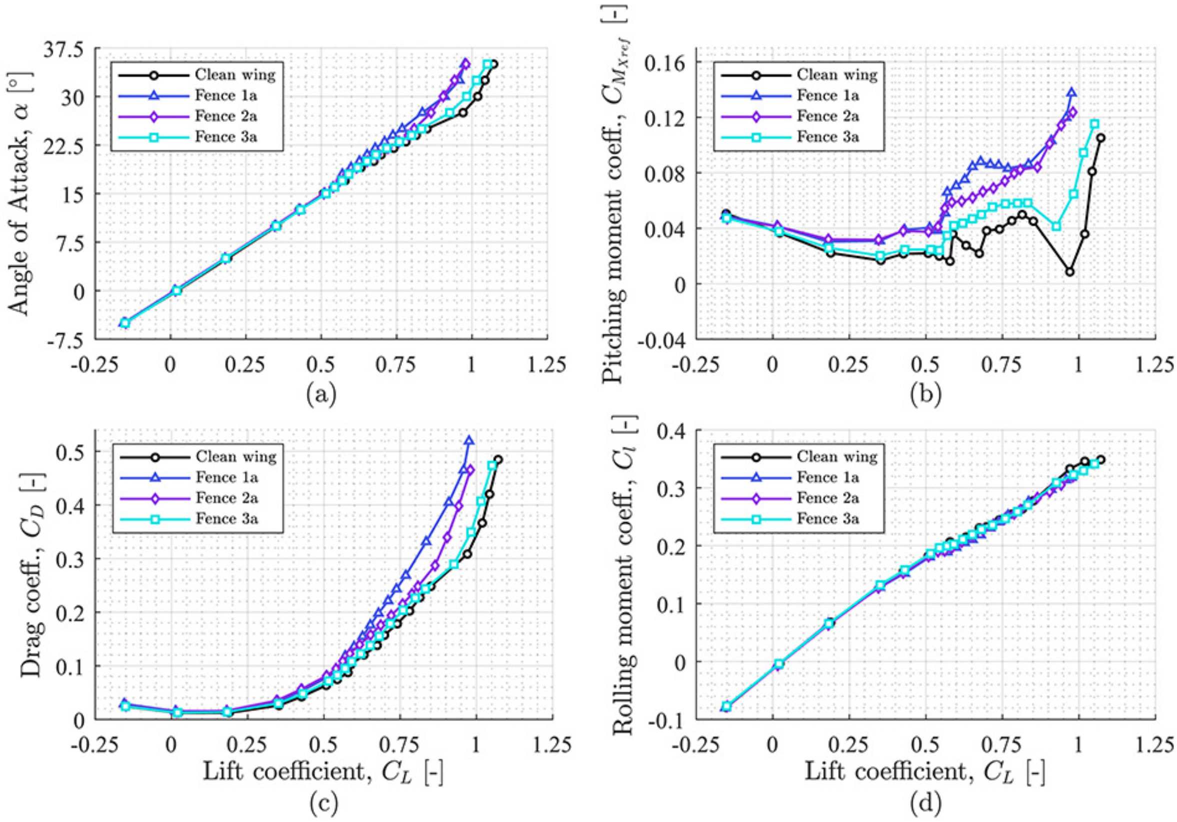

Figure 4.8: Aerodynamic coefficients of the clean Flying V wing with fence variation a at locations 1 to 3, results from W1

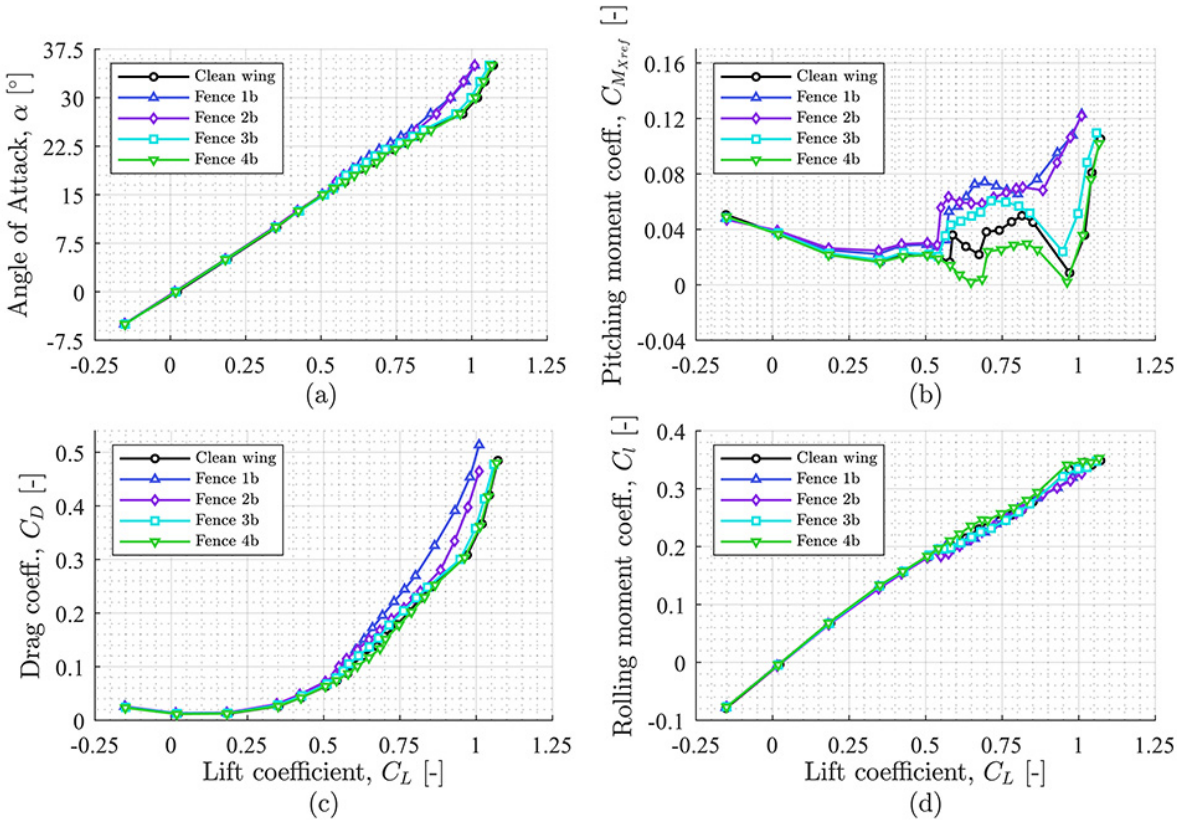

Figure 4.9: Aerodynamic coefficients of the clean Flying V wing with fence variation b at locations 1 to 4, results from W1

In Figure 4.9 the aerodynamic characteristics of the Flying V equipped with a fence with height $h = 0.25t$ at spanwise location 1, 2, 3 and 4 ($\eta = 0.19$, 0.40 , 0.51 and 0.63) are shown. The effect of the fences on the clean wings' pitching moment coefficient is shown in Figure 4.9(c). This figure shows that the installation of all fences, except for fence 4, increases the pitching moment coefficient for $C_L > 0.2$. Fence 4 follows the same trend as the clean wing up to a lift coefficient of $C_L = 0.55$. Between a lift coefficient of $C_L = 0.55$ and 0.96, fence 4 prevents the erratic behavior seen in the pitching moment curve of the clean wing. The pitching moment characteristic of fence 4 follows the same trend as the baseline, but at a lower absolute value of the pitching moment coefficient. In regards of the angle of attack with lift coefficient, shown in Figure 4.9(a), fence 4 follows the clean wings' curve over the whole range of lift coefficients. Fences at spanwise locations 1, 2 and 3 yield a lower lift coefficient at the same angle of attack as the baseline when the lift coefficient is higher than $C_L = 0.4$, 0.63 and 0.7 respectively. The same is trend is observed in Figure 4.9(b), where the drag coefficient with lift coefficient is shown. Again the application of fence 4 to the wing results in almost the same aerodynamic performance as the baseline. Fence 1 clearly deteriorates the aerodynamic performance of the Flying V wind tunnel model, increasing the drag with 40 counts at a lift coefficient of $C_L = 0.63$. This difference increases with increasing lift coefficient. The rolling moment of the baseline wing is not influenced by the application of fence 4 and up to a lift coefficient of $C_L = 0.74$ this holds for fence 2 and 3 as well, see Figure 4.9(d). At this lift coefficient the rolling moment coefficient slope suddenly flattens when fence 2 or 3 is installed, where that of the baseline and fence 4 are constant up to a lift coefficient of $C_L = 0.81$. The application of fence 1 results in a more linear rolling moment characteristic with respect to the clean wing. From a lift coefficient of $C_L = 0.35$ and higher, the rolling moment coefficient of wing plus fence 1 is lower than that of the baseline and all other fences.

Based on the observations made from Figure 4.9, the following hypotheses are formed. The elimination of the region of erratic behavior by fence 4 as seen in the pitching moment coefficient between $C_L = 0.55$ and 0.70, is thought to be the results of increased vortex strength of the kink vortex over the outboard wing. This results in an aft shift in aerodynamic center location for that specific C_L-region. For a lift coefficient between $C_L = 0.80$ and 0.95, the vortices on the inboard wing strengthen. This results in an inboard and forward movement of the aerodynamic center. Between $C_L = 0.85$ and 0.95 the vortex generated by the leading edge kink and fence 4 increases in strength, moving the aerodynamic center outboard and aft, before breaking down at $C_L = 0.95$. This increases the nose-down pitching moment as well as the rolling moment.

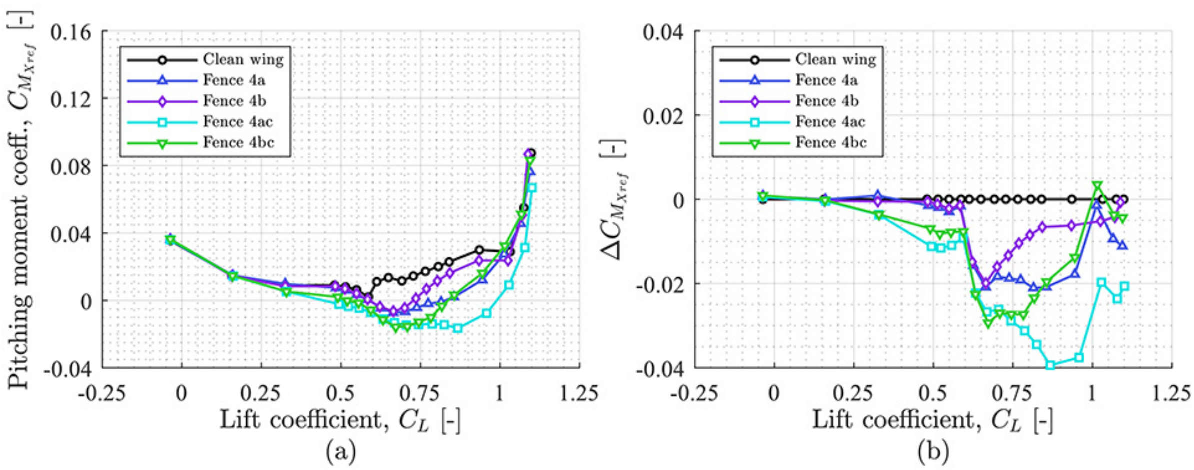

Figure 4.10: Pitching moment coefficient (a) and delta with respect to clean wing (b) of four fence 4 designs

In Figure 4.10(a) the pitching moment coefficient for all fence 4 designs is presented. It can be seen that all designs of fence 4 prevent the sharp break in the pitching moment coefficient curve of the clean wing at $C_L = 0.54$. Application of each fence results in the same trend of the pitching moment coefficient. The slope of the pitching moment coefficient curve is strongly negative, after which a more gradual decrease of pitching moment coefficient is observed, which in turn is followed by a dip in pitching moment coefficient, reaching the minimum absolute value over the whole range of lift coefficients, before the pitching moment starts to increase irrecoverably. However, the lift coefficient where this break is observed, depends on which version of fence 4 is installed. For both fence 4a, fence 4b and fence 4bc, the break occurs at $C_L = 0.7$. The installation of fence 4b and fence 4bc results in the same positive gradient after the break, but the absolute value of the pitching moment is lower when the fence spanning the total local chord is installed than when the part chord fence is installed. The installation of the fence spanning the total local chord and with height $h = 0.5t$, fence 4bc, results in a postponement of the break in pitching moment coefficient, which eventually occurs at $C_L = 0.87$. For all lift coefficients lower than $C_L = 0.87$, the installation of last mentioned fence results in a negative pitching moment coefficient gradient with lift coefficient.

In Figure 4.10(b) the difference in pitching moment coefficient characteristic between the four fence designs is expressed as $\Delta C_{M_{\text{xref}}}$, with respect to the clean wing. The most interesting that can be observed is that between $C_L = 0.63$ and $C_L = 1$ fence 4b and fence 4bc seem to have an almost equal effect on the pitching moment coefficient of the Flying V wind tunnel model. An outlier is fence 4ac, which for $C_L > 0.75$ decreases the pitching moment coefficient of the Flying V a lot more than all other fences. This confirms the expectation that this fence affects the pitching moment coefficient most.

4.4. Combined Trip Strip and Vortilon Effects

In this section the effect of the addition of a vortilon to the strip-on configuration of the Flying V is discussed. The strip-on configuration is shown in Figure 2.1, the spanwise location of the vortilons in Figure 2.5 and the results of the wind tunnel measurements of the Flying V in strip-on configuration equipped with vortilons in Figures 4.11 to 4.14. For all measurements the vortilons are installed one at a time.

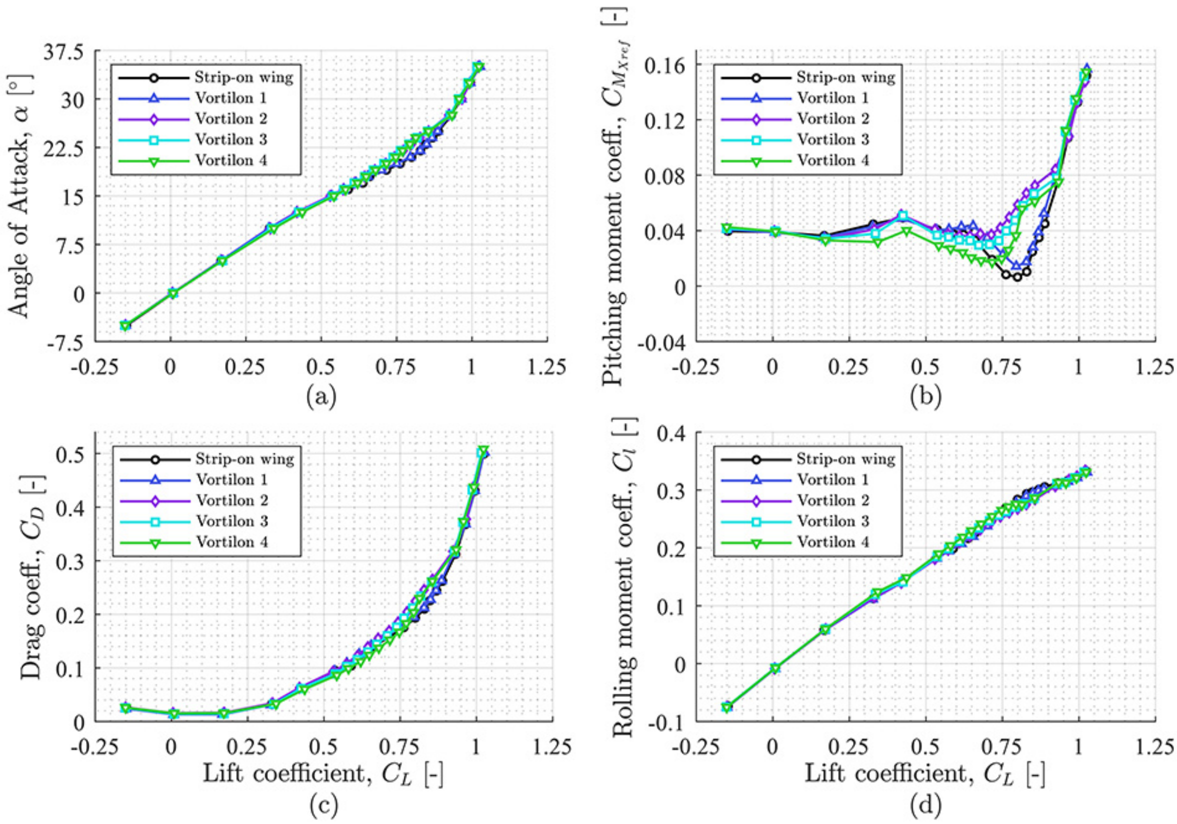

Figure 4.11: Aerodynamic coefficients of the Flying V wing in strip-on configuration with vortilons at locations 1 to 4

In Figure 4.11 the aerodynamic coefficients of the Flying V in strip-on configuration with a vortilon at spanwise locations 1 to 4 ($\eta = 0.07$ to 0.27) are shown. First in Figure 4.11(a), it is observed that apart from vortilon 1 all vortilons results in slightly more linear lift coefficient curve than that of the clean wing for $C_L = 0.55$ to 0.95. Second, the pitching moment coefficients are shown in Figure 4.11(b).

Again the vortilons at locations 2 to 4 show a greater effect than vortilon 1. Vortilons 2, 3 and 4 shift the unstable pitch break of the strip-on wing from $C_L = 0.80$ to $C_L = 0.70$, thus decreasing the usable $C_{L_{\text{max}}}$. However, up to that lift coefficient vortilon 4 results in a more linear nose-down pitching moment coefficient curve compared to the strip-on wing. Vortilons 2, 3 and 4 result in a slightly increased drag coefficient between $C_L = 0.55$ and 0.95, where vortilon 1 does not seem to influence the drag coefficient characteristic, see Figure 4.11(c). Finally in Figure 4.11(d) the rolling moment coefficient is shown. Only a small difference can be observed between $C_L = 0.80$ and 0.90, where vortilons 2, 3 and 4 slightly decrease the rolling moment coefficient compared to the strip-on and vortilon 1 cases.

Comparing the effect of these vortilons on the clean (Figure 4.4) and strip-on (Figure 4.11) wing it is observed that these vortilons affect the aerodynamic coefficients more when they are installed on the strip-on wing. It is suspected that due to the trip strips the flow over the wing is more attached, where on the clean wing vortices are formed at lower lift coefficients. As these vortilons result in small disturbances, they will only affect the flow when their effect is stronger than other flow phenomena on the wing. When the flow is attached, the vortex originating from the vortilon seems strong enough to influence the flow over the wing.

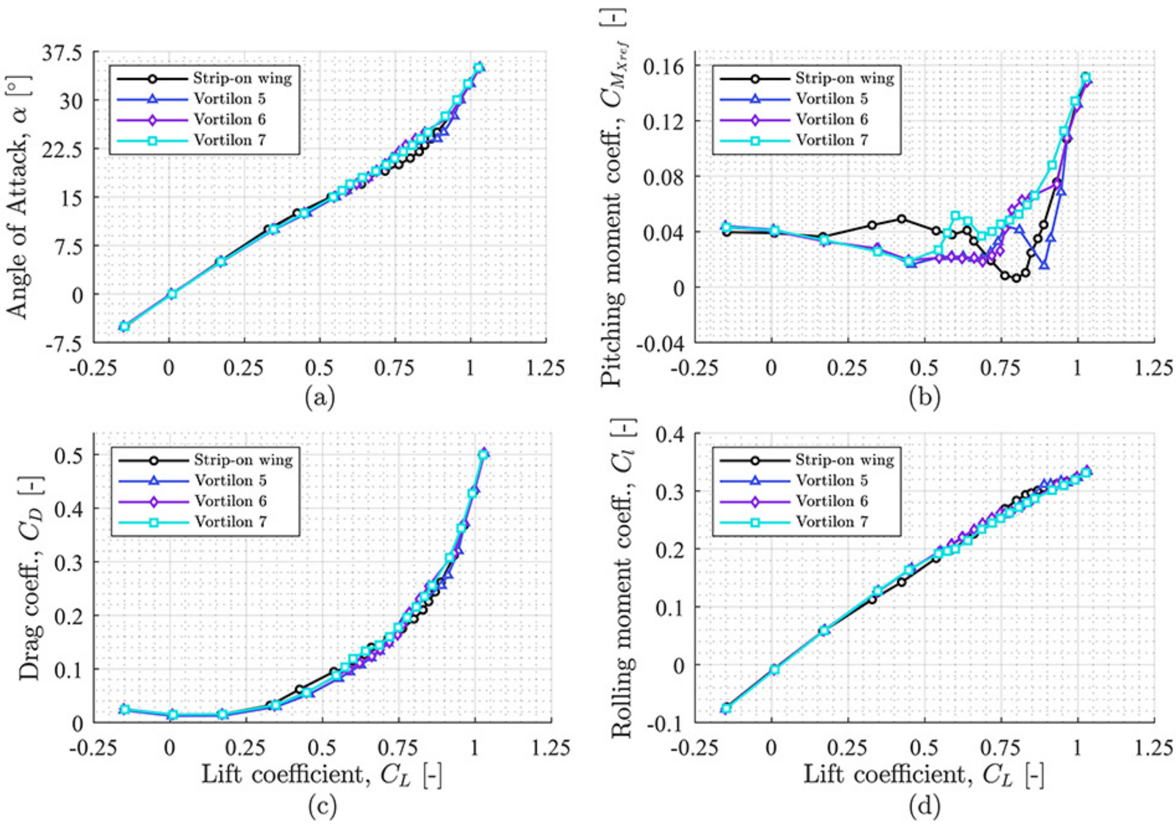

Figure 4.12: Aerodynamic coefficients of the Flying V wing in strip-on configuration with vortilons at locations 5 to 7

The lift coefficient characteristic of the vortilon 5, 6 and 7 ($\eta = 0.33$ to 0.47) cases, shown in Figure 4.12(a), is more linear compared to the strip-on wing lift coefficient characteristic. A difference between vortilon 5 and vortilon 6 is visible at $C_L = 0.75$, where the lift coefficient gradient of vortilon 5 suddenly increases. At $C_L = 0.90$ and greater, the lift coefficient of the strip-on wing equals that of the vortilon 5 and 6 cases. Looking at Figure 4.12(b), the pitching moment coefficient with lift coefficient for the Flying V wing in strip-on configuration and the vortilons is shown. In the region from $C_L = -0.15$ to 0.45, the pitching moment coefficient slope is more negative for all wing plus vortilon combinations than the slope of the strip-on wing. On top of that, the increase in pitching moment coefficient of the strip-on case is prevented by installation of each of the three vortilons. For $C_L > 0.45$ the pitching moment coefficient of the vortilon 7 case suddenly increases, rendering that add-on less interesting in this research. Vortilon 5 and 6 however, yield an almost constant value for the pitching moment coefficient from $C_L = 0.45$ to 0.70. Both the vortilon 5 and 6 pitching moment coefficients increase sharply, but at $C_L = 0.75$ the pitching moment coefficient gradient of wing plus vortilon 5 changes from strongly positive to strongly negative until the pitching moment coefficient increases irrecoverably at $C_L = 0.90$. The strip on wing has a usable maximum lift coefficient of $C_{L\max} = 0.80$. The installation of vortilon 5 results in a usable $C_{L\max}$ of 0.45, the installation of vortilon 6 in a usable $C_{L\max}$ of 0.75 and the installation of vortilon 7 in a usable $C_{L\max}$ of 0.90. Shifting to Figure 4.12(c), the drag coefficient of the strip-on wing with vortilons is shown. It is observed that between $C_L = 0.30$ and 0.75 all three vortilons result in a decrease in drag coefficient. Between $C_L = 0.75$ and 0.95 installation of the vortilons results in an increase in drag coefficient. Up to a lift coefficient of $C_L = 0.75$ vortilon 7 follows the strip-on wings' drag coefficient most closely compared to the other two. For $C_L > 0.75$ vortilon 5 follows the drag coefficient characteristic of the strip-on wing most closely. In Figure 4.12(d) the rolling moment coefficient is shown. It can be observed that the installation of each of the vortilons results in a more linear rolling moment coefficient characteristic.

Based on the wind tunnel measurements, literature[23] and previous research into the Flying V [15], it is suspected that the vortilons presented in Figure 4.12 form a vortex that interacts with the vortex on the inboard part of the wing. All three vortilons delay the formation of the inboard vortex up to lift coefficient of $C_L = 0.45$ by producing a counter-rotating vortex. The vortex produced by vortilon 5 and 6 however, seems to affect the inboard vortex up to a lift coefficient of $C_L = 0.70$. These vortices result in an aft movement of the aerodynamic center, which in turn leads to a smaller pitching moment coefficient compared to the strip-on wing. After these lift coefficients, the vortilon vortex strengthens the inboard vortex. This results in an forward movement of the aerodynamic center and therefore an increase in pitching moment coefficient.

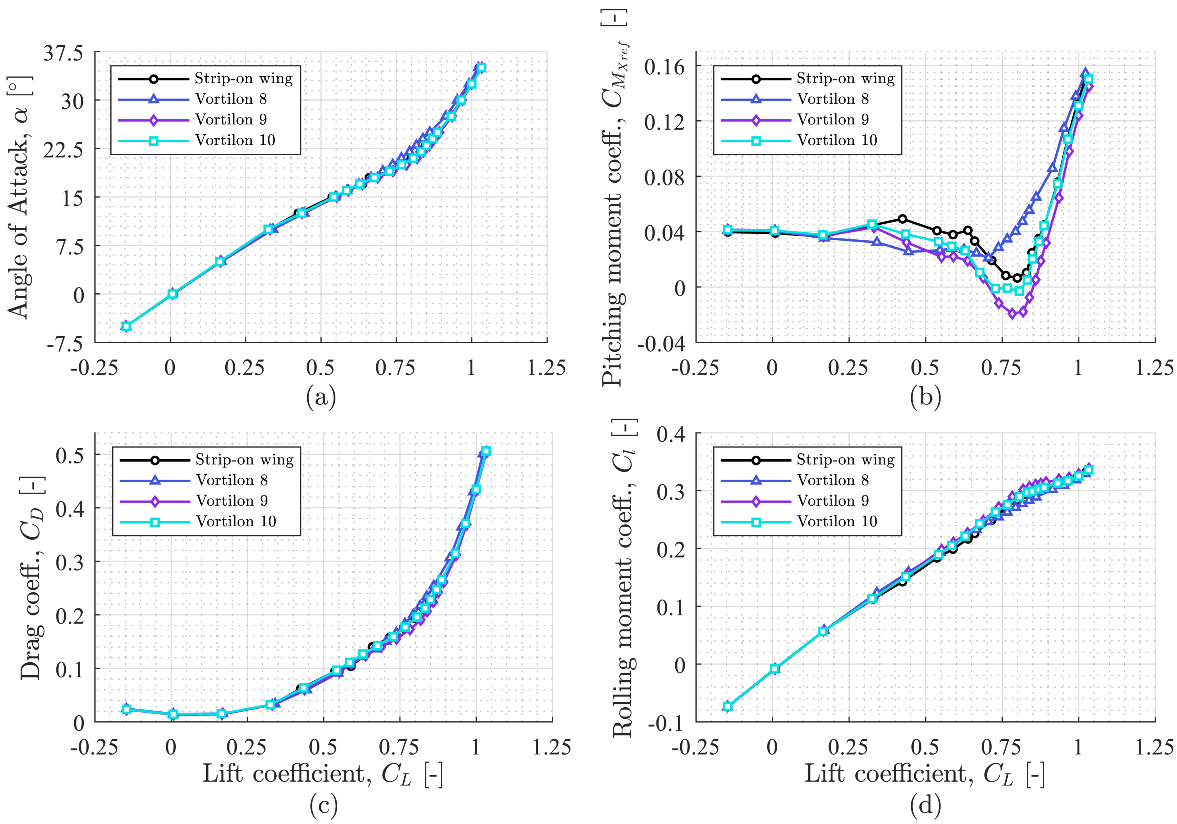

Figure 4.13: Aerodynamic coefficients of the Flying V wing in strip-on configuration with vortilons at locations 8 to 10

As with the results for vortilons 8, 9 and 10 ($\eta = 0.54$ to 0.67) installed on the clean wing, see Figure 4.6, installing the same vortilons on the strip-on wing has little to no effect on the lift, and drag coefficient, see Figure 4.13(a,c). However, the pitching moment coefficient of the strip-on wing is subject of change when vortilon 8, 9 or 10 is installed. From Figure 4.13(b) it is observed that all three vortilons increase the nose-down pitching moment. Vortilon 8 decreases the pitching moment coefficient of the strip-on wing from $C_L = 0.15$ to 0.70 but the unstable pitch break now occurs at

$C_L = 0.70$ instead of $C_L = 0.80$ for the strip-on wing. Vortilon 9 and 10 increase the nose-down pitching moment for $C_L > 0.30$ and the unstable pitch break occurs at the same lift coefficient as that of the clean wing. The increased nose-down pitching moment coefficient in the vortilon 8 and 9 cases corresponds with an increased rolling moment coefficient compared to the strip-on wing, see Figure 4.13(d).

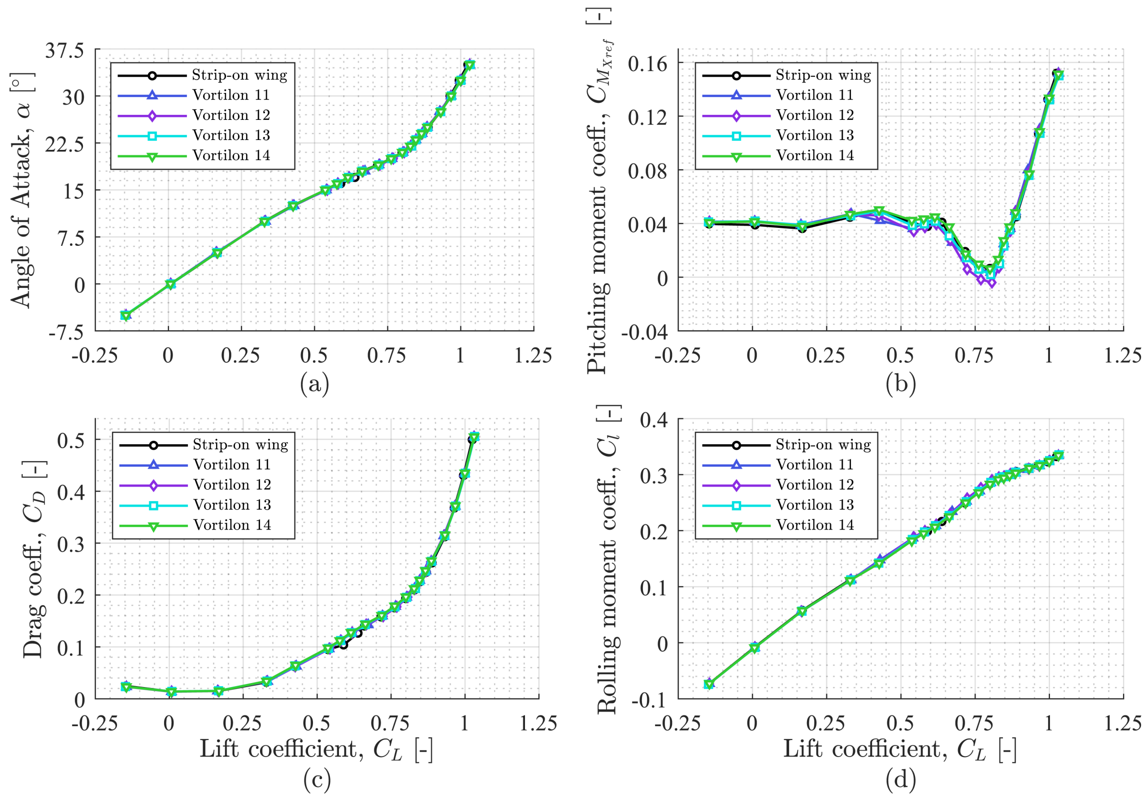

Figure 4.14: Aerodynamic coefficients of the Flying V wing in strip-on configuration with vortilons at locations 11 to 14

As expected from the clean wing results for vortilons 11 to 14 ($\eta = 0.74$ to 0.94), see Figure 4.7, installing these vortilons on the strip-on wing, see Figure 4.14 has no effect on the aerodynamic coefficients of the Flying V. It is thought that the size of the vortilons was too small to have any effect on the flow over the wing.

4.5. Combined Trip Strip and Fence Effects

In this section the effect of the addition of a fence to the strip-on configuration of the Flying V wind tunnel model will be discussed. The strip-on configuration is shown in Figure 2.1, the spanwise location of the vortilons in Figure 2.5 and Figures 4.15 and 4.16 show the results of the wind tunnel measurements of the Flying V wing in strip-on configuration equipped with fences. Flow visualisation pictures are included in Figure 4.17 and a comparison between the installation of fence 4 on the clean- and strip-on wing is shown in Figure 4.18.

In Figure 4.15 the aerodynamic characteristics of the strip-on Flying V equipped with a fence with height $h = 0.5t$ at spanwise location 1, 2 and 3 are shown. Installing fence 1, 2 or 3 on the strip-on wing results in different effects than when these fences are installed on the clean wing (Figure 4.8), but the effect is the same for the lift and drag coefficient characteristic, see Figure 4.15(a,c). When installed on the clean wing, all fences resulted in an increased nose-up pitching moment. Fence 2 and 3 on the strip-on wing result in an increase in nose-down pitching moment between $C_L = 0.35$ and 0.70, see Figure 4.15(b). Another difference with respect to the clean wing with fences is a change in rolling moment coefficient between the strip-on wing and the strip-on wing with a fencea, see Figure 4.15(d). The installation of fence 1 shows the most pronounced effect, reducing the rolling moment of the strip-on wing between $C_L = 0.70$ and 0.95. The installation of fence 2 and 3 reduces the rolling moment coefficient of the strip-on wing between $C_L = 0.80$ and 0.95.

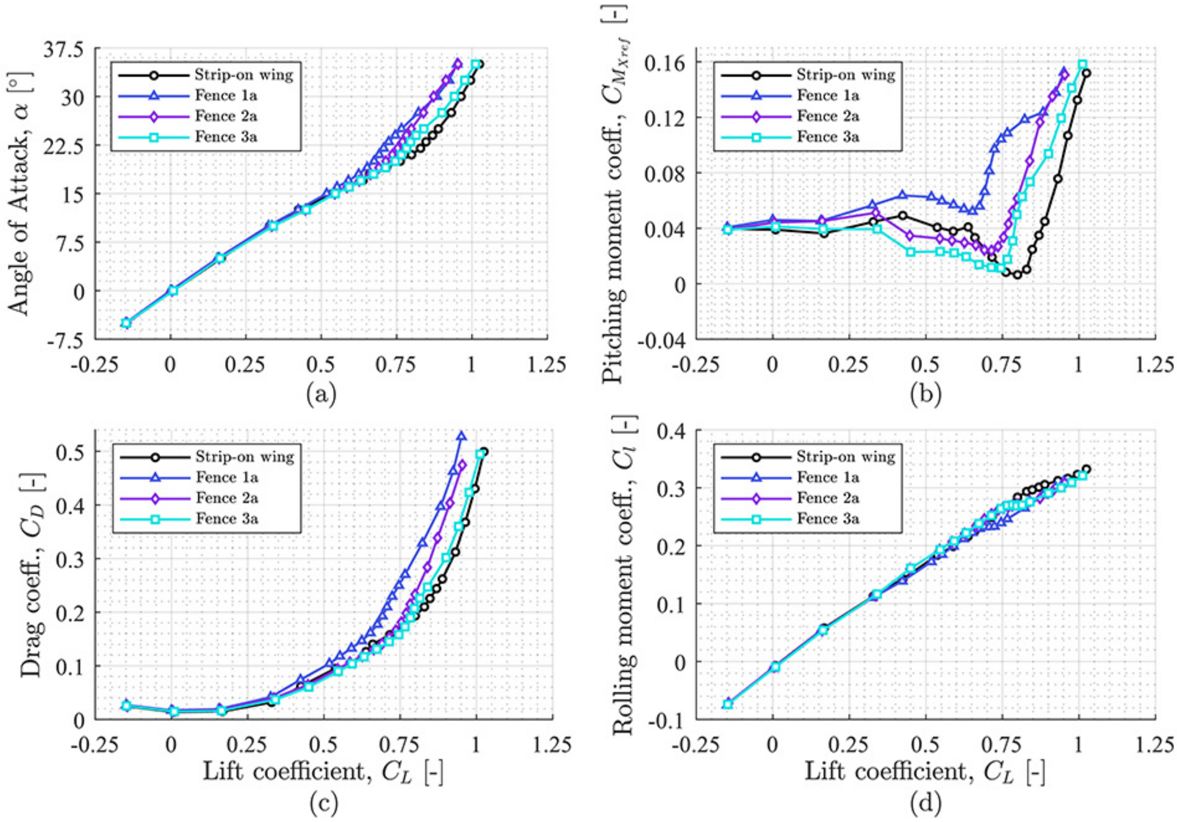

Figure 4.15: Aerodynamic coefficients of the Flying V in strip-on configuration with fence variation a

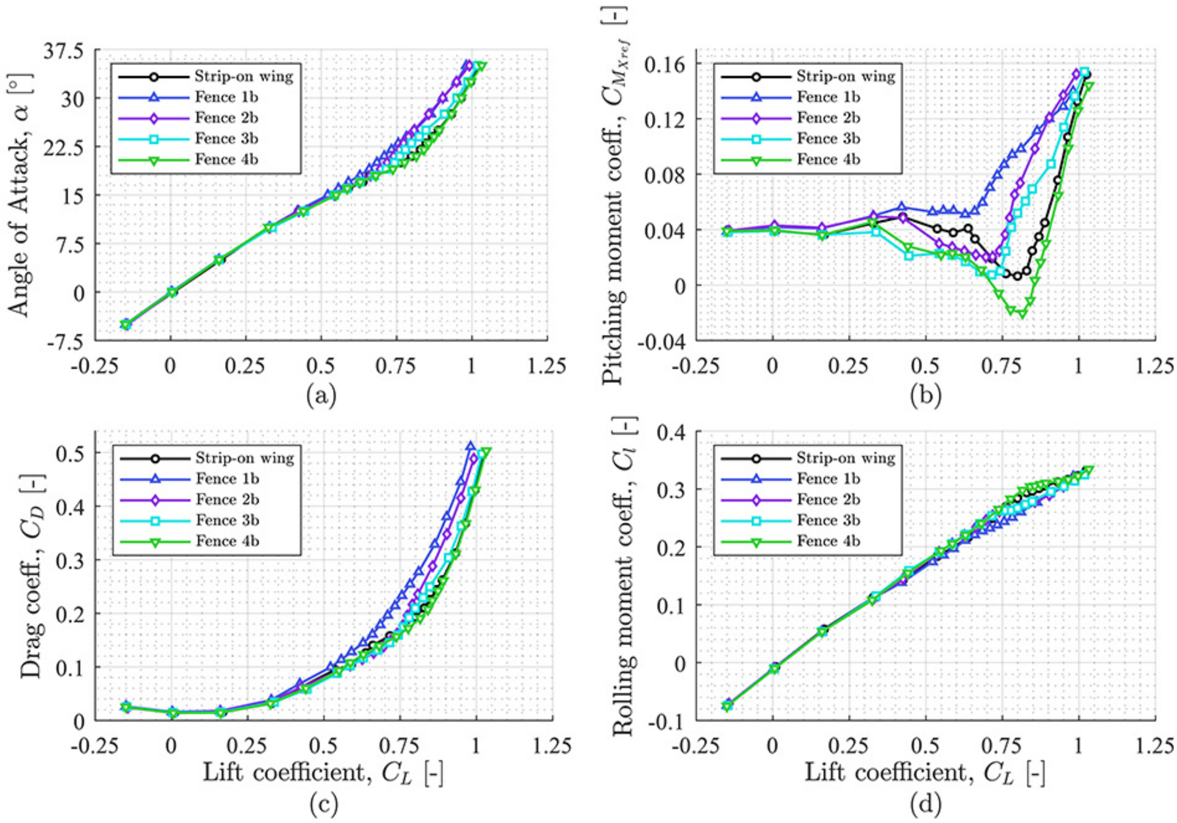

Figure 4.16: Aerodynamic coefficients of the Flying V in strip-on configuration with fence variation b

In Figure 4.16 the effects of fences with height $h = 0.25t$ at locations 1 to 4 on the aerodynamic coefficients of the strip-on Flying V are shown. In Figure 4.16(b), the pitching moment coefficient characteristics can be seen. The baseline, the wing in strip-on configuration, as well as all fence cases except for fence 3, exhibit a sudden increase in pitching moment coefficient curve slope at $C_L = 0.20$, where both fence 3 and 4 drop off in a steep manner at $C_L = 0.35$. Fence 2 shows the same drop off in pitching moment coefficient, but at $C_L = 0.40$, where at the same lift coefficient the pitching moment coefficient of the strip-on wing and fence 1 decrease in a more gradual manner. Where the strip-on wing results show a wobble around $C_L = 0.65$, fence 2 decreases with constant gradient but departs earlier than the strip-on wing. The pitching moment coefficient behavior of fence 3 is similar to that of the strip-on wing, however the absolute value is lower up to $C_L = 0.75$. The pitching moment coefficient behavior of fence 4 is similar to that of the strip-on wing and also lower in absolute value. However, the pitching moment departs at the same lift coefficient as that of the strip-on wing, at $C_L = 0.80$. The lift coefficient curve with angle of attack is more linear for all fence results except for fence 4. As can be seen in Figure 4.16(a), this results in a loss of lift coefficient at the higher angles of attack for fence 1, 2 and 3. The lift coefficient with angle of attack for fence 4 follows the strip-on wing curve. The same trend is seen in terms of drag coefficient, see Figure 4.16(c), where the fence 4 results are almost equal to the strip-on wing. A standout is fence 1, with a significant higher drag coefficient compared to that of the strip-on wing. In terms of rolling moment, see Figure 4.16(d), again fence 4 yields the same results as the strip-on wing. Especially fence 1 and to some extend fence 2 and 3 show a lower rolling moment coefficient at higher lift coefficients, $C_L > 0.63$, than the strip-on wing.

Based on the wind tunnel measurements, it is thought that fence 3b and 4b start to develop a vortex at a lift coefficient of $C_L = 0.30$. These fence vortices result in increased lift on the outboard wing, shifting the aerodynamic center aft. This results in a lower pitching moment coefficient, see Figure 4.16(b), compared to the strip-on wing up to a lift coefficient of $C_L = 0.75$ for fence 3b and for all lift coefficients for fence 4b. The slightly higher rolling moment coefficients for fence 3b and 4b at these lift coefficients confirm this theory, see Figure 4.16(d).

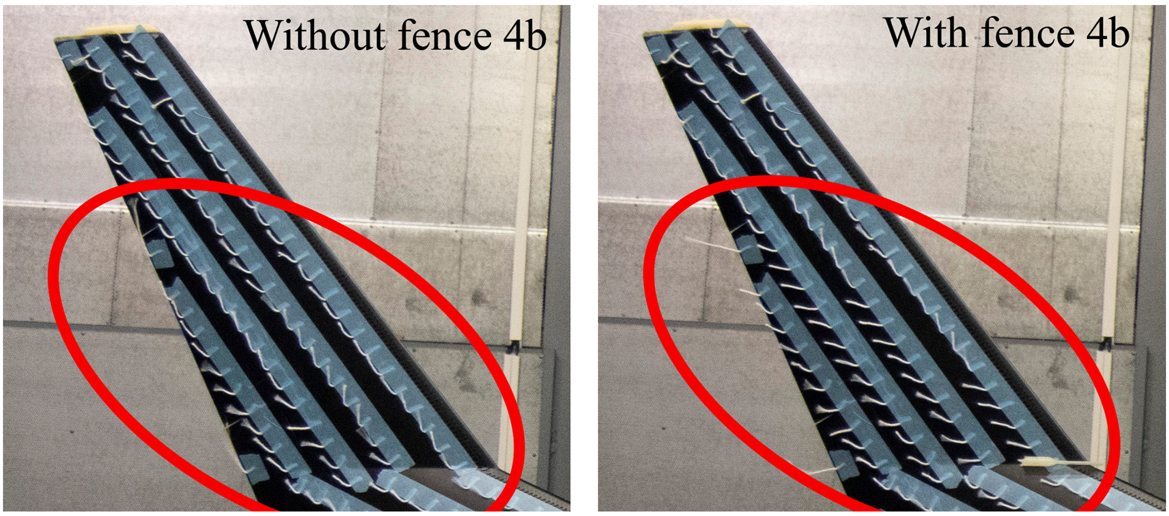

Figure 4.17: Tuft comparison of outboard wing in strip-on configuration without (left) and with (right) fence 4b at $C_L = 0.53$ and $\alpha = 15°$

Zooming in on the effect of fence 4b, tufts are applied to the wing to visualize the flow over the surface of the wing, see Figure 4.17. It is clear that when fence 4b is attached to the strip-on wing, a clean boundary layer is established and cross-flow is almost eliminated. This results in an increase in lift coefficient on the outboard wing, compared to the strip-on wing. Because this increase in lift lies aft of the center of gravity of the wing, the pitching moment is smaller for the strip-on wing with fence 4b, which indeed can be seen in Figure 4.16(b). However, the trend of both strip-on wing and the strip-on wing plus fence 4 are very similar, suggesting flow phenomena over other parts of the wing also influence the pitching moment coefficient.

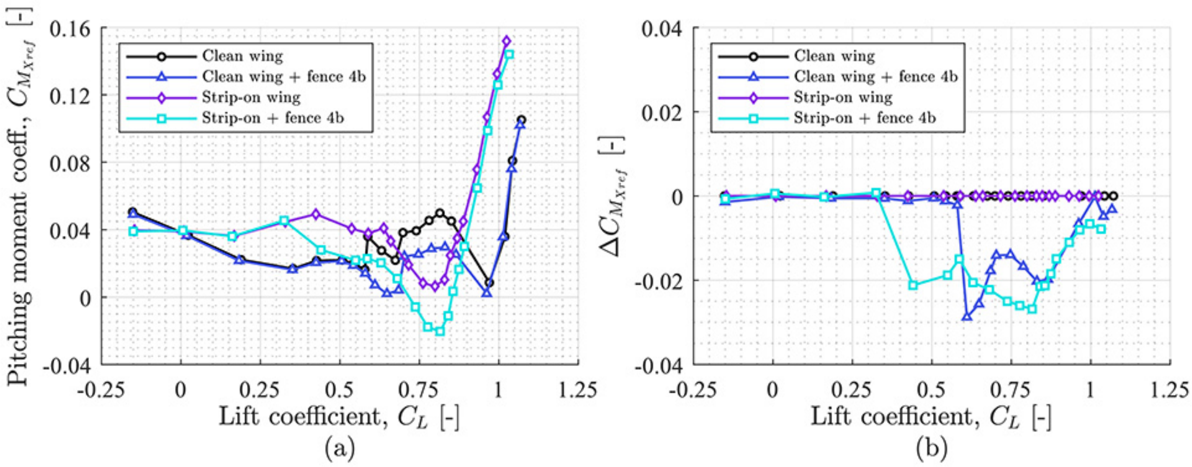

Figure 4.18: Influence of trip strips on fence 4b effect on pitching moment coefficient (a), and delta with respect to clean- and strip-on wing, respectively (b)

Looking at the $\Delta C_{M_{\text{xref}}}$-plot of Fence 4b for its two respective baselines, see Figure 4.18(b), it can be observed that when the trip strips are applied to the wing, fence 4b becomes more effective in lowering the pitching moment coefficient. Furthermore, fence 4b either has a neutral or positive effect on the pitching moment coefficient of the Flying V wind tunnel model.

5 Conclusions & Recommendations

This research has been performed with the ultimate goal of postponing the unstable pitch break to increase the usable $C_{L_{\text{max}}}$ of the Flying V. In order to achieve this goal, the effect of the presence of a trip strip as well as the position and size of vortilons and fences has been investigated.

5.1. Conclusion

The application of trip strips to the pressure and suction side of the wing results in a neutral pitching moment coefficient curve slope from $C_L = -0.15$ to 0.65 compared to a negative slope for the clean wing. The application of trip strips reduces the usable $C_{L_{\text{max}}}$ from $C_L = 0.95$ to 0.80. However, improvement in surface flow was observed on the outboard wing ($\eta > 0.63$) when the trip strips were applied. Therefore, trip strips should only be applied on the outboard wing of the Flying V.

The experiments on positioning of the vortilons clarifies that the most effective locations for vortilon placement are spanwise locations 9 and 10, $\eta = 0.60$ and 0.67 respectively. Locations 9 and 10 are located before and after the leading edge kink in spanwise direction. Vortilons placed at those locations showed improvement in pitching moment coefficient characteristic between $C_L = 0.70$ and 0.95 and $C_L = 0.55$ and 0.70 respectively, without postponing the unstable pitch break. When the trip strips and a vortilon are combined, the most effective spanwise location to install a vortilon changes to $\eta = 0.33$, 0.40 and 0.47. Installation of either of these vortilons results in a negative pitching moment coefficient curve slope, compared to a neutral slope of the strip-on wing. For vortilons at spanwise locations 5 and 6 ($\eta = 0.33$ and 0.40) this effect is observed between $C_L = -0.15$ and 0.70 and for a vortilon at spanwise location 7 ($\eta = 0.47$) between $C_L = -0.15$ and 0.45. Installing a vortilon at locations 6 and 7 reduces the usable $C_{L_{\text{max}}}$ to 0.70 and 0.45, respectively. The installation of a vortilon at location 5 postpones the unstable pitch break and as a result increases the usable $C_{L_{\text{max}}}$ to 0.90.

The most effective spanwise location to install a fence is found to be location 4, where $\eta = 0.63$. Placing a fence at spanwise location 4, coinciding with the leading edge kink, postpones the unstable pitch break and reduces the absolute value of the pitching moment coefficient in general. A fence twice as high elongates it's positive effect on the pitching moment coefficient to a 0.35 higher lift coefficient. A fence spanning from leading edge to trailing edge on the suction surface results in a near constant negative pitching moment coefficient curve slope. Next to that advantage, this fence prevents the abrupt unstable pitch break making the increase in pitching moment coefficient gradual and predictable. It is recommended to install this fence (fence 4ac) on the Flying V. The combination of the trip strips and a fence results in a decreased pitching moment coefficient, depending on the spanwise location the fence is installed in. The installation of a fence at locations 2, 3 and 4 ($\eta = 0.40$, 0.51 and 0.63) results in a decreased pitching moment coefficient between $C_L = 0.45$ and 0.70, $C_L = 0.35$ and 0.75 and $C_L > 0.15$, respectively. However, the installation of a fence in location 1 ($\eta = 0.19$) reduces the usable $C_{L_{\text{max}}}$ to 0.65, the installation of a fence in location 2 and 3 reduces the usable $C_{L_{\text{max}}}$ to 0.70 and the installation of a fence in location 4 has no influence on the usable $C_{L_{\text{max}}}$ when combined with the trip strips.

5.2. Recommendations

The present study has resulted in new insights in the effect of trip strips, vortilons and fences on the Flying V and ways to improve the aerodynamic characteristics of the Flying V. During this study several factors were found that could be improved to increase the confidence in wind tunnel measurement data. First, the main improvement lies in a redesign of the wind tunnel setup. Reference angles for angle of attack, yaw angle and roll angle of the model should be added in such a way they can be achieved every time the experiment is setup. Second, the position and orientation in which the the wind tunnel model is installed on the wind tunnel setup should be fixed, to guarantee aforementioned angles. Third, the rotating table motor is controlled in such a way that a vibration is observed during balance measurements. This should be solved. Fourth and last, the current setup is prone to play in several parts. The redesign should focus on a setup that is rigid and stiff from wind tunnel floor or jet to wind tunnel model, and everything in between.

Furthermore, based on the results found in this study several topics for future work are identified:

- A set of wind tunnel experiments to determine the change in flow around the Flying V for a full span model compared to the half span model
- Investigation of the effect of a combination of add-ons on the flow around and aerodynamic characteristics of the Flying V. Based on the present study a combination of fence x and x, vortilon x and fence x or vortilon x and vortilon x is suggested
- Investigation of the effect of a different sized and/or shaped trip strip on the suction and/or pressure side of the outboard wing
- Investigation of the effect of a change in size and orientation of the vortilons, especially on the outboard wing
- Investigation of the effect of a suction surface only fence compared to a fence wrapped around the leading edge
- As the leading edge kink was found to be the most interesting region regarding influence on pitching moment coefficient, research into kink smoothing or otherwise changing the shape of the leading edge kink would be worthwhile

Bibliography

[1] Palermo, M., "The Longitudinal Static Stability and Control Characteristics of a Flying V Scaled Model," Tech. rep., Delft University of Technology, 2019.

[2] Ruiz Garcia, A., "Aerodynamic Model Identification of the Flying V using Wind Tunnel Data," Tech. rep., Delft University of Technology, 2019.

[3] van Empelen, S. A., "Engine Integration of the Flying V," Tech. rep., Delft University of Technology, 2020.

[4] EEA, "European aviation environmental report 2019," Tech. rep., 2019.

[5] Clean Sky, "Welcome to the Clean Sky | Clean Sky," .

[6] Future Sky, "Future sky," , 2020.

[7] Horizon 2020, "The EU Framework Programme for Research and Innovation," in "Report of Pres. Barroso's Science and Technology Advisory Council (STAC) : The Future of Europe is science - October 2014," p. 159, 2014, doi:10.2777/3719.

[8] Airbus, "ZEROe - Hydrogen - Airbus," , 2020.

[9] AirBus, "E-Fan X - Electric flight - Airbus," , 2020.

[10] Airbus, "Imagine travelling in this blended wing body aircraft - Innovation - Airbus," , 2020.

[11] Website, T. D. F.-V., "https://www.tudelft.nl/lr/flying-v/," .

[12] Liebeck, R. H., Page, M. A., and Rawdon, B. K., "Blended-Wing-Body subsonic commercial transport," in "36th AIAA Aerospace Sciences Meeting and Exhibit," American Institute of Aeronautics and Astronautics Inc, AIAA, 1998, doi:10.2514/6.1998-438.

[13] Benad, J., "a New Aircraft Configuration for Commercial Passenger Transport," in "Deutscher Luft- und Raumfahrtkongress," , 2015, pp. 1–8, doi:http://dx.doi.org/10.1016/S0140-6736(17)32758-7.

[14] Faggiano, F., "Aerodynamic Design of a Flying V Aircraft," Tech. rep., TU Delft, 2016, doi:10.2514/6.2017-3589.

[15] Viet, R. A., "Analysis of the flight characteristics of a highly swept cranked flying wing by means of an experimental test," Tech. rep., Delft University of Technology, 2019.

[16] Palermo, M. and Vos, R., "Experimental Aerodynamic Analysis of a 4.6%-Scale Flying-V Subsonic Transport," in "AIAA Scitech 2020 Forum," American Institute of Aeronautics and Astronautics (AIAA), Delft, 2020, doi:10.2514/6.2020-2228.

[17] Walker, M. M. and Bons, J. P., "The Effect of Passive and Active Boundary-Layer Fences on Swept-Wing Performance at Low Reynolds Number," in "2018 AIAA Aerospace Sciences Meeting," American Institute of Aeronautics and Astronautics, Reston, Virginia, January, 2018, pp. 1–15, doi:10.2514/6.2018-0793.

[18] Nickel, K. and Wohlfahrt, M., *Tailless Aircraft in Theory and Practice*, AIAA inc., Washington DC, 1994.

[19] Solfelt, D. A. and Mapley, R. C., "CFD analysis of a T-38 wing fence," in "46th AIAA Aerospace Sciences Meeting and Exhibit," AIAA inc., Reno, Nevada, January, 2008, doi:10.2514/6.2008-331.

[20] Buchholz, M. D. and Tso, J., "Lift Augmentation on Delta Wing with Leading-Edge Fences and Gurney Flap," *Journal of Aircraft*, Vol. 37, No. 6, 2000, pp. 1050–1057, doi:10.2514/2.2710.

[21] Rao, D. M. and Johnson, T. D. J., "Subsonic Pitch-Up Alleviation on a 74 Deg. Delta Wing," Tech. rep., 1981.

[22] Hummel, D., "Effects of Boundary Layer Formation on the Vortical Flow above Slender Delta Wings," in "RTO AVT Specialists' Meeting on "Enhancement of NATO Military Flight Vehicle Performance by Management of Interacting Boundary Layer Transition and Separation," NATO, Prague, Czech Republic, October, 2004, pp. 4–7.

[23] Phillips, E., Taubert, L., Wygnanski, I., and Menge, M., "Passive and Active Leading Edge devices on a simple swept back wing," in "AIAA Aviation Forum," AIAA inc., Dallas, Texas, June, 2019, pp. 1–18, doi:10.2514/6.2019-3393.

A

Tuft Flow Visualization Photos

In this appendix all tuft flow visualizations can be found. All flow visualizations are carried out at a wind speed of $V = 18.7$ m/s and for angles of attack $\alpha = [10, 15, 17.5, 20, 22, 25, 30]$. Flow visualizations are carried out for the following cases:

- The clean wing
- The strip-on wing
- The strip-on wing with:
  - Fence 1a
  - Fence 1b
  - Fence 4b
  - Fence 1b and fence 4b combined
  - Vortilon 2
  - Vortilon 8
  - Vortilon 9
  - Vortilon 2 and vortilon 9 combined

A.1. Clean Wing

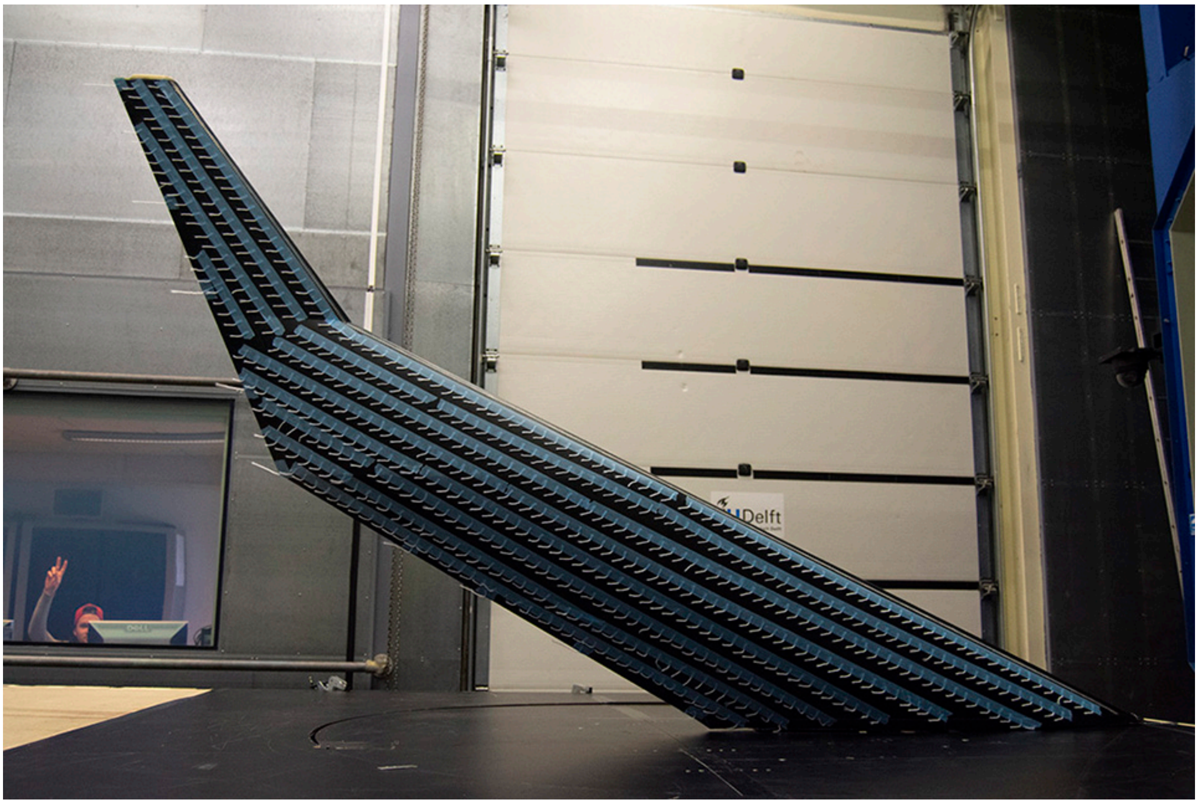

Figure A.1: Clean wing at $\alpha = 0^{\circ}$ and $V = 18.7$ m/s

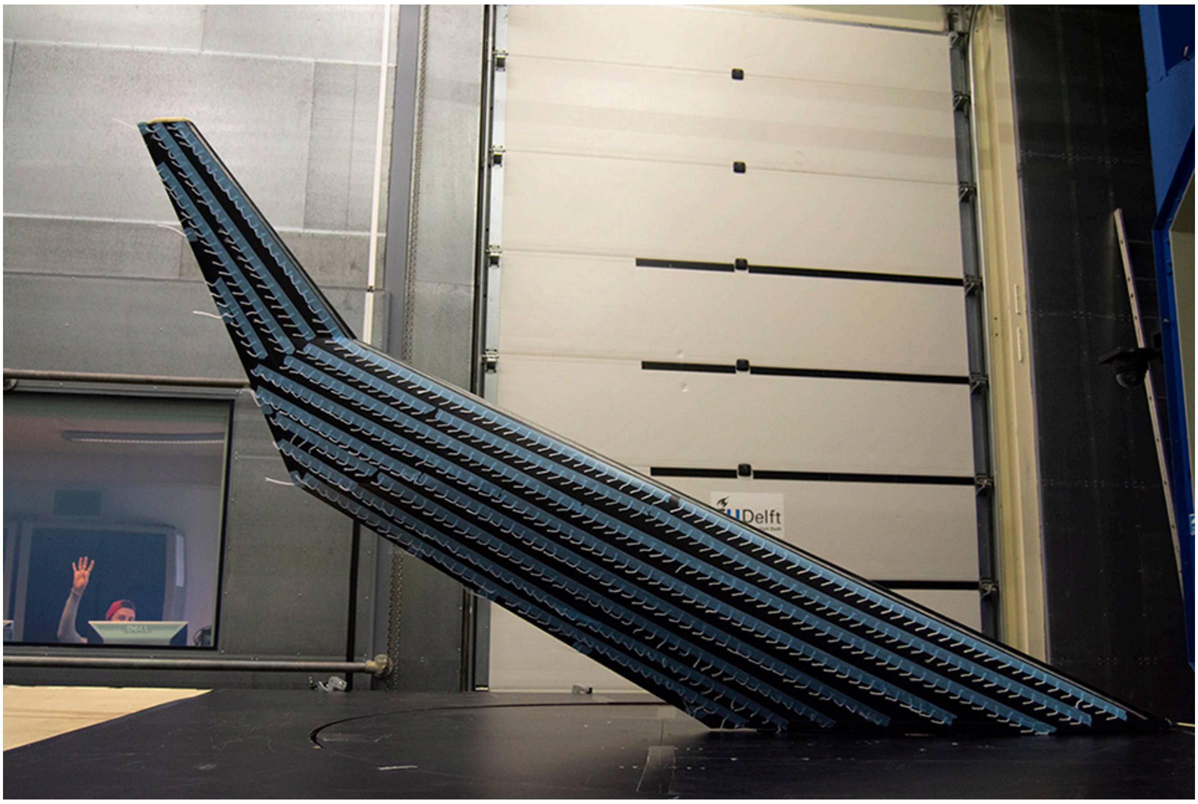

Figure A.2: Clean wing at $\alpha = 10^{\circ}$ and $V = 18.7$ m/s

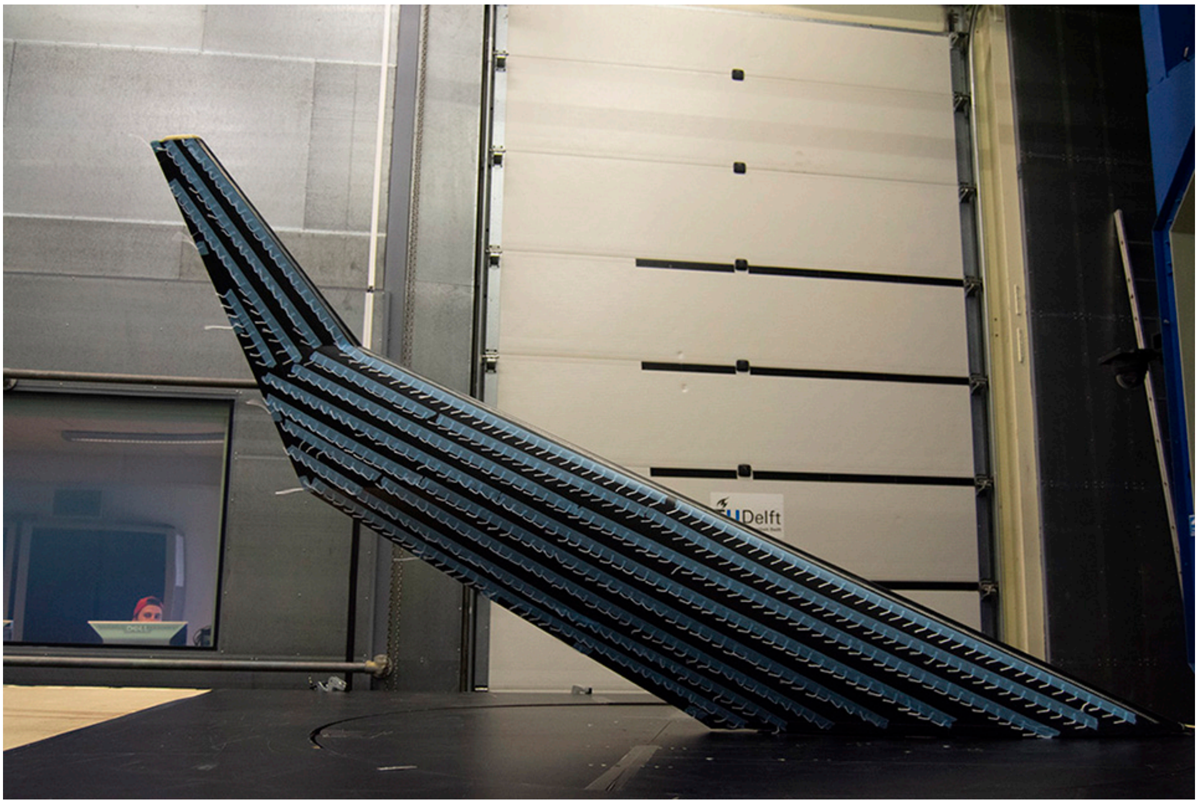

Figure A.3: Clean wing at $\alpha = 15°$ and $V = 18.7$ m/s

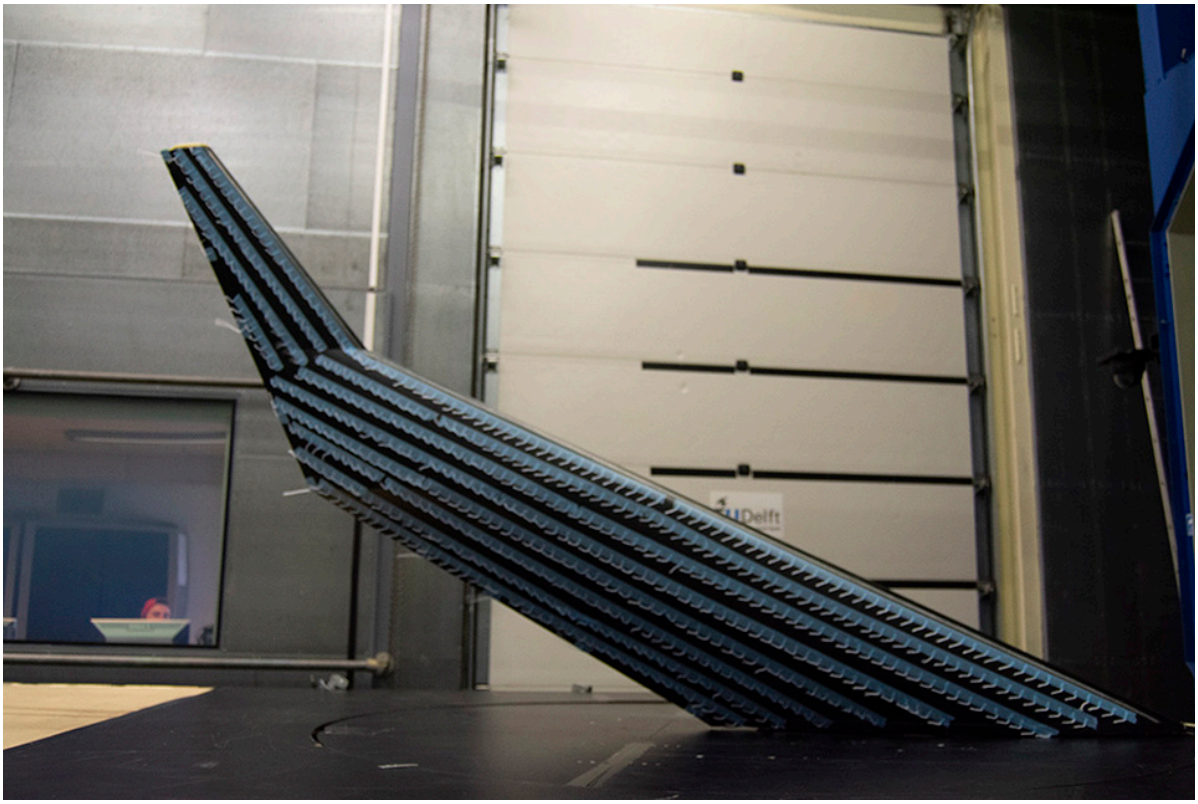

Figure A.4: Clean wing at $\alpha = 17°$ and $V = 18.7$ m/s

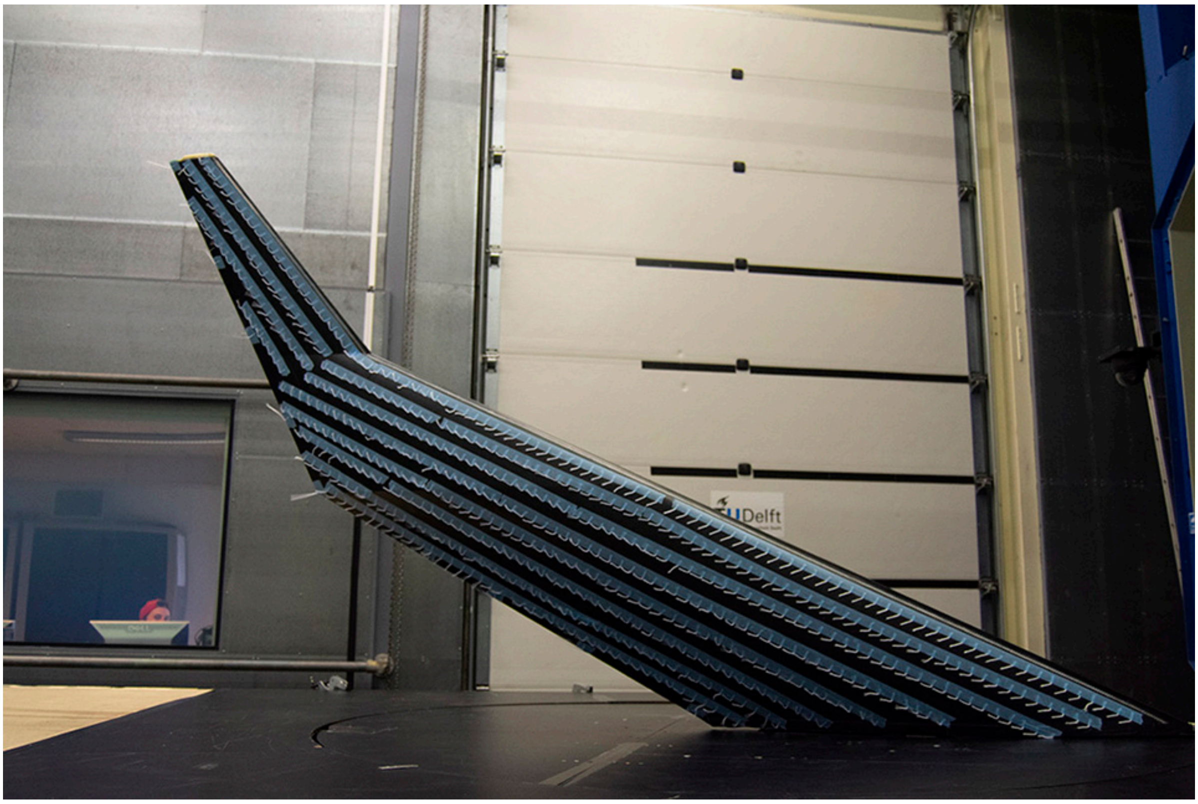

Figure A.5: Clean wing at $\alpha = 20^{\circ}$ and $V = 18.7$ m/s

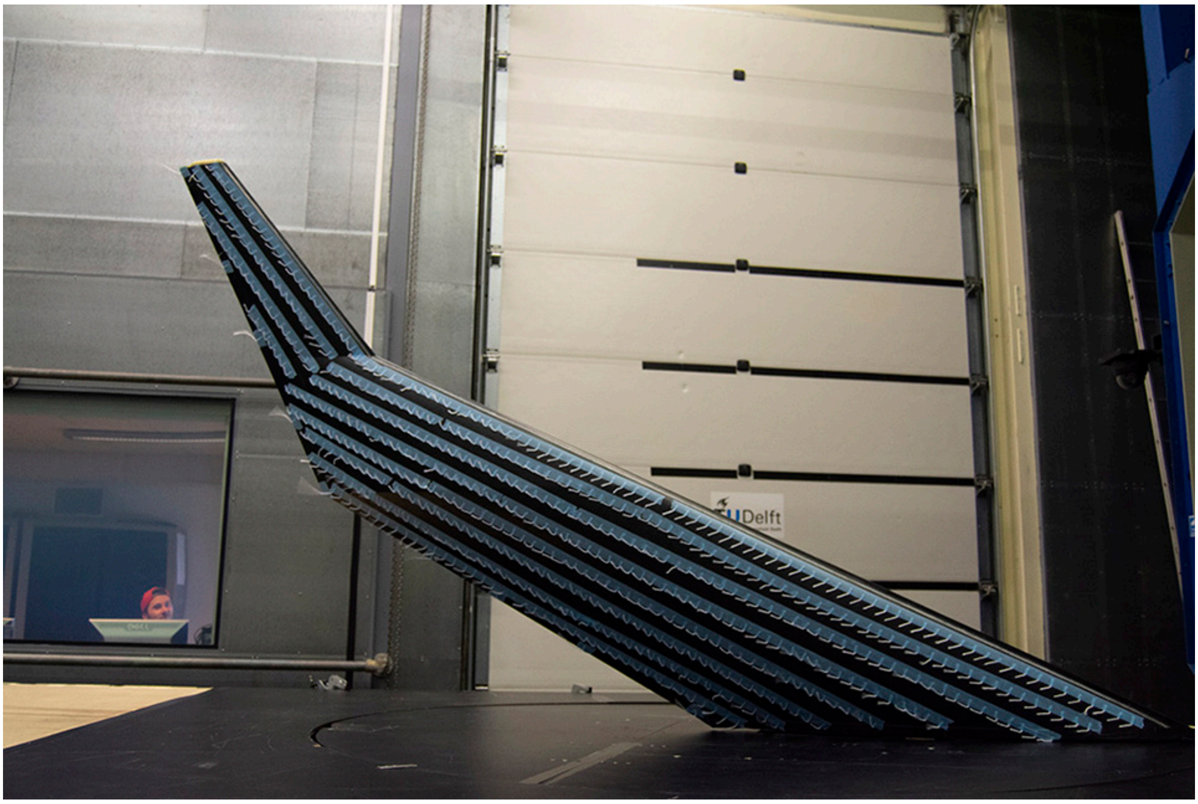

Figure A.6: Clean wing at $\alpha = 22^{\circ}$ and $V = 18.7$ m/s

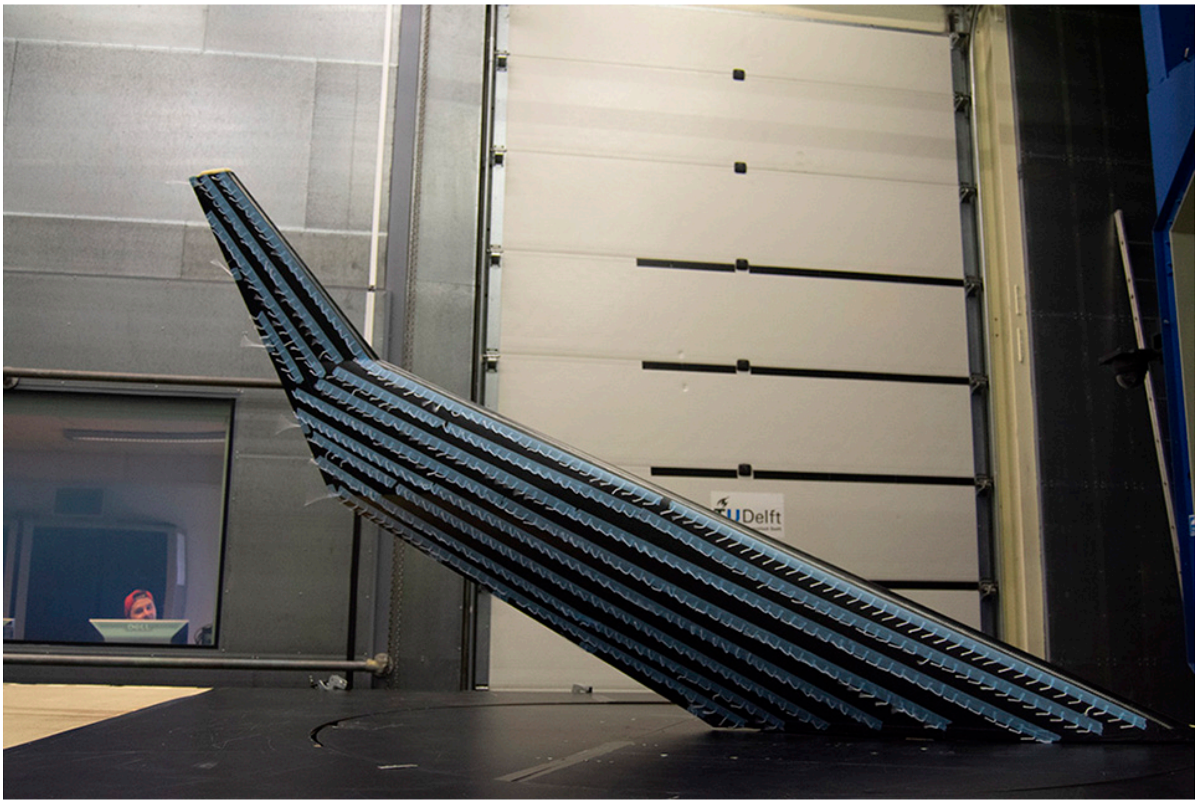

Figure A.7: Clean wing at $\alpha = 25^{\circ}$ and $V = 18.7$ m/s

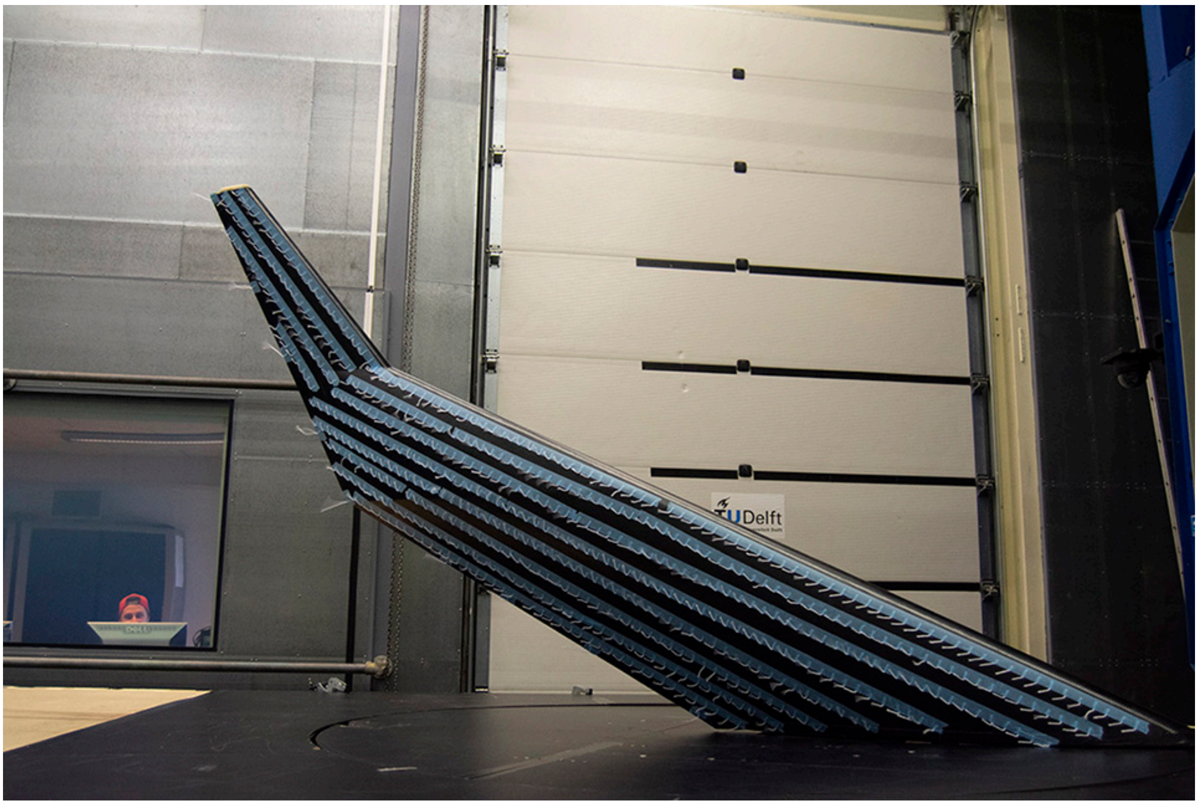

Figure A.8: Clean wing at $\alpha = 30^{\circ}$ and $V = 18.7$ m/s

A.2. Strip-on Wing

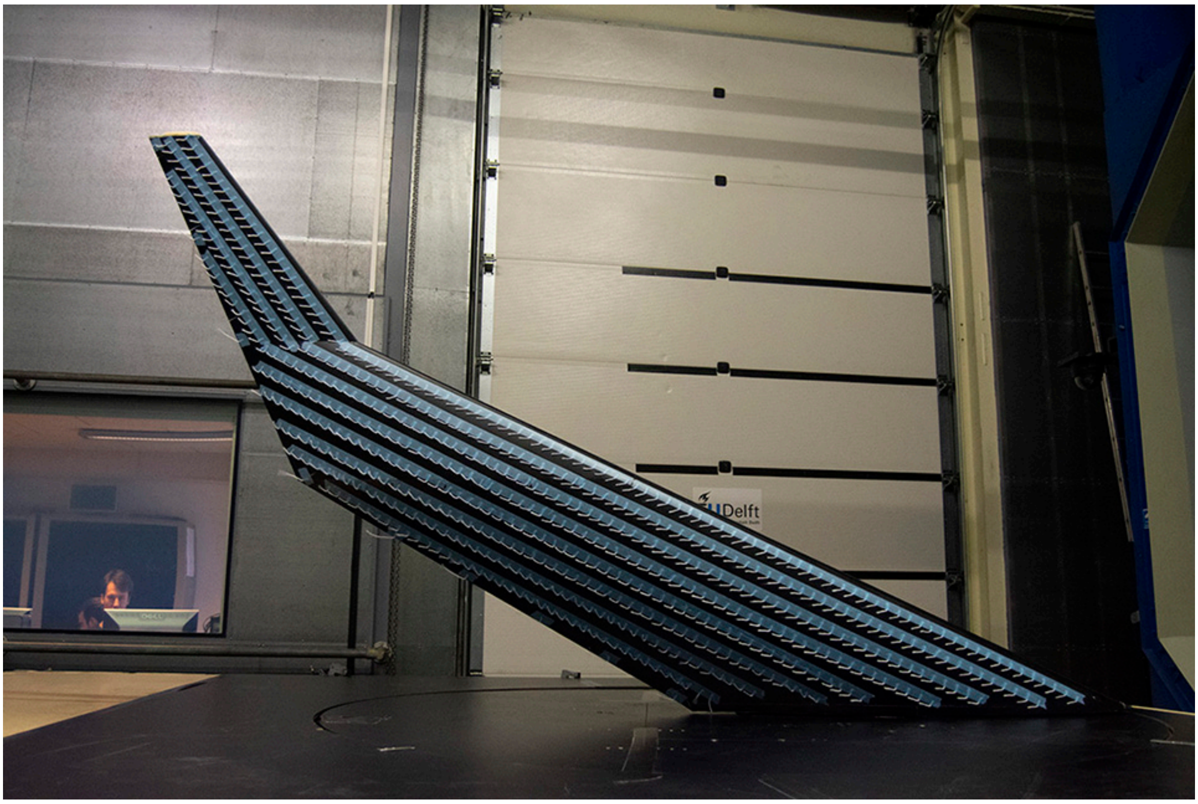

Figure A.9: Strip-on wing at $\alpha = 10^{\circ}$ and $V = 18.7$ m/s

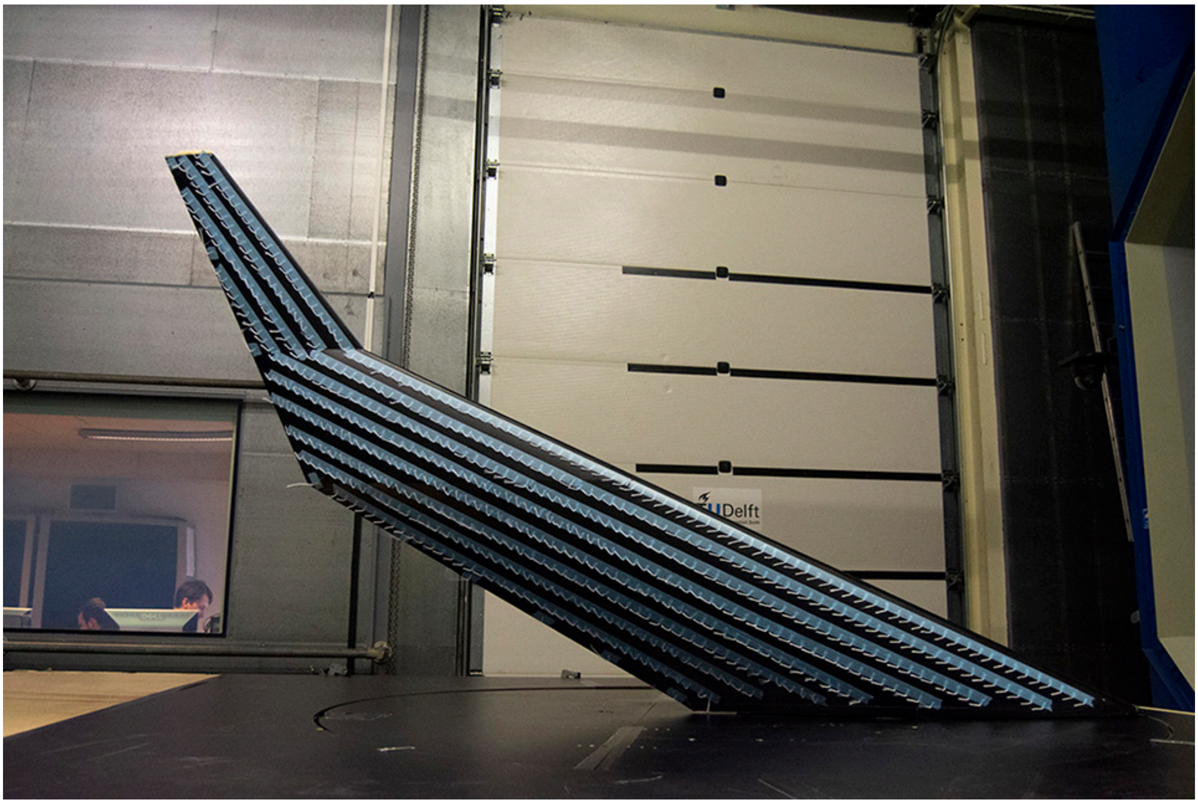

Figure A.10: Strip-on wing at $\alpha = 15^{\circ}$ and $V = 18.7$ m/s

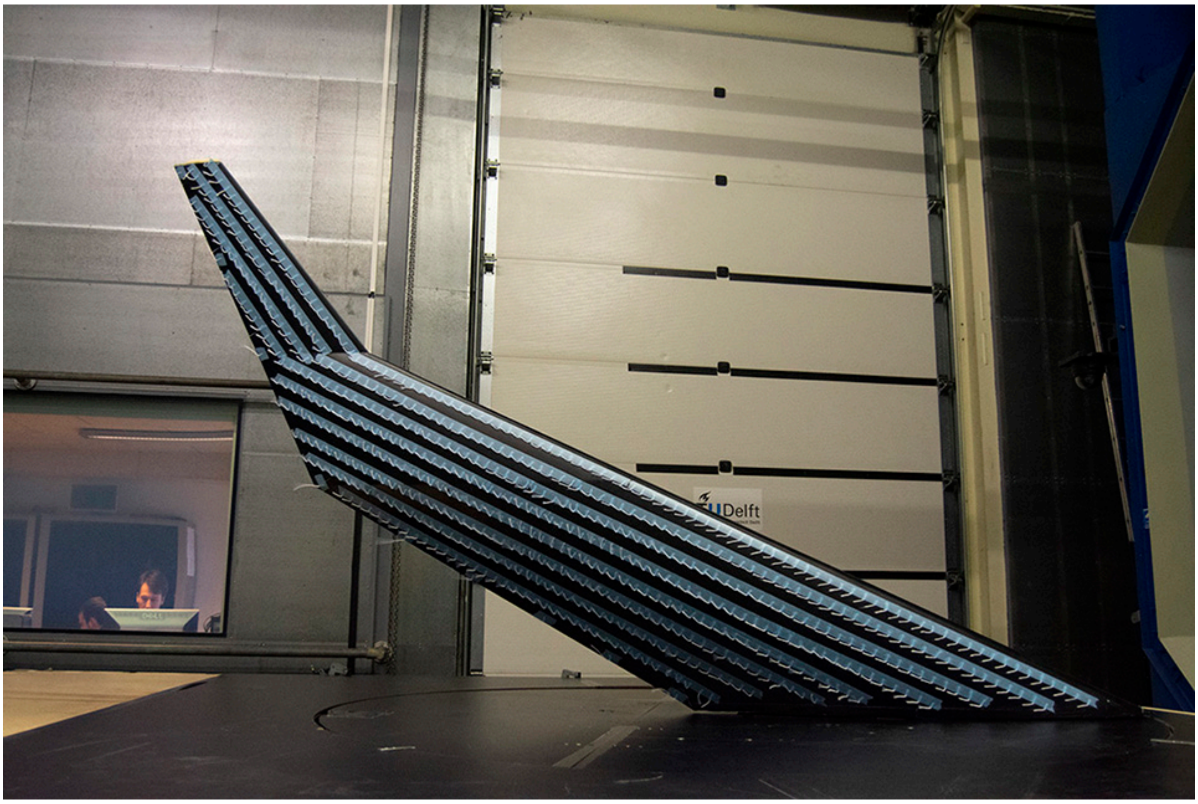

Figure A.11: Strip-on wing at $\alpha = 17.5°$ and $V = 18.7$ m/s

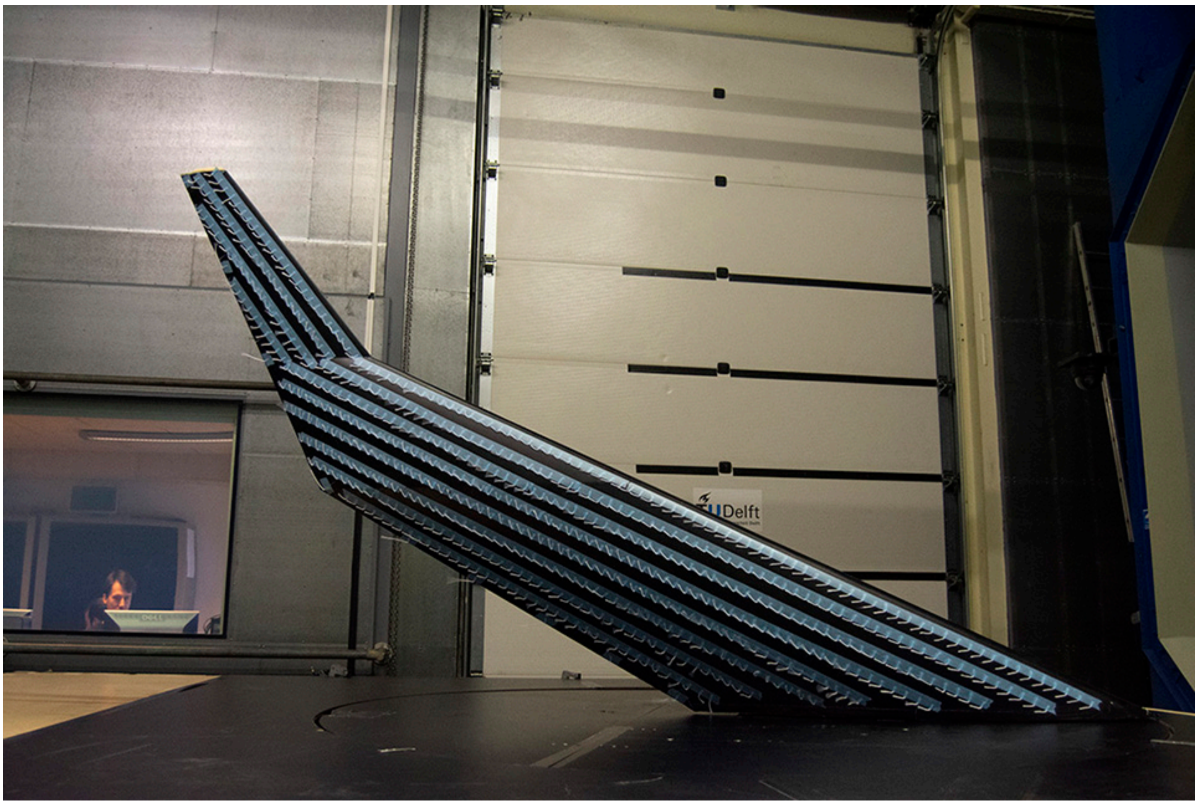

Figure A.12: Strip-on wing at $\alpha = 20°$ and $V = 18.7$ m/s

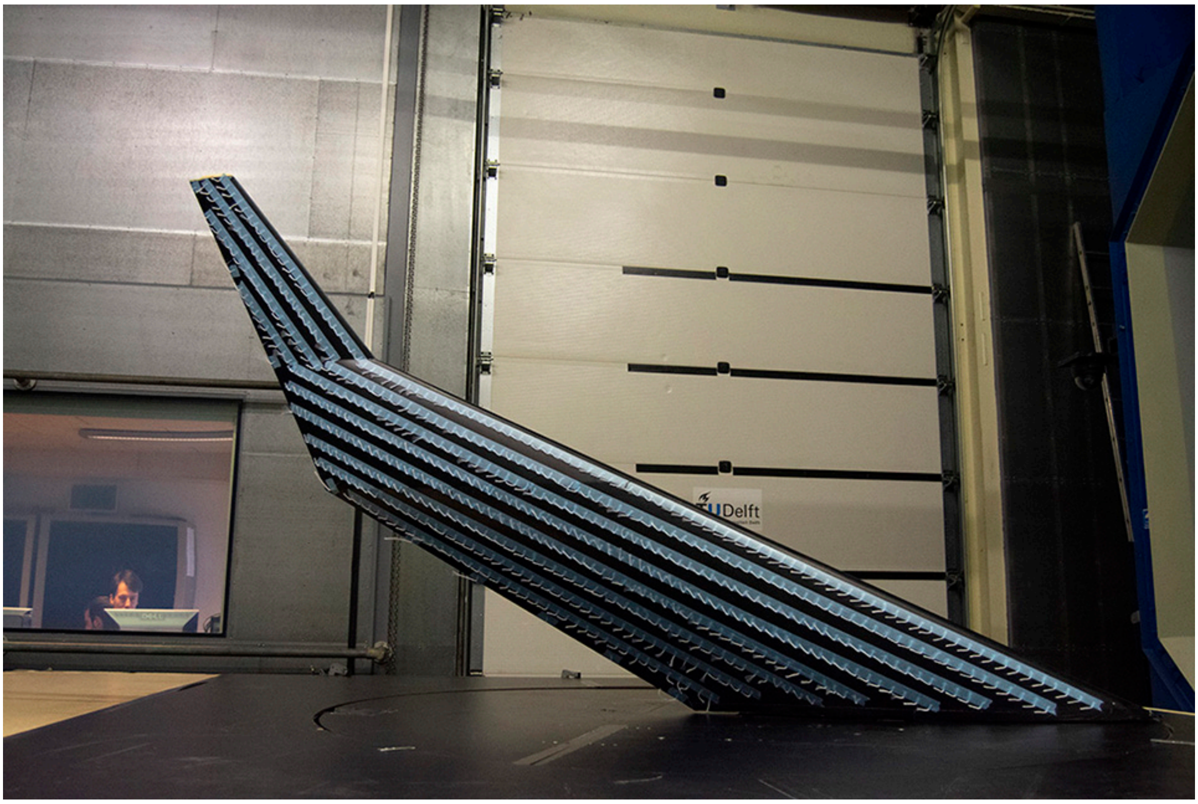

Figure A.13: Strip-on wing at $\alpha = 22°$ and $V = 18.7$ m/s

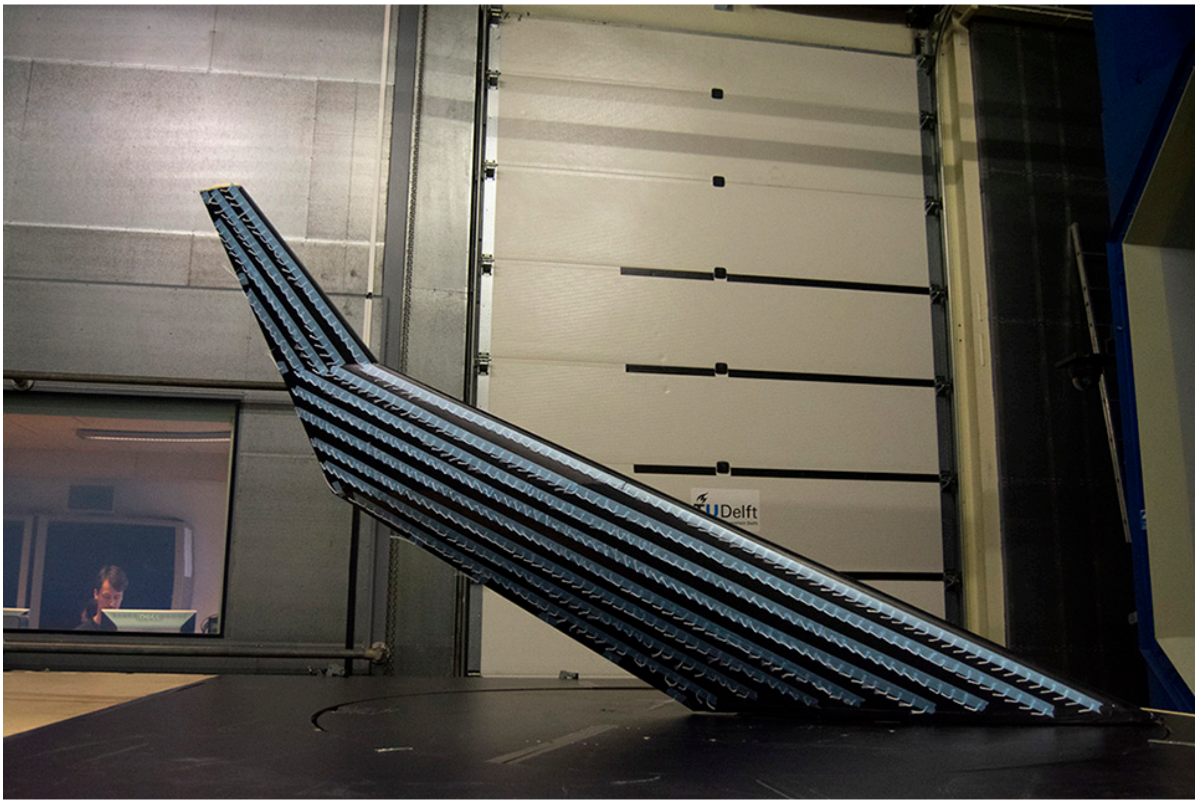

Figure A.14: Strip-on wing at $\alpha = 25°$ and $V = 18.7$ m/s

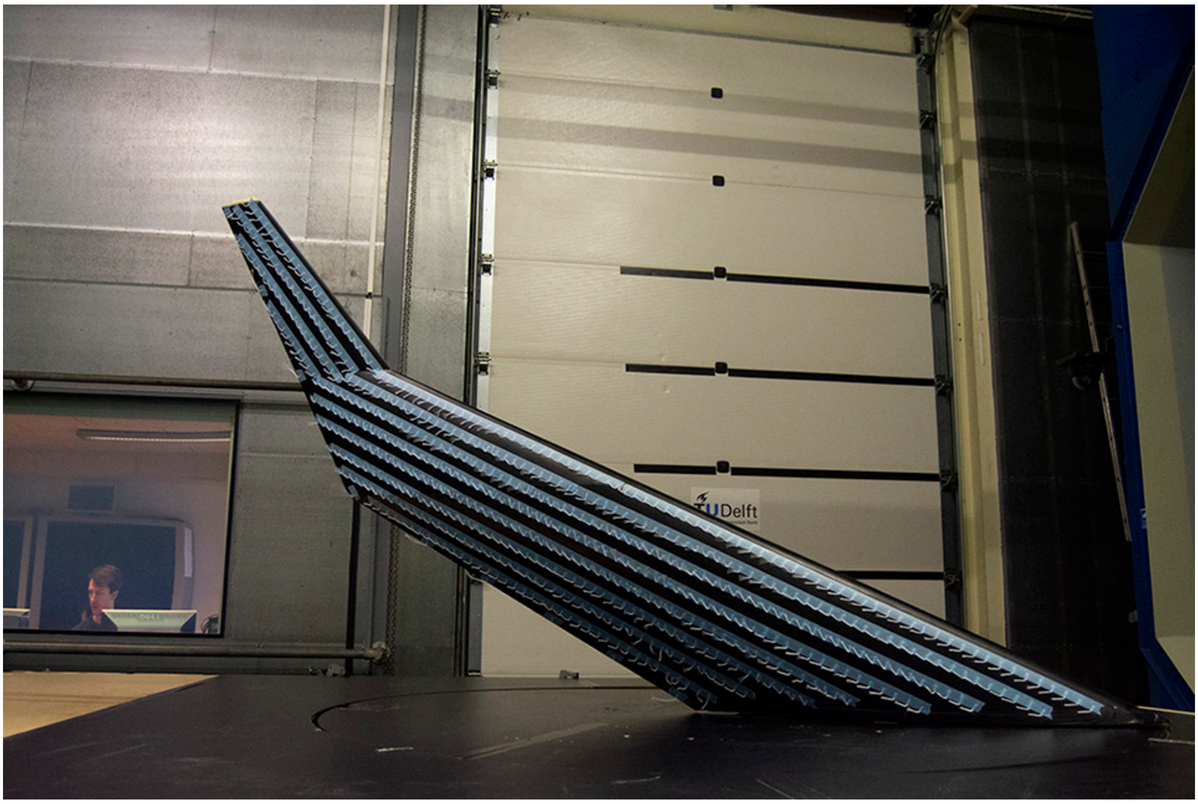

Figure A.15: Strip-on wing at $\alpha = 30^{\circ}$ and $V = 18.7$ m/s

A.3. Strip-on Wing + Fence 1a

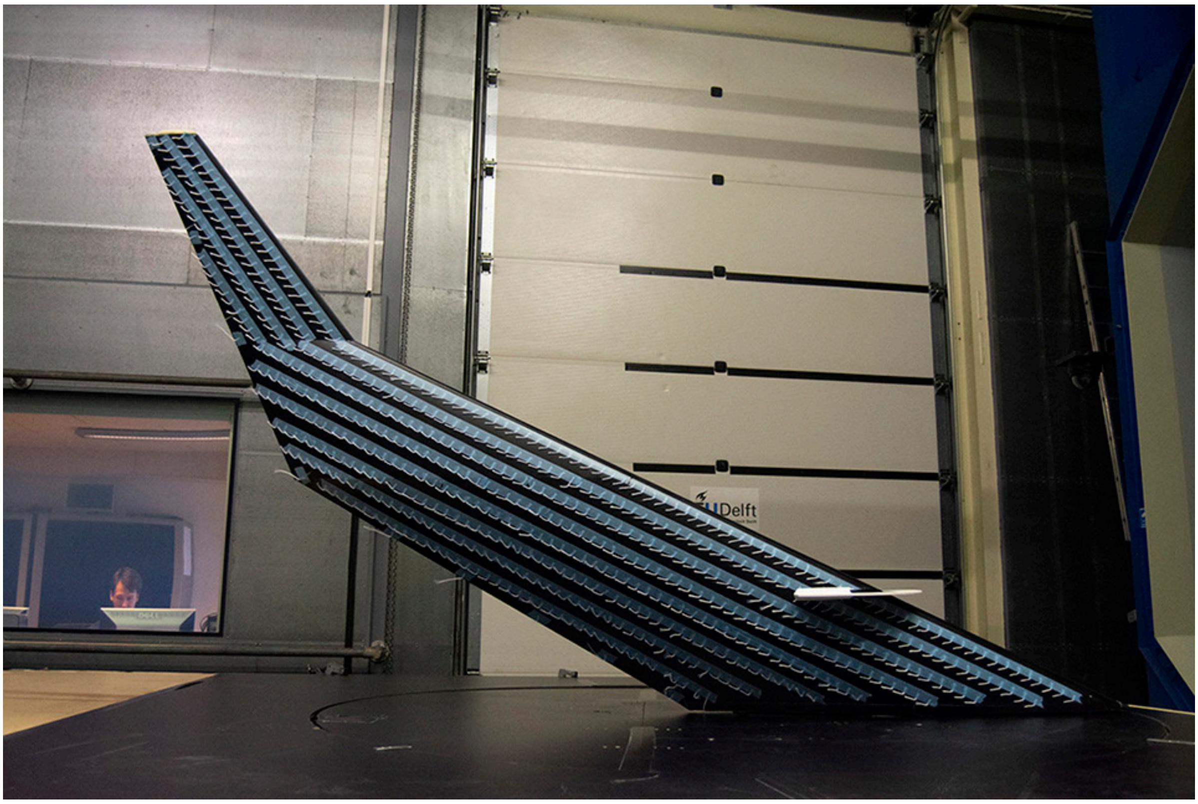

Figure A.16: Strip-on wing with fence 1a at $\alpha = 10^{\circ}$ and $V = 18.7$ m/s

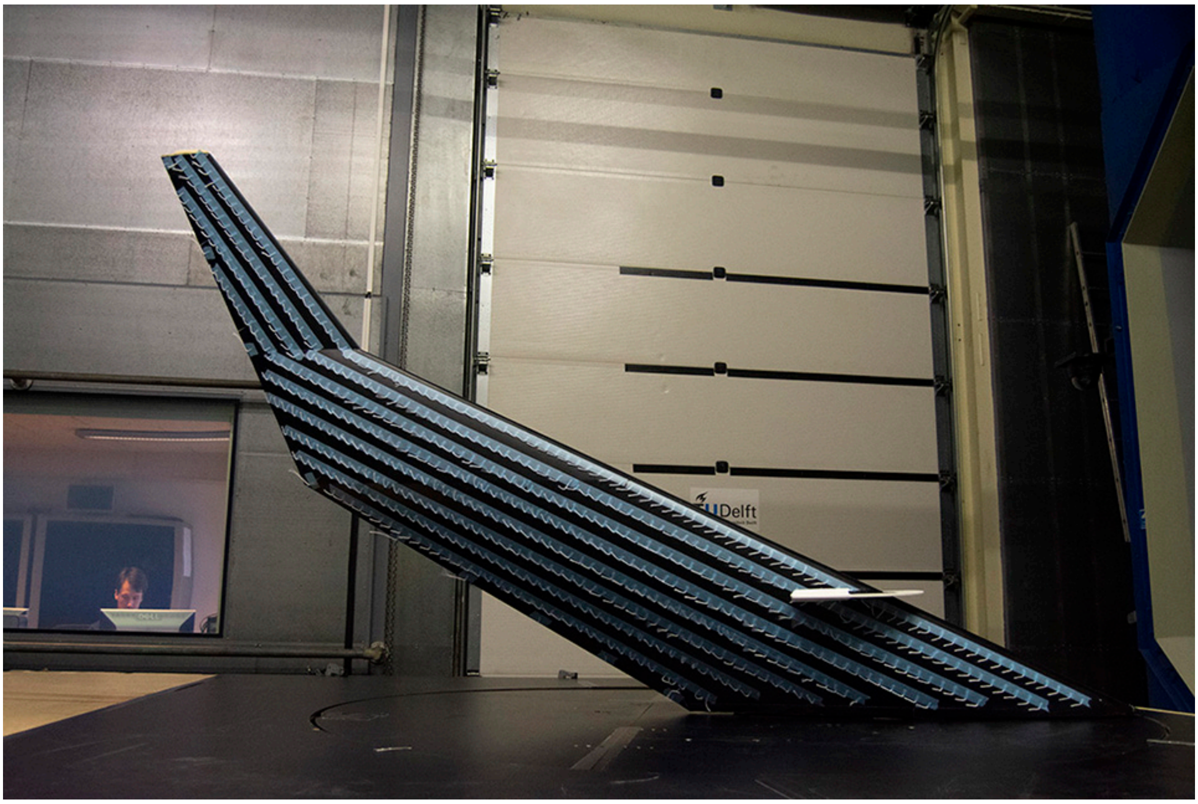

Figure A.17: Strip-on wing with fence 1a at $\alpha = 15°$ and $V = 18.7$ m/s

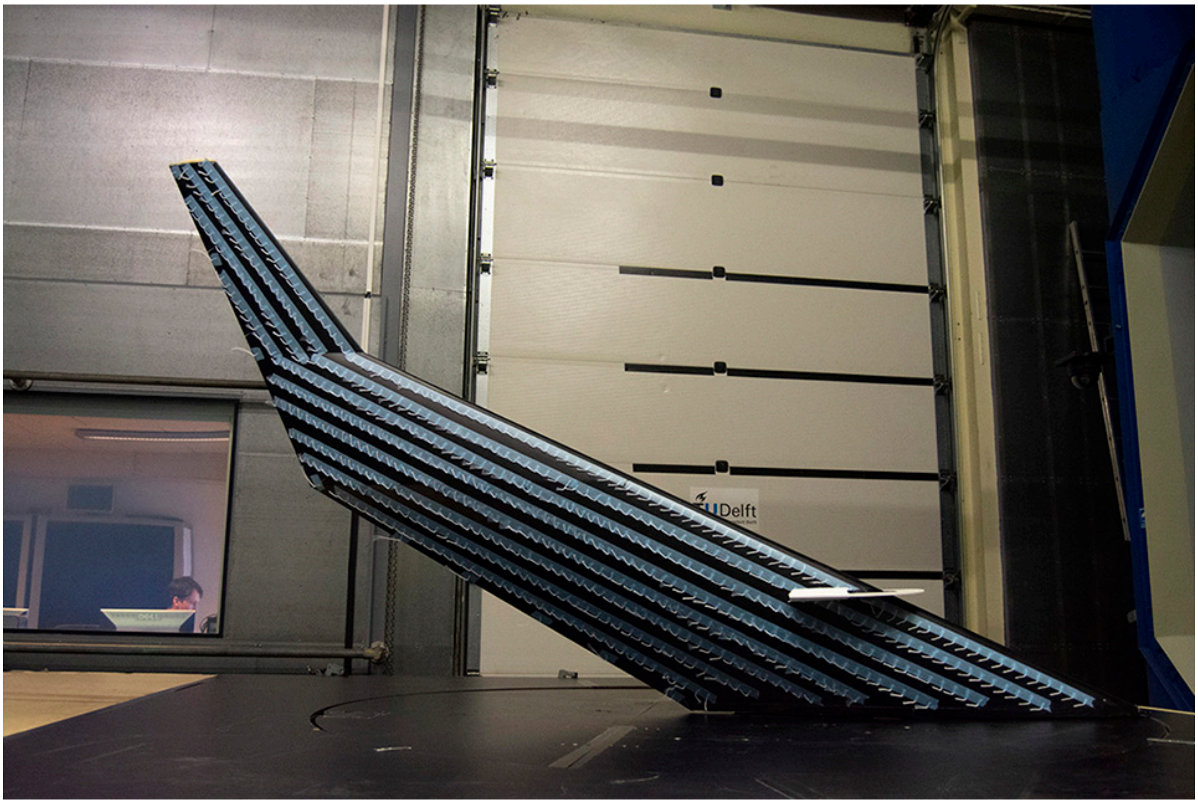

Figure A.18: Strip-on wing with fence 1a at $\alpha = 17.5°$ and $V = 18.7$ m/s

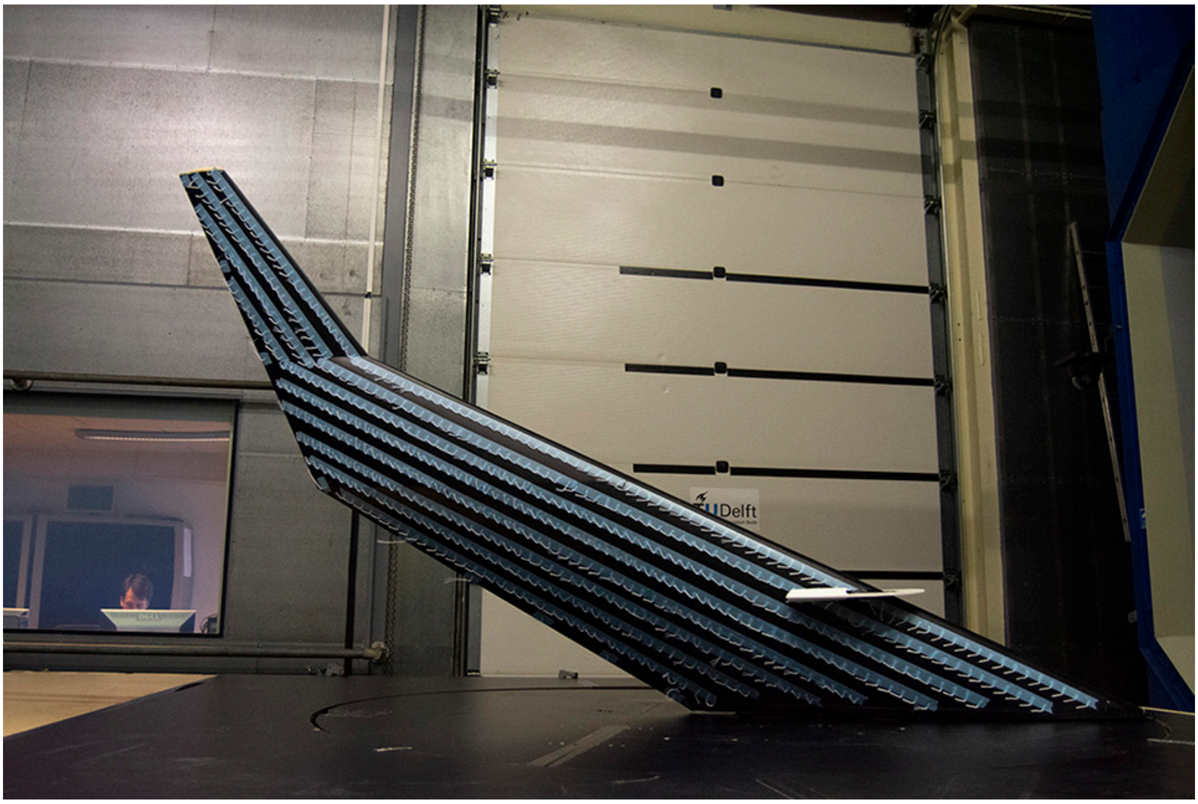

Figure A.19: Strip-on wing with fence 1a at $\alpha = 20°$ and $V = 18.7$ m/s

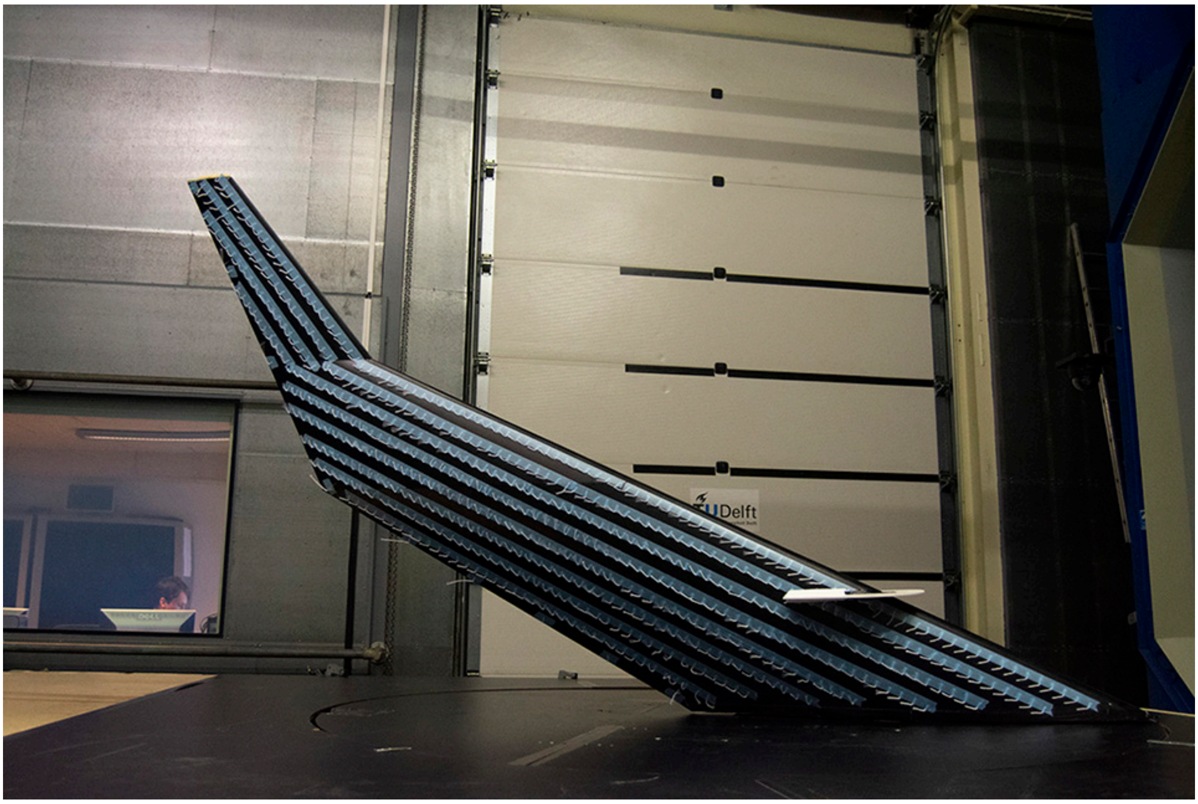

Figure A.20: Strip-on wing with fence 1a at $\alpha = 22°$ and $V = 18.7$ m/s

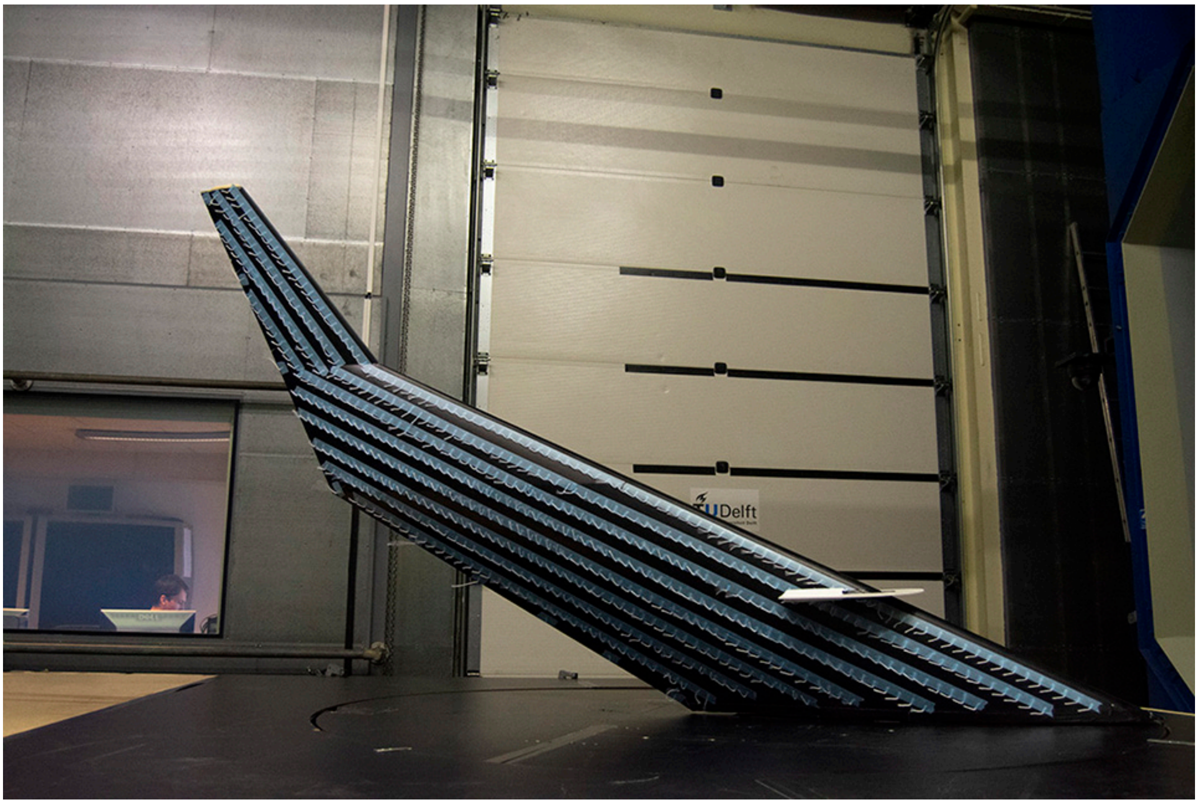

Figure A.21: Strip-on wing with fence 1a at $\alpha = 25^{\circ}$ and $V = 18.7$ m/s

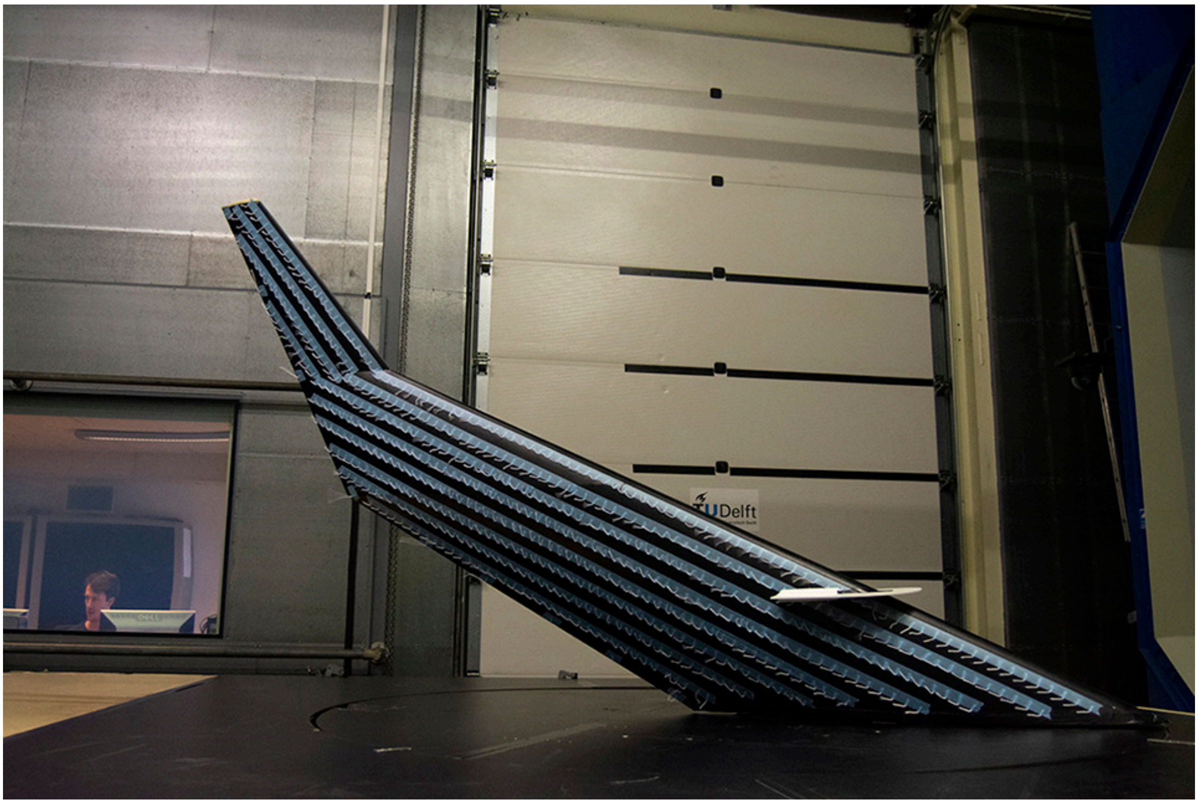

Figure A.22: Strip-on wing with fence 1a at $\alpha = 30^{\circ}$ and $V = 18.7$ m/s

A.4. Strip-on Wing + Fence 1b

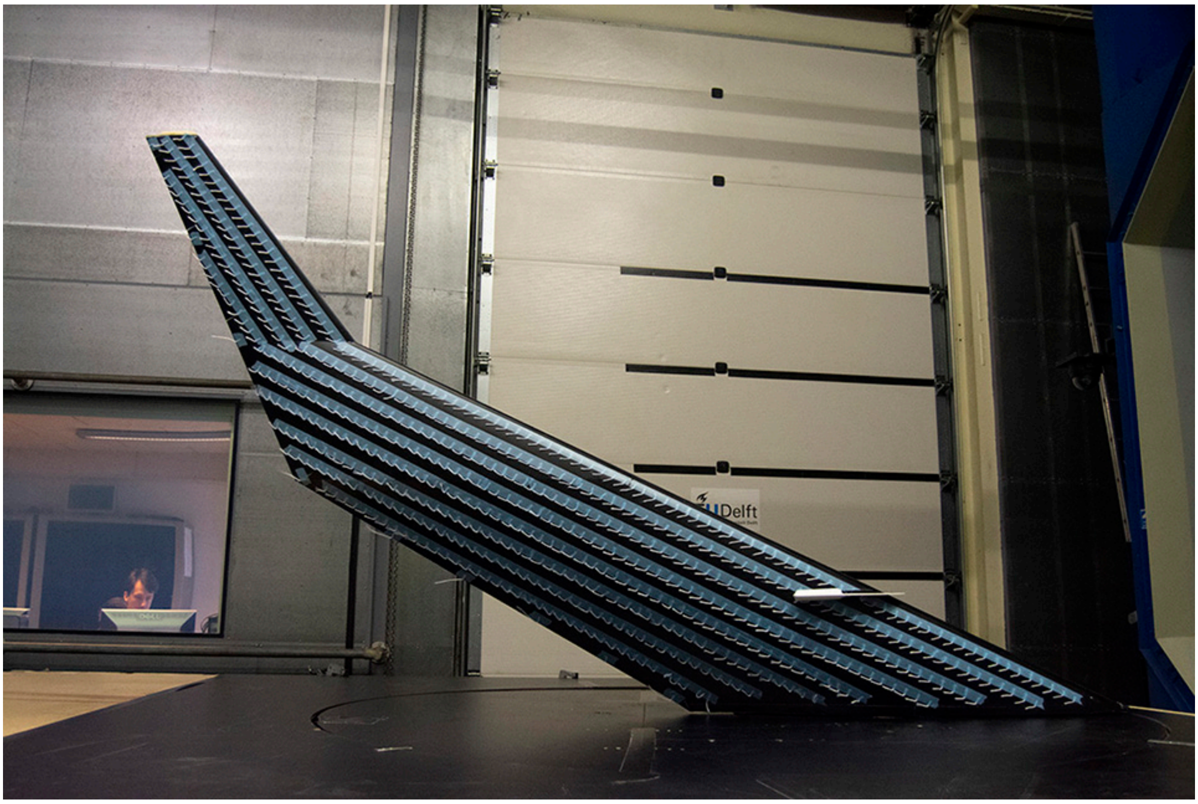

Figure A.23: Strip-on wing with fence 1b at $\alpha = 10^{\circ}$ and $V = 18.7$ m/s

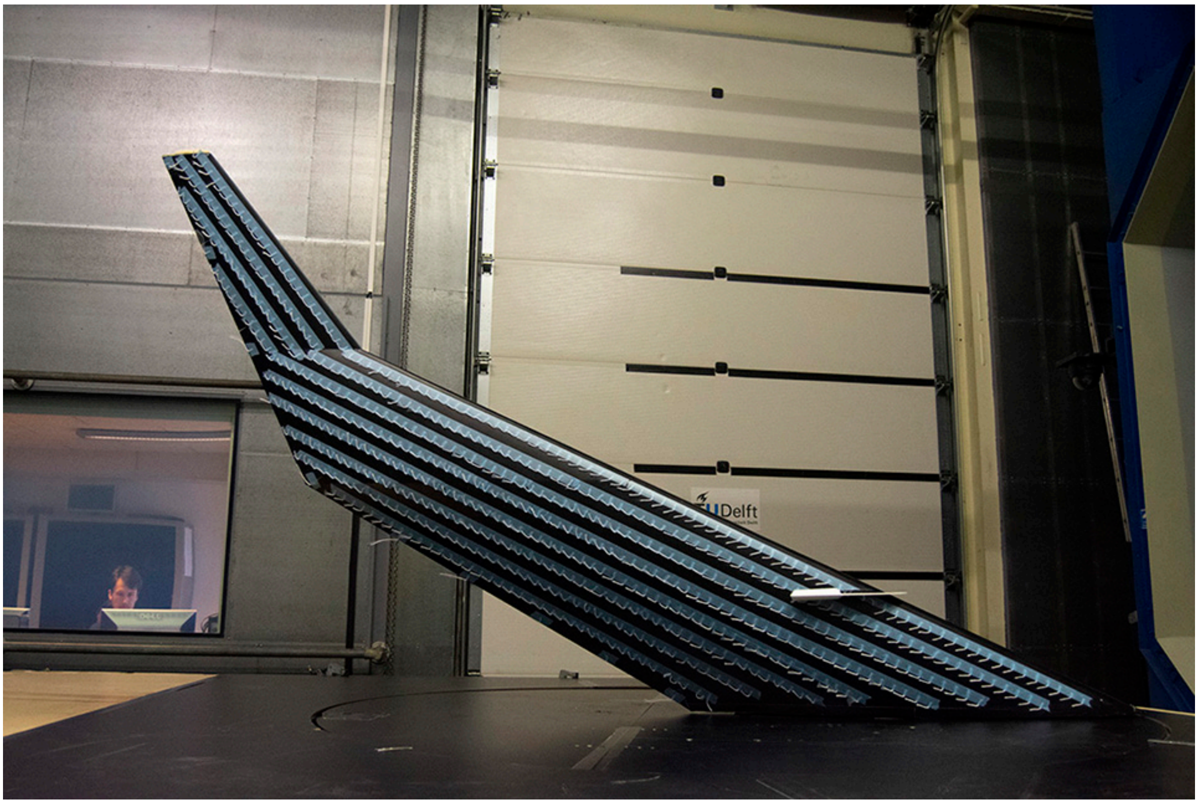

Figure A.24: Strip-on wing with fence 1b at $\alpha = 15^{\circ}$ and $V = 18.7$ m/s

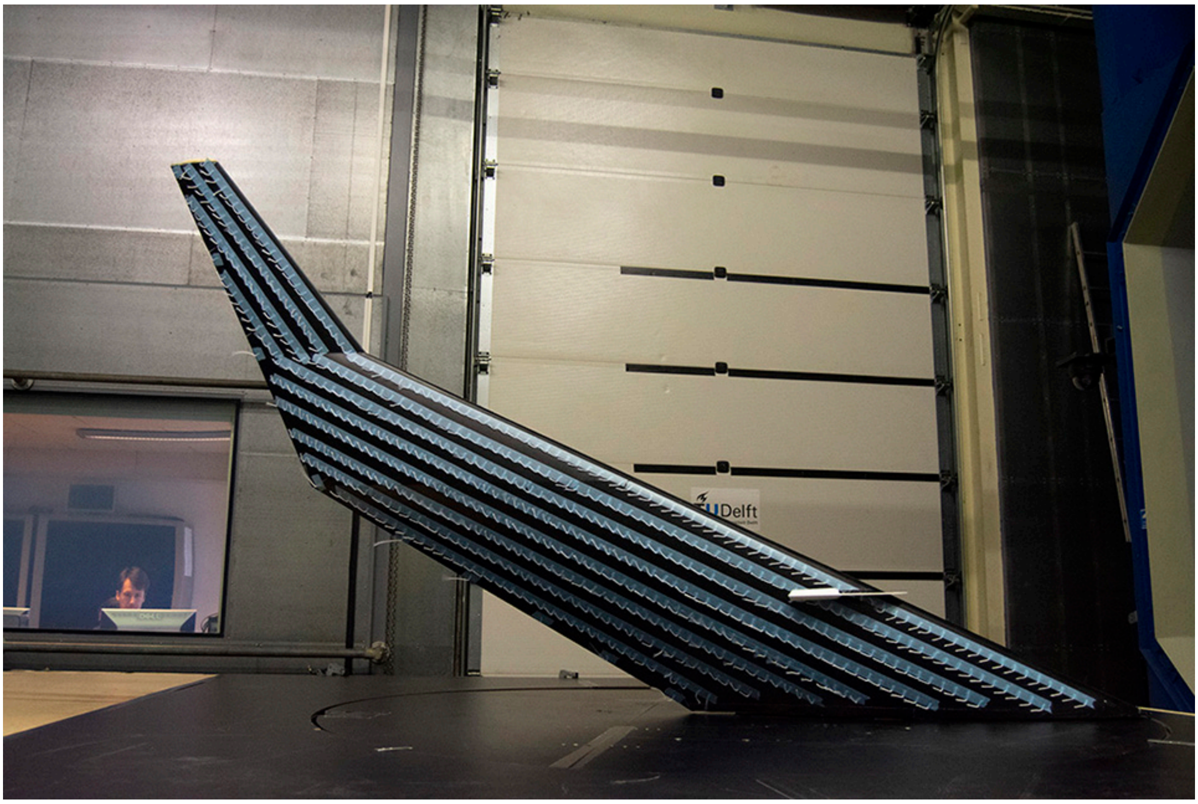

Figure A.25: Strip-on wing with fence 1b at $\alpha = 17.5^{\circ}$ and $V = 18.7$ m/s

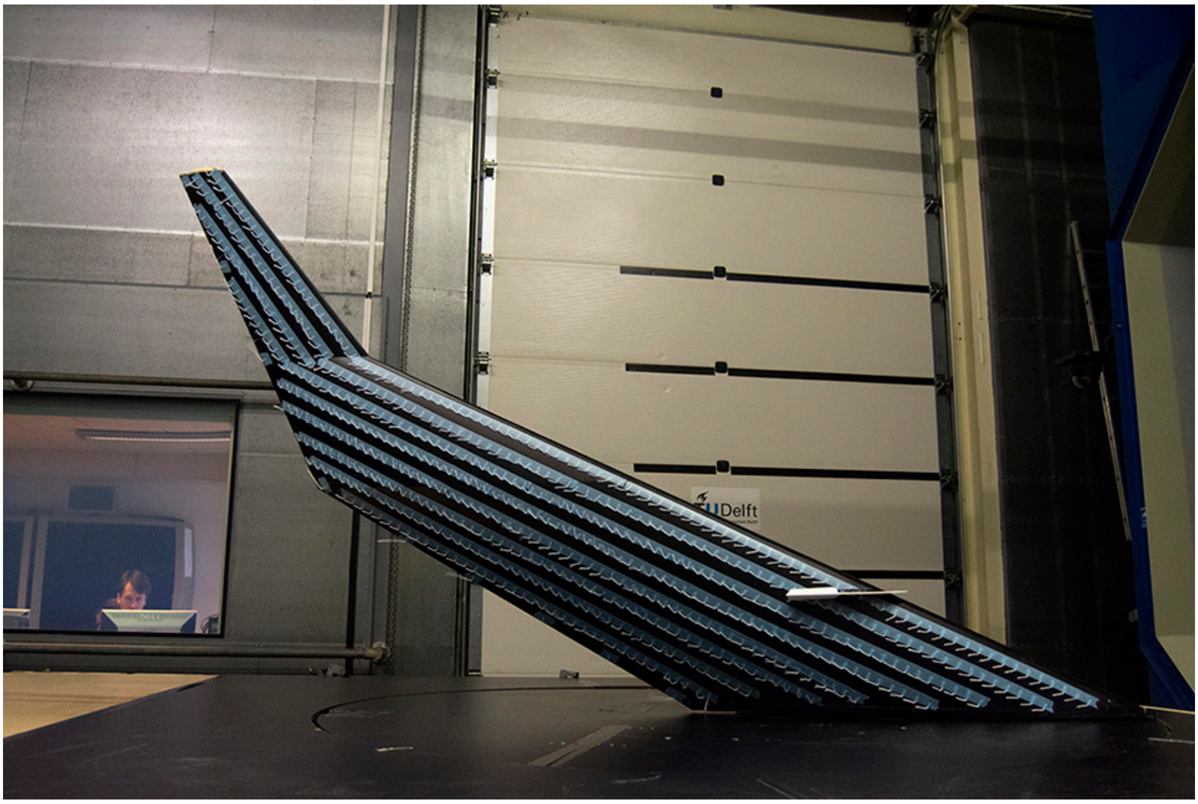

Figure A.26: Strip-on wing at with fence 1b $\alpha = 20^{\circ}$ and $V = 18.7$ m/s

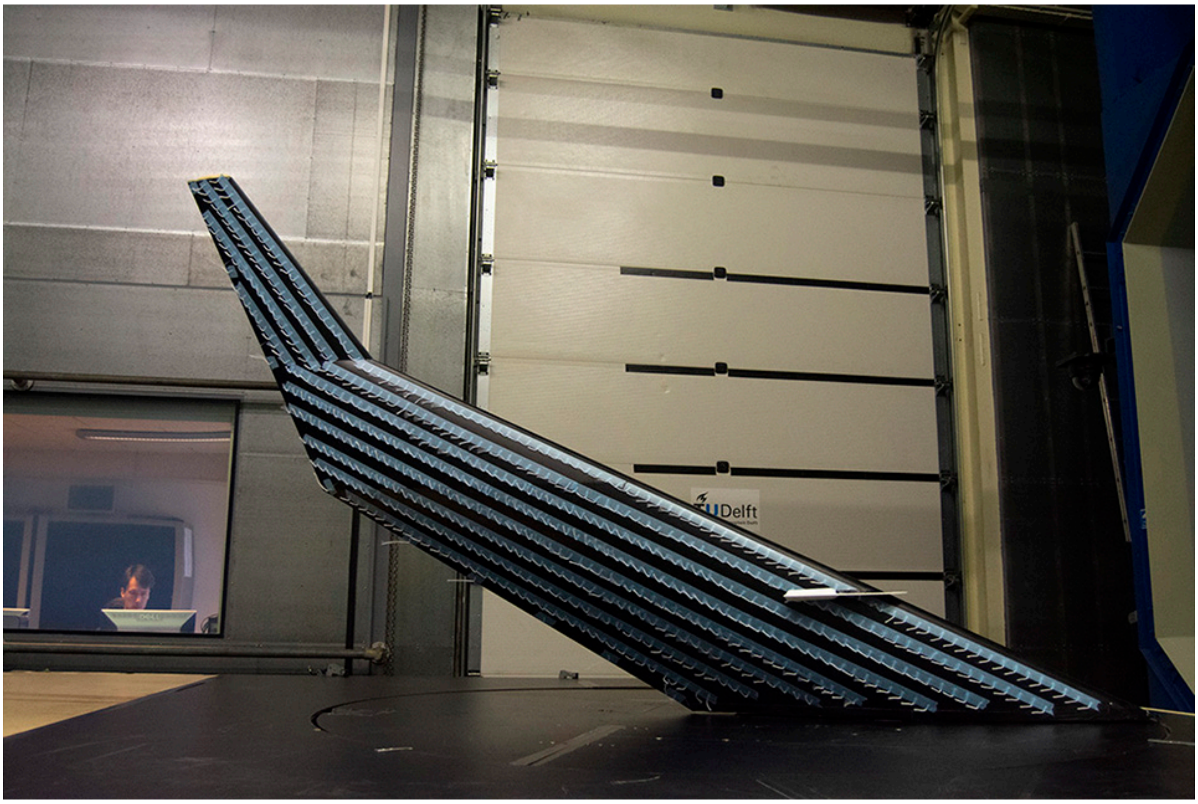

Figure A.27: Strip-on wing at with fence 1b $\alpha = 22^{\circ}$ and $V = 18.7$ m/s

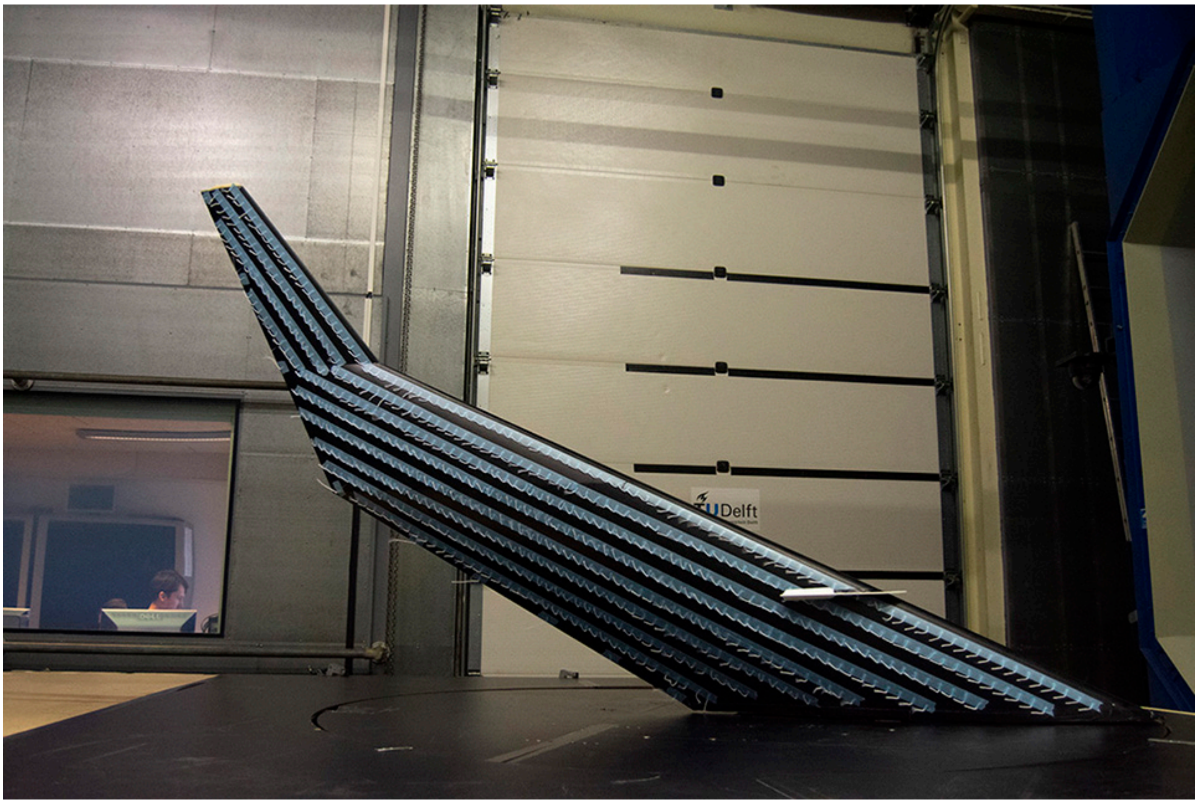

Figure A.28: Strip-on wing with fence 1b at $\alpha = 25^{\circ}$ and $V = 18.7$ m/s

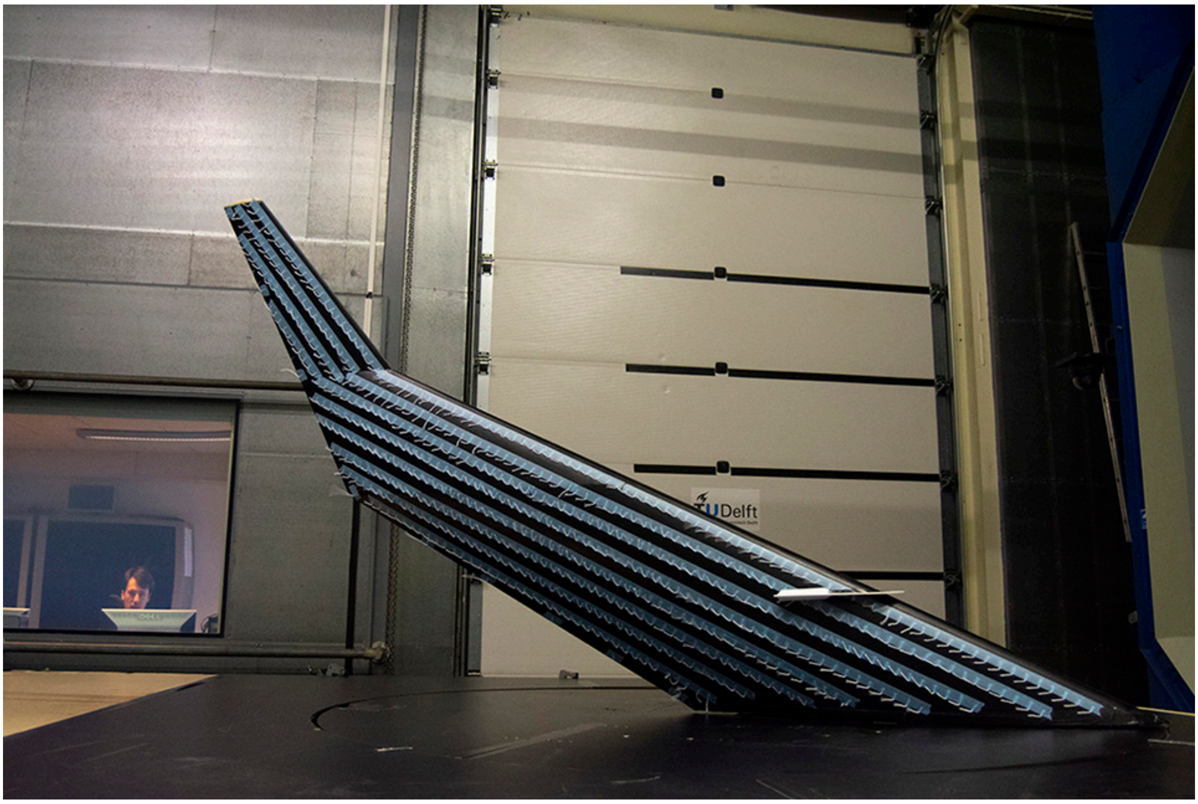

Figure A.29: Strip-on wing with fence 1b at $\alpha = 30^\circ$ and $V = 18.7$ m/s

A.5. Strip-on Wing + Fence 1b

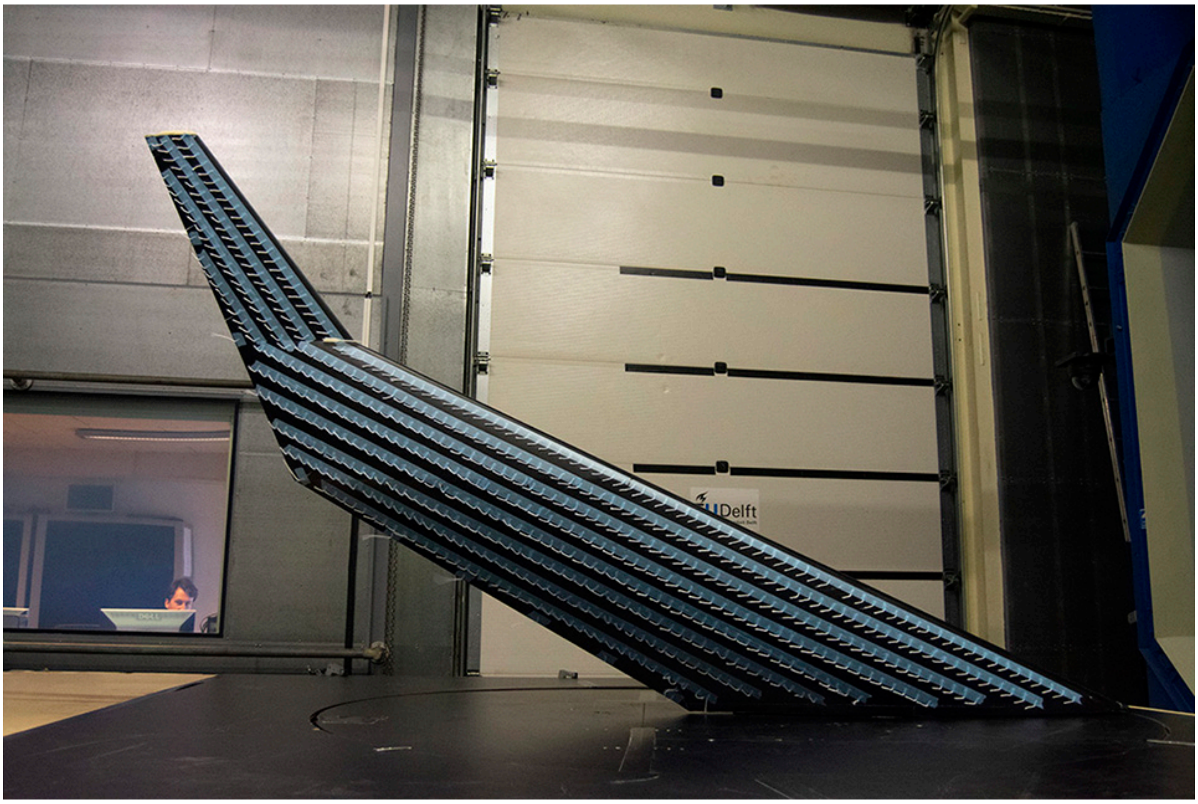

Figure A.30: Strip-on wing with fence 4b at $\alpha = 10^\circ$ and $V = 18.7$ m/s

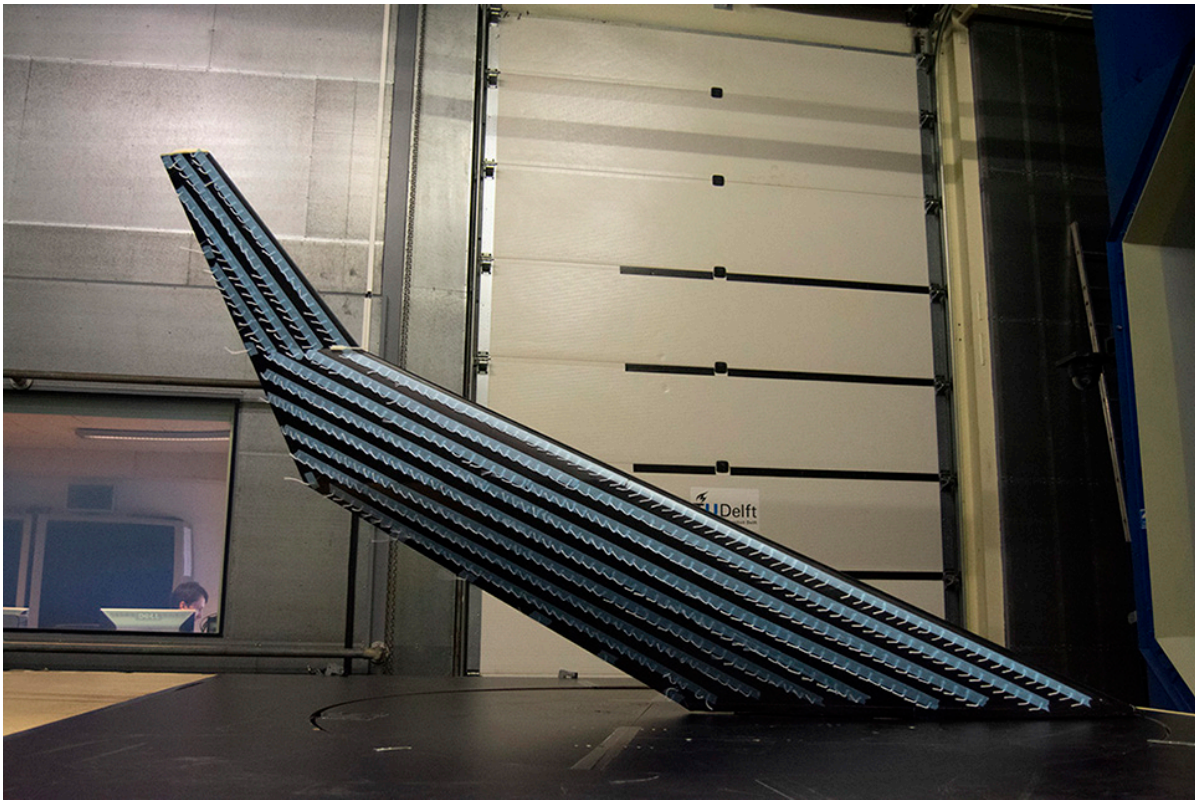

Figure A.31: Strip-on wing with fence 4b at $\alpha = 15^{\circ}$ and $V = 18.7$ m/s

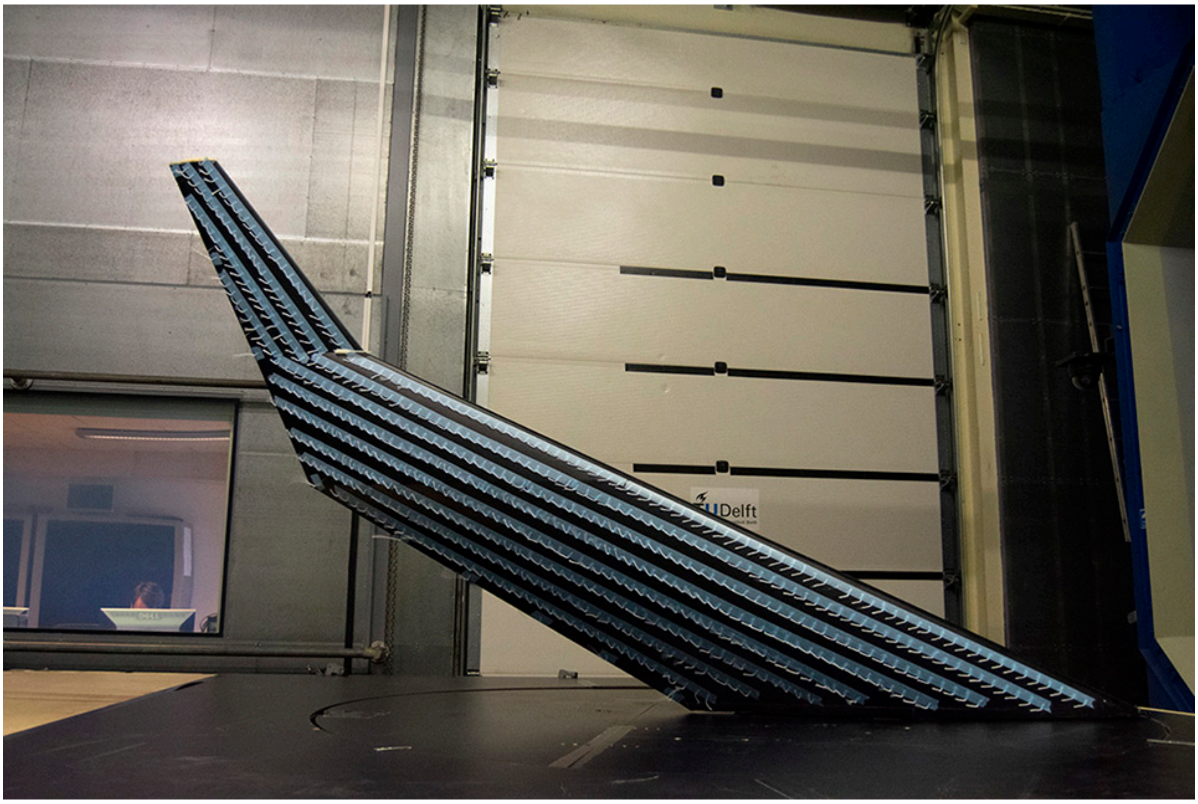

Figure A.32: Strip-on wing with fence 4b at $\alpha = 17.5^{\circ}$ and $V = 18.7$ m/s

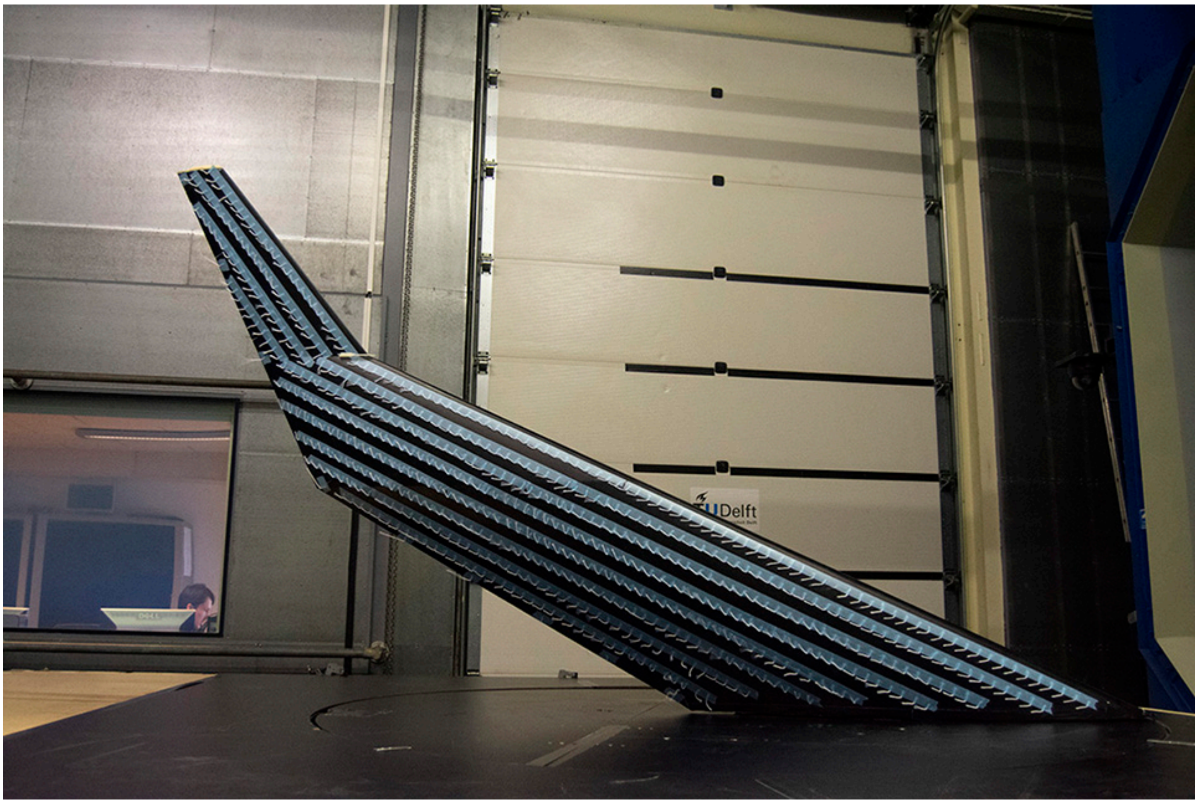

Figure A.33: Strip-on wing at with fence 4b $\alpha = 20°$ and $V = 18.7$ m/s

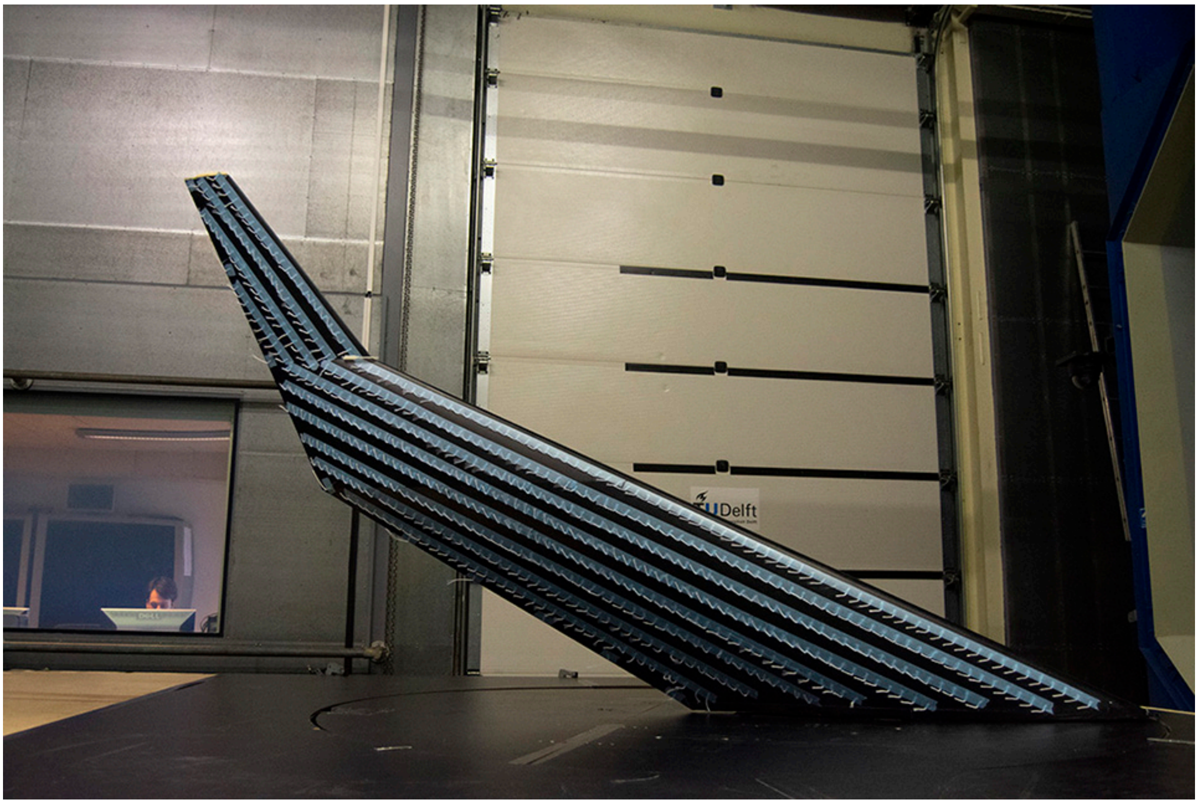

Figure A.34: Strip-on wing at with fence 4b $\alpha = 22°$ and $V = 18.7$ m/s

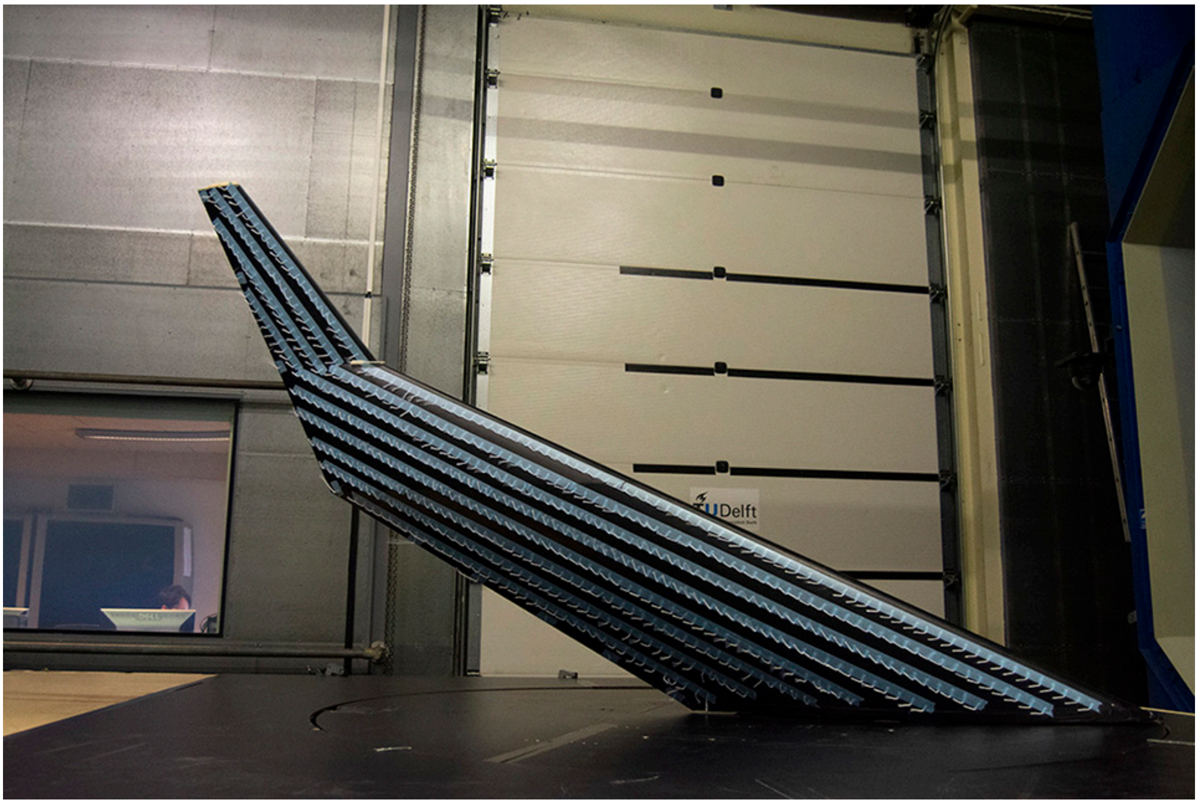

Figure A.35: Strip-on wing with fence 4b at $\alpha = 25^{\circ}$ and $V = 18.7$ m/s

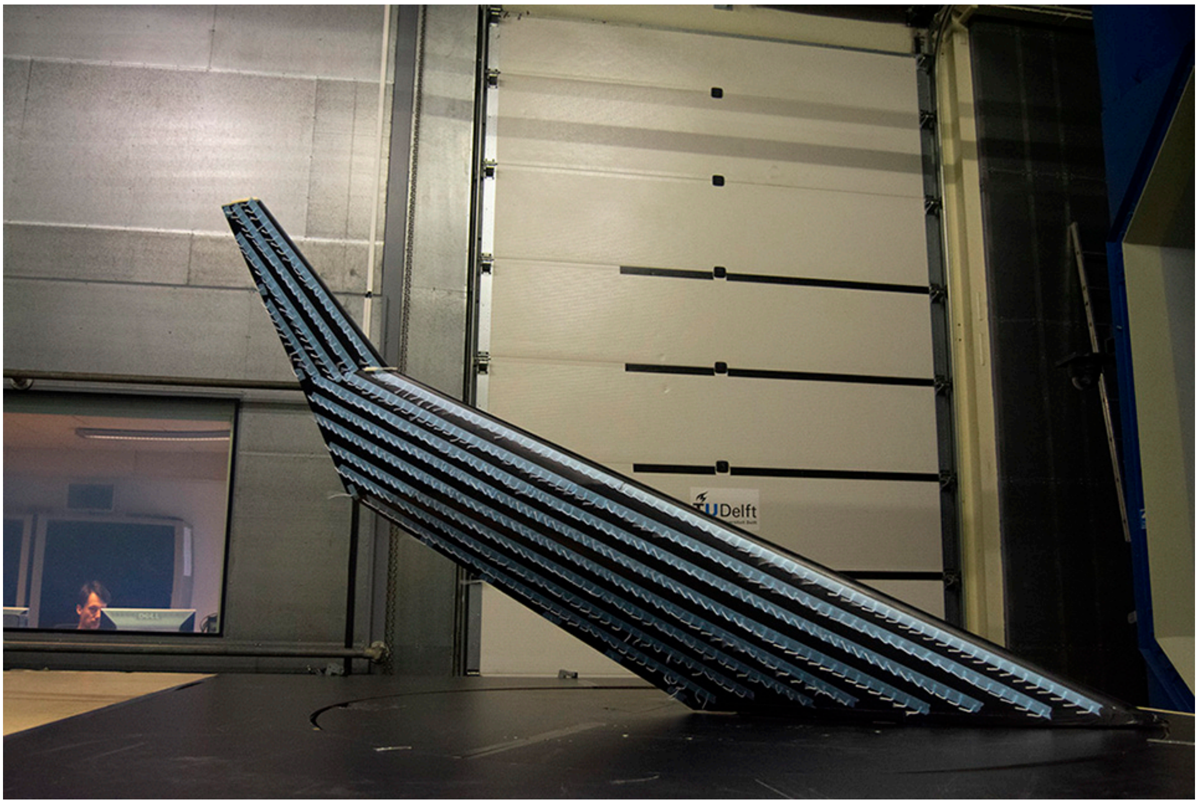

Figure A.36: Strip-on wing with fence 4b at $\alpha = 30^{\circ}$ and $V = 18.7$ m/s

A.6. Strip-on Wing + Fence 1b and Fence 4b

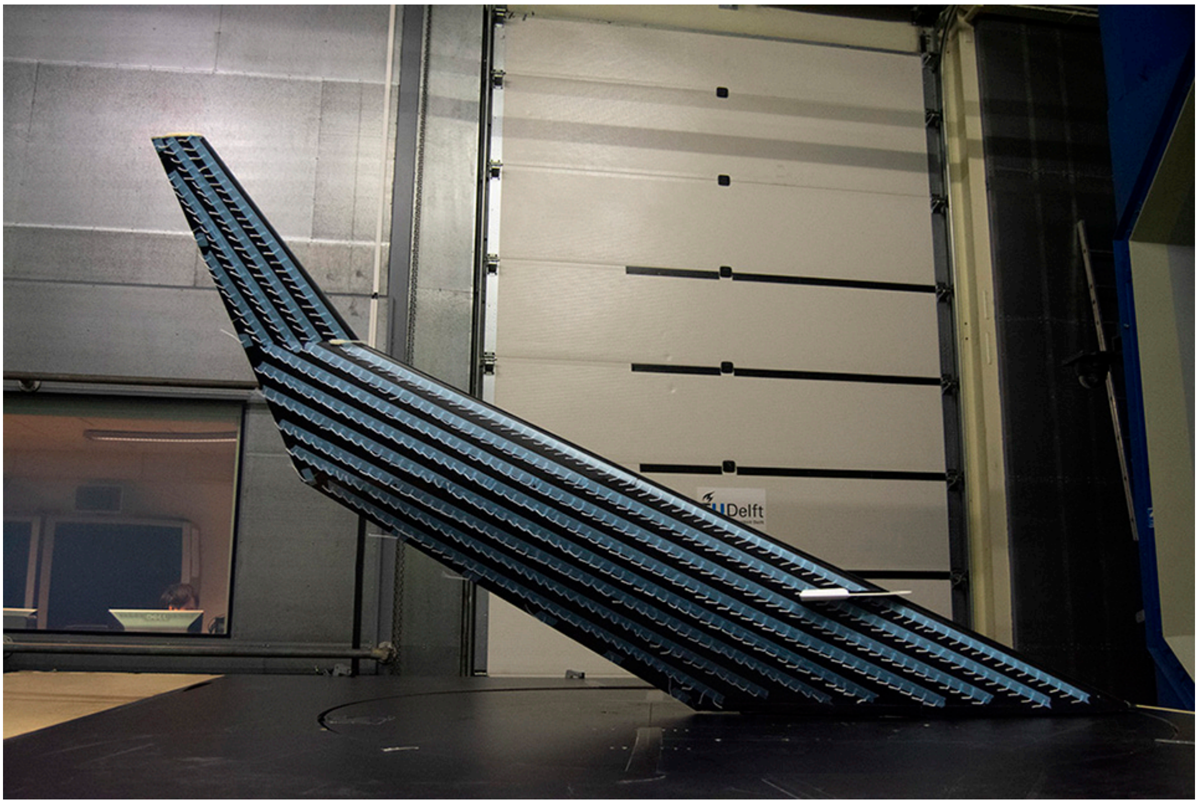

Figure A.37: Strip-on wing with fence 1b and fence 4b at $\alpha = 10^{\circ}$ and $V = 18.7$ m/s

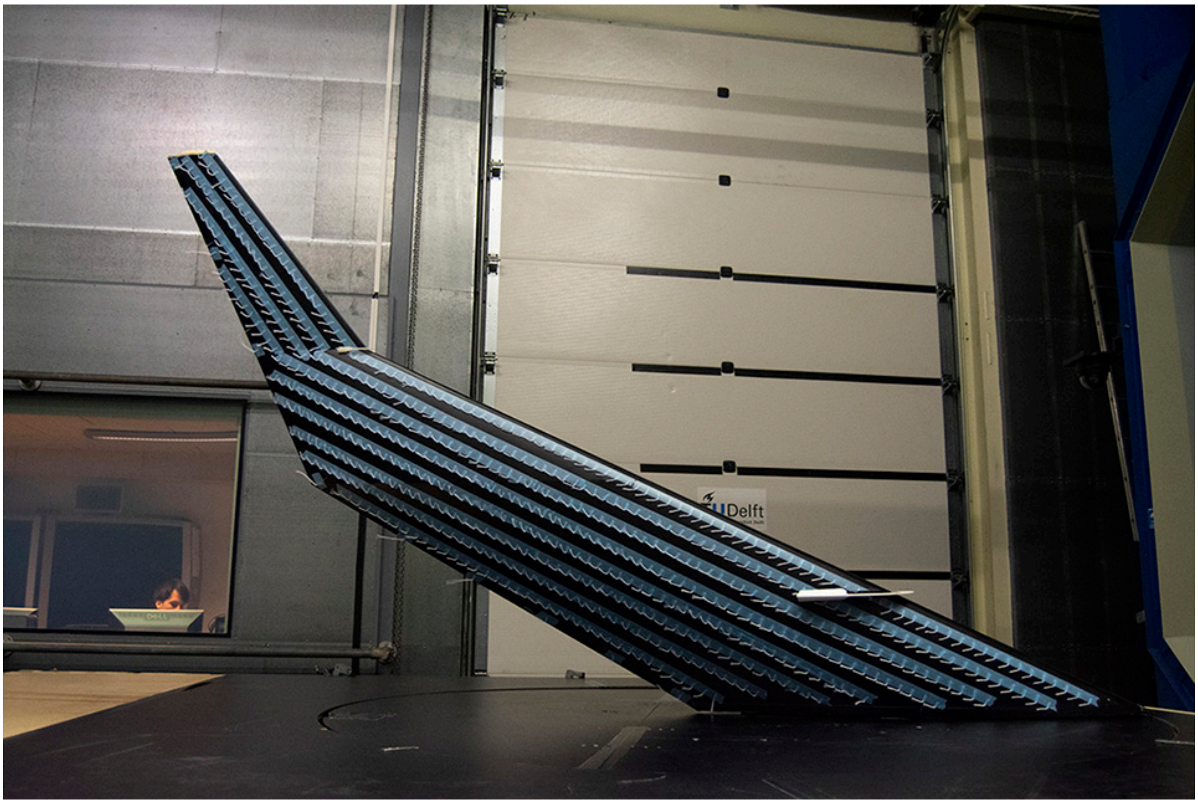

Figure A.38: Strip-on wing with fence 1b and fence 4b at $\alpha = 15^{\circ}$ and $V = 18.7$ m/s

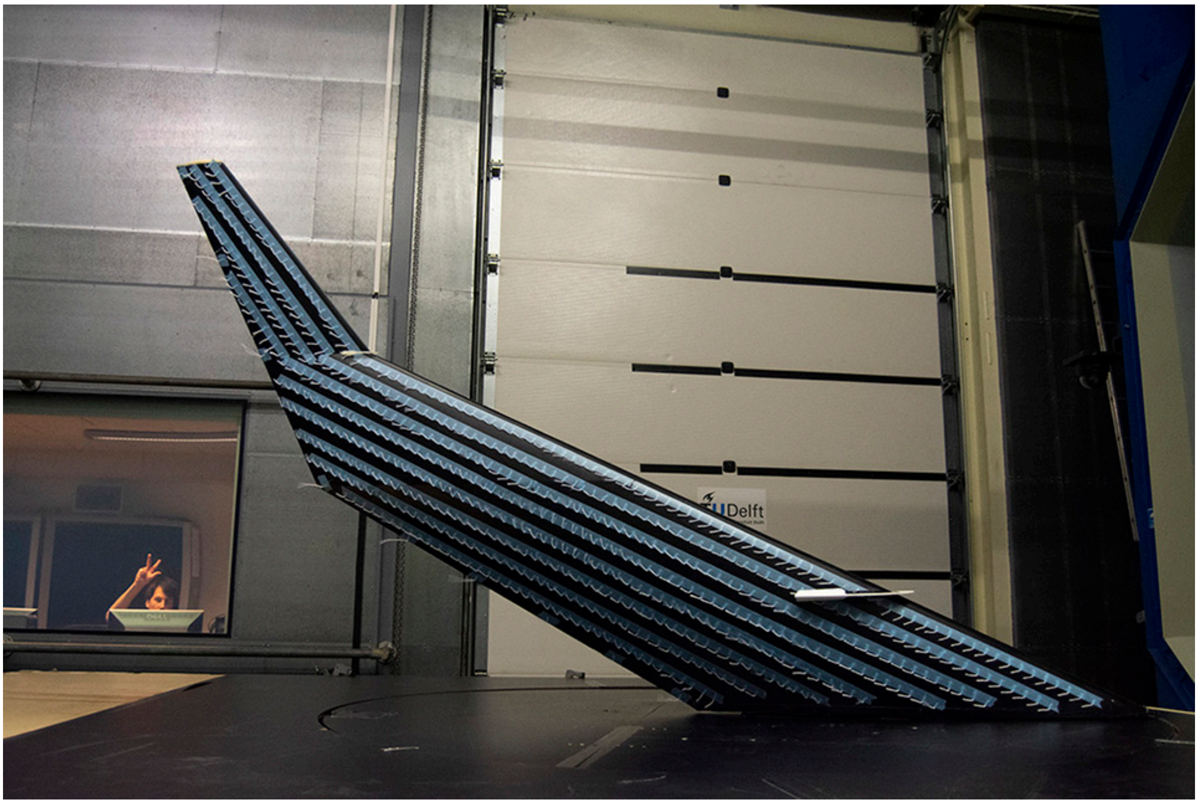

Figure A.39: Strip-on wing with fence 1b and fence 4b at $\alpha = 17.5^{\circ}$ and $V = 18.7$ m/s

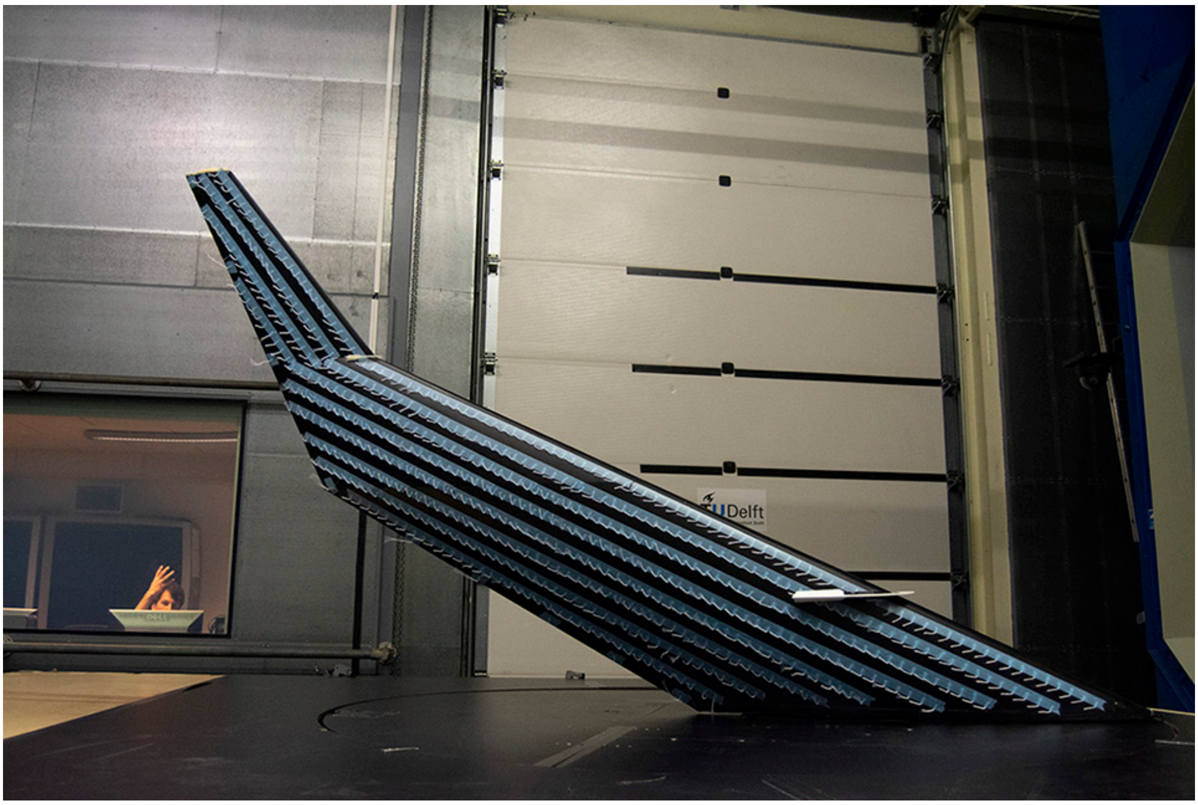

Figure A.40: Strip-on wing with fence 1b and fence 4b at $\alpha = 20^{\circ}$ and $V = 18.7$ m/s

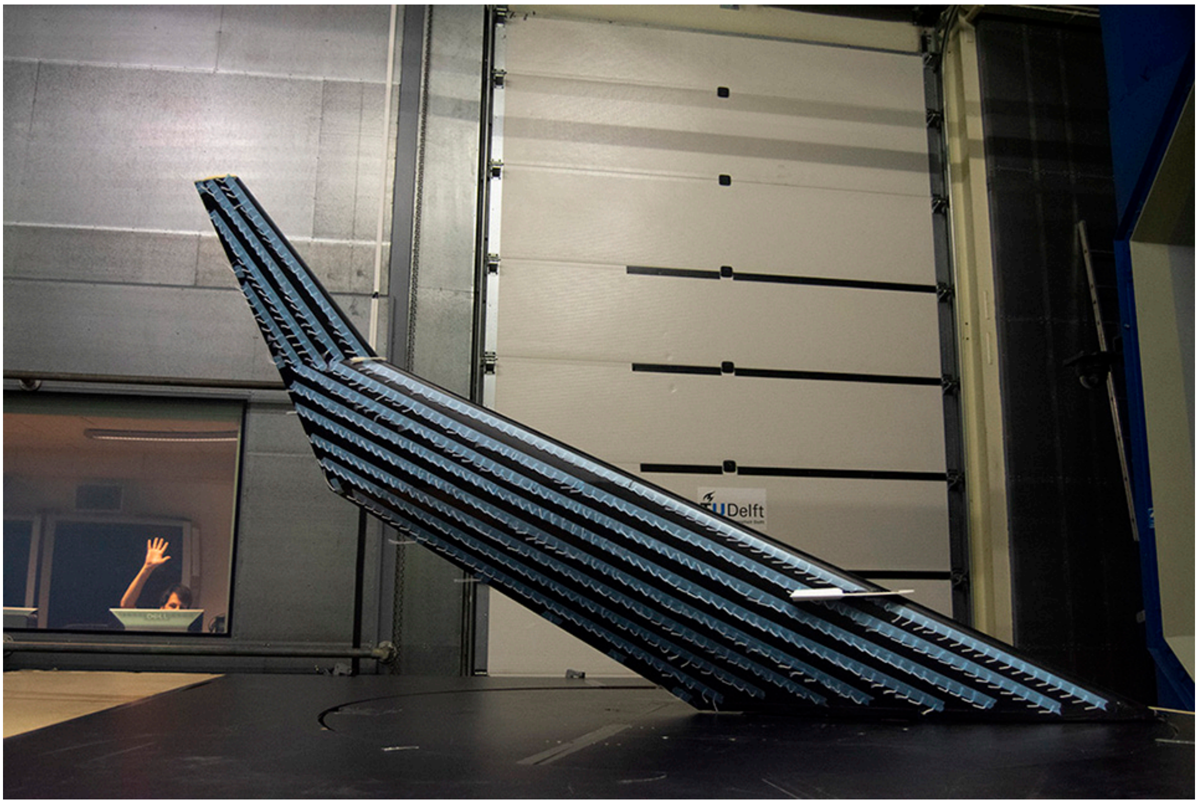

Figure A.41: Strip-on wing with fence 1b and fence 4b at $\alpha = 22^{\circ}$ and $V = 18.7$ m/s

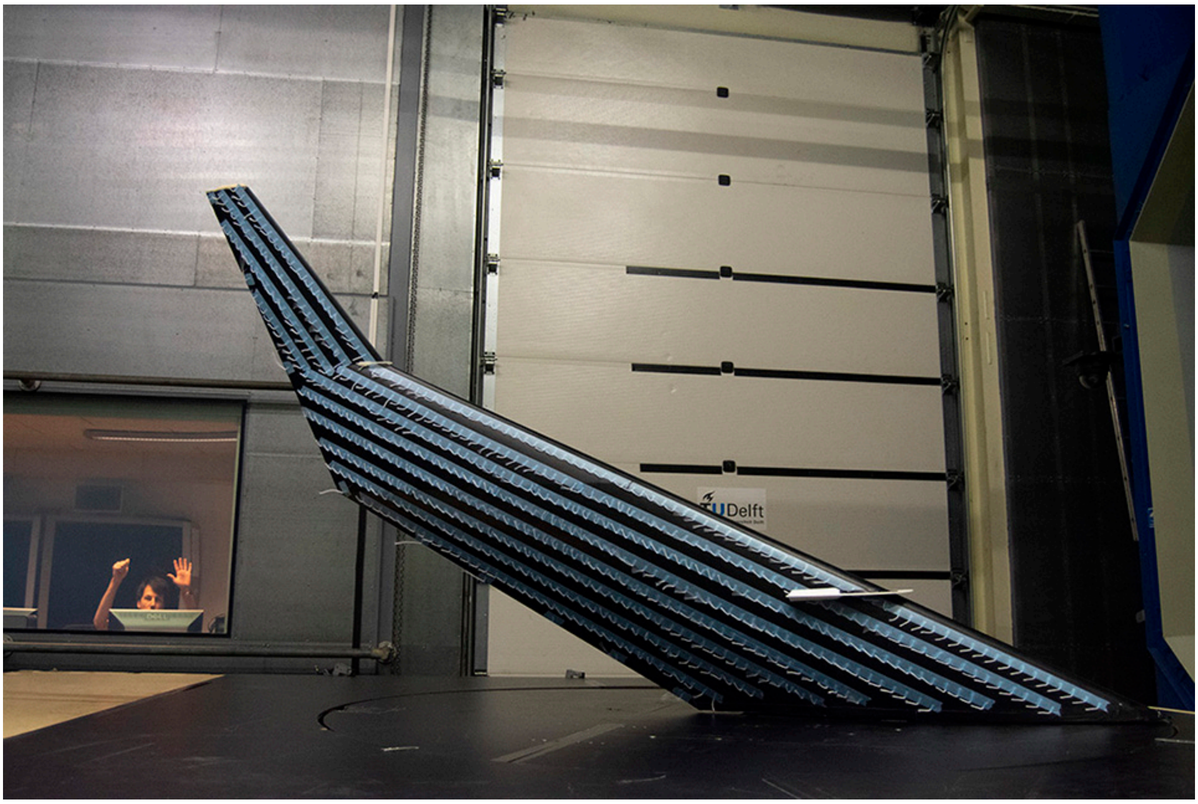

Figure A.42: Strip-on wing with fence 1b and fence 4b at $\alpha = 25^{\circ}$ and $V = 18.7$ m/s

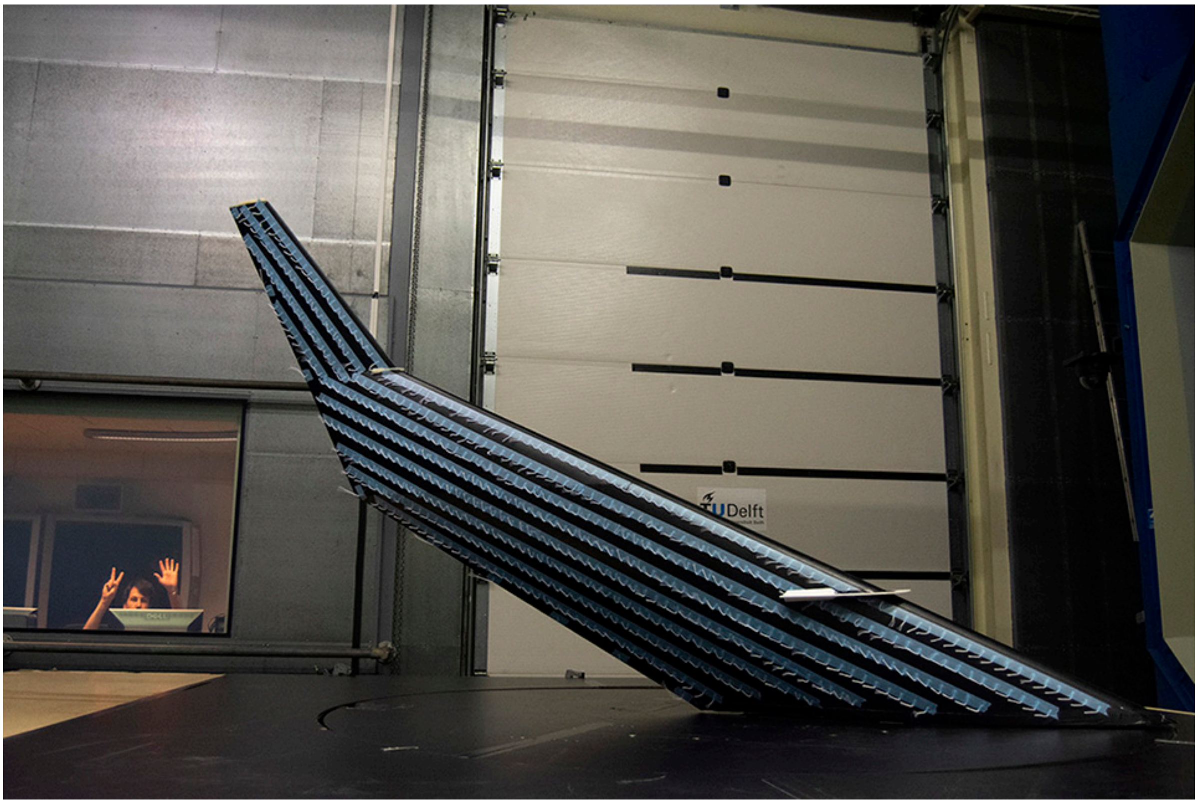

Figure A.43: Strip-on wing with fence 1b and fence 4b at $\alpha = 30^{\circ}$ and $V = 18.7$ m/s

A.7. Strip-on Wing + Vortilon 2

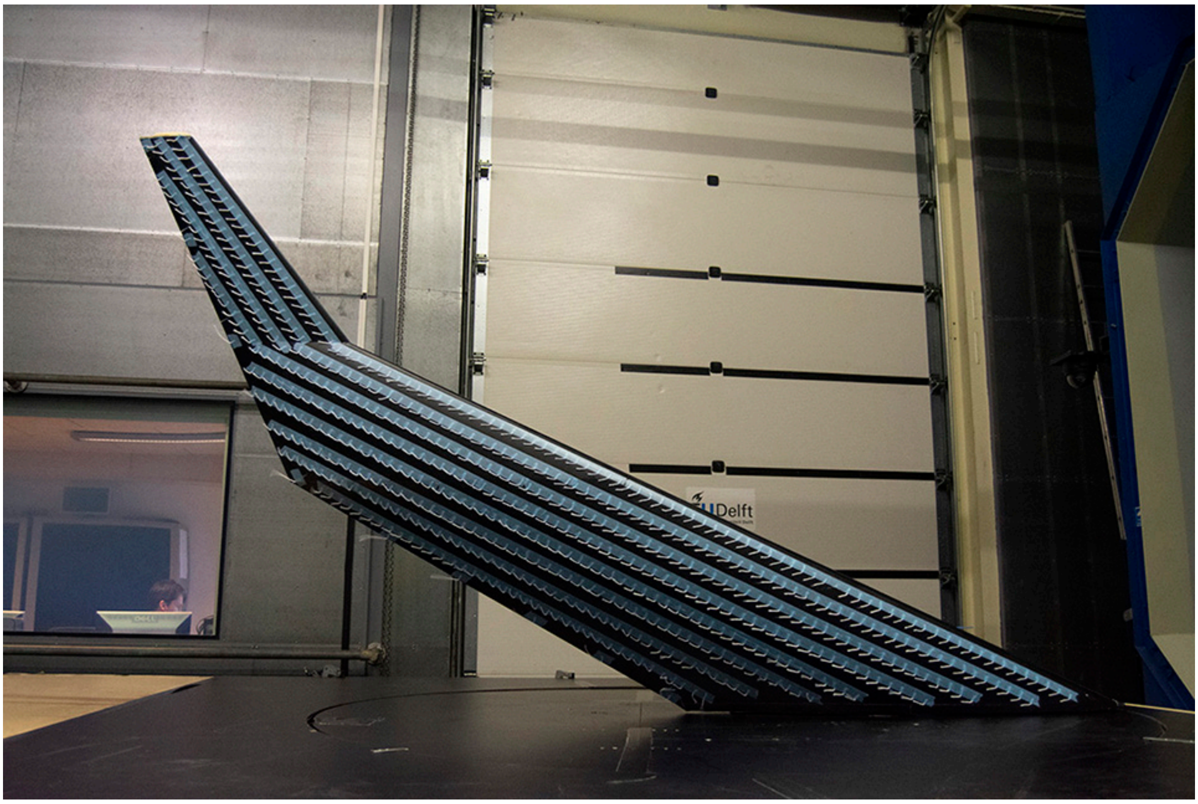

Figure A.44: Strip-on wing with vortilon 2 at $\alpha = 10^{\circ}$ and $V = 18.7$ m/s

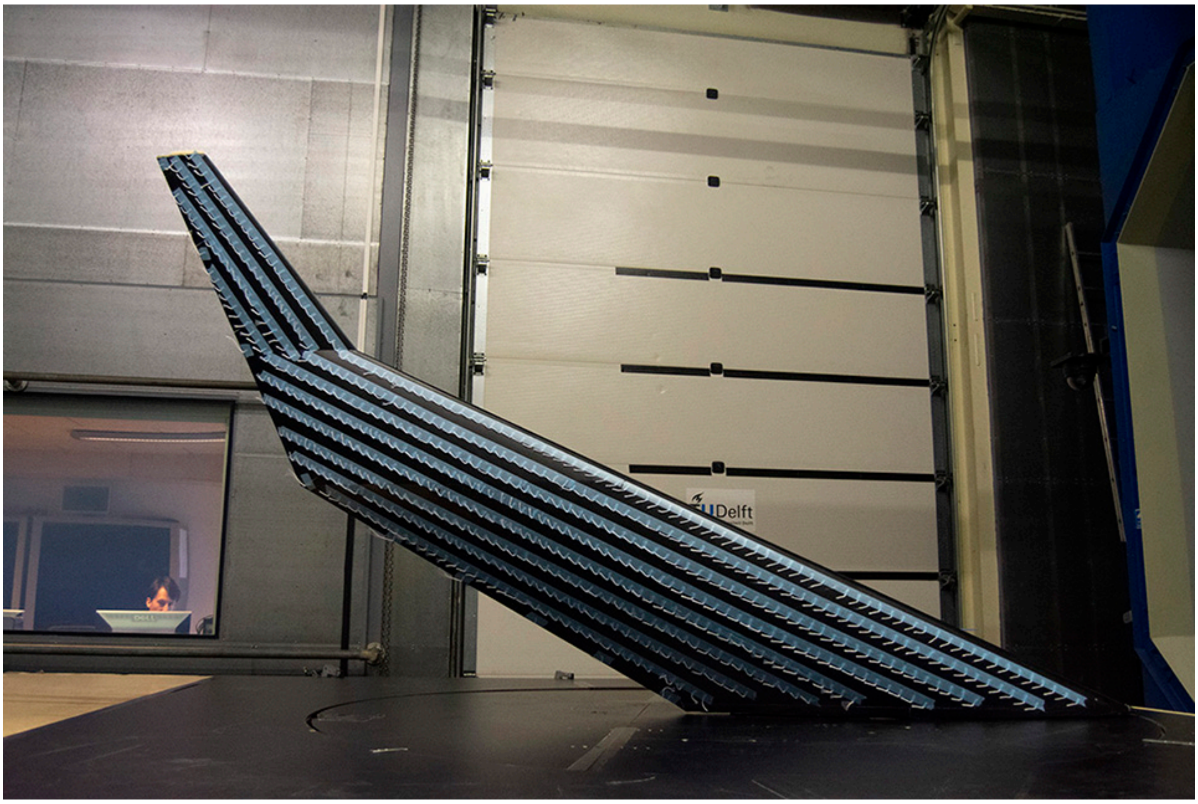

Figure A.45: Strip-on wing with vortilon 2 at $\alpha = 15°$ and $V = 18.7$ m/s

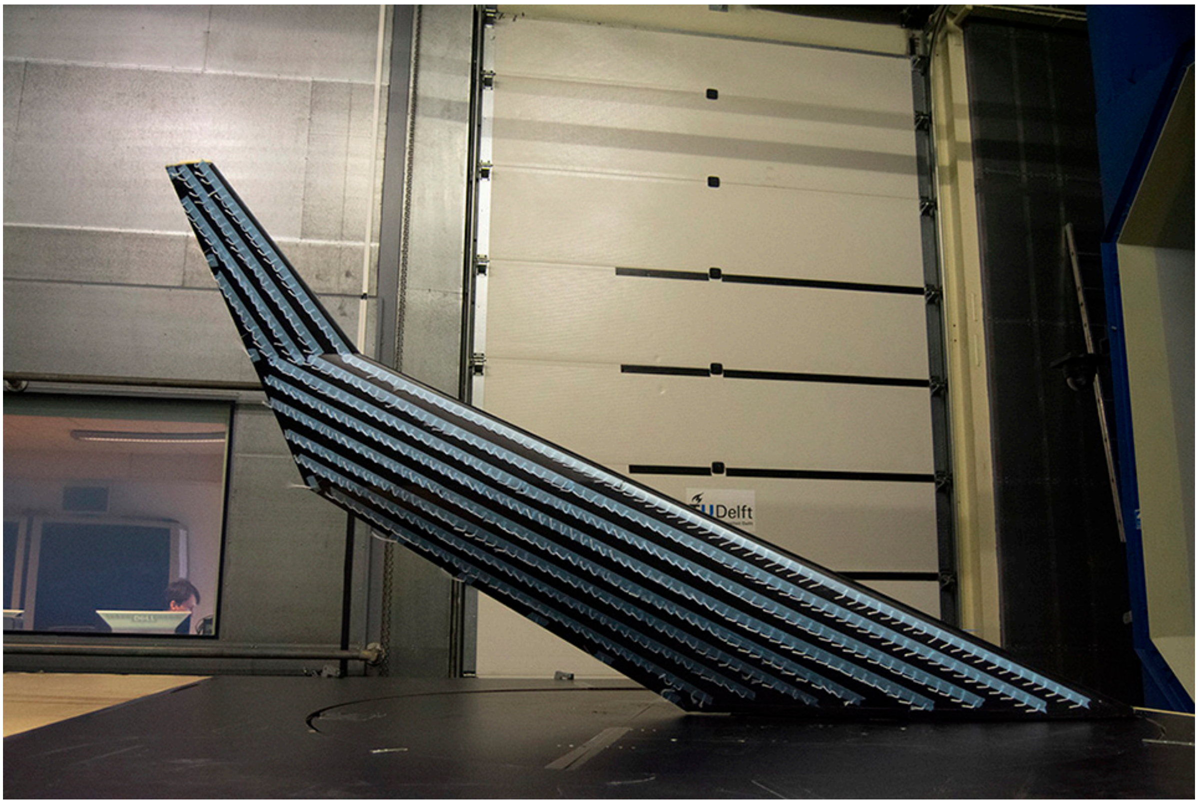

Figure A.46: Strip-on wing with vortilon 2 at $\alpha = 17.5°$ and $V = 18.7$ m/s

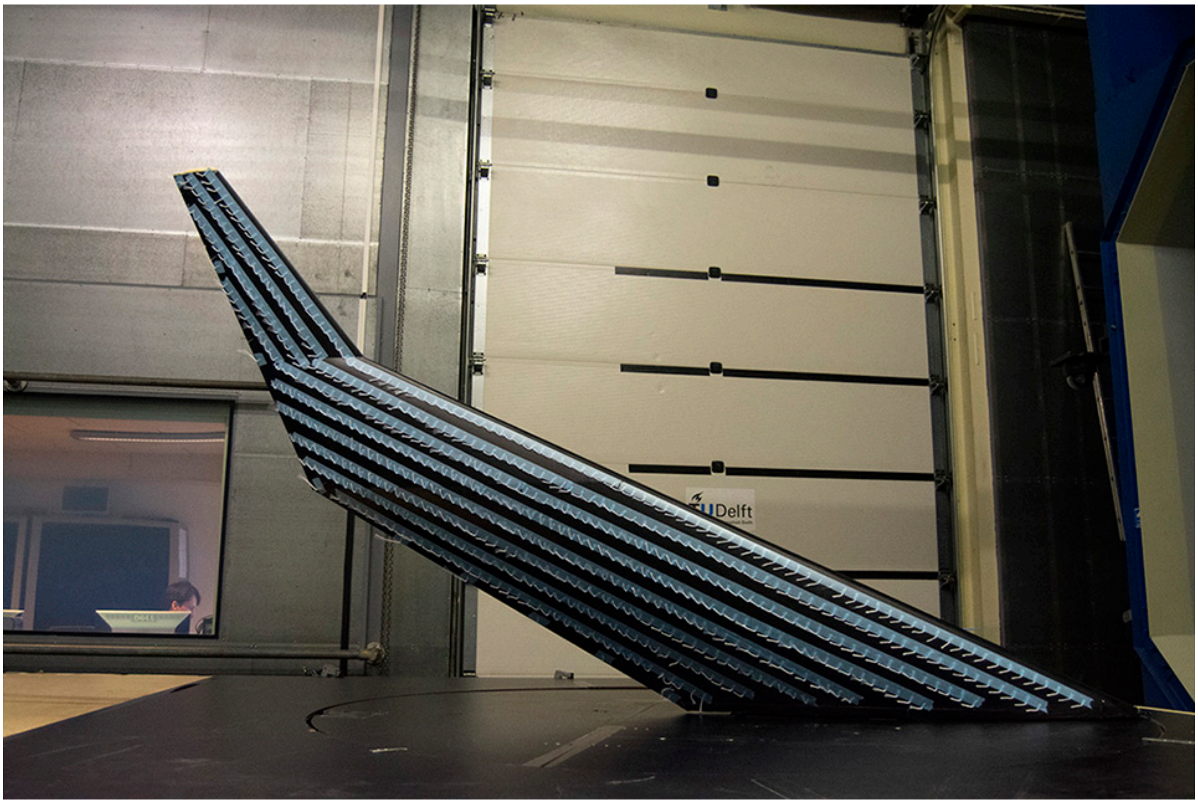

Figure A.47: Strip-on wing with vortilon 2 at $\alpha = 20^\circ$ and $V = 18.7$ m/s

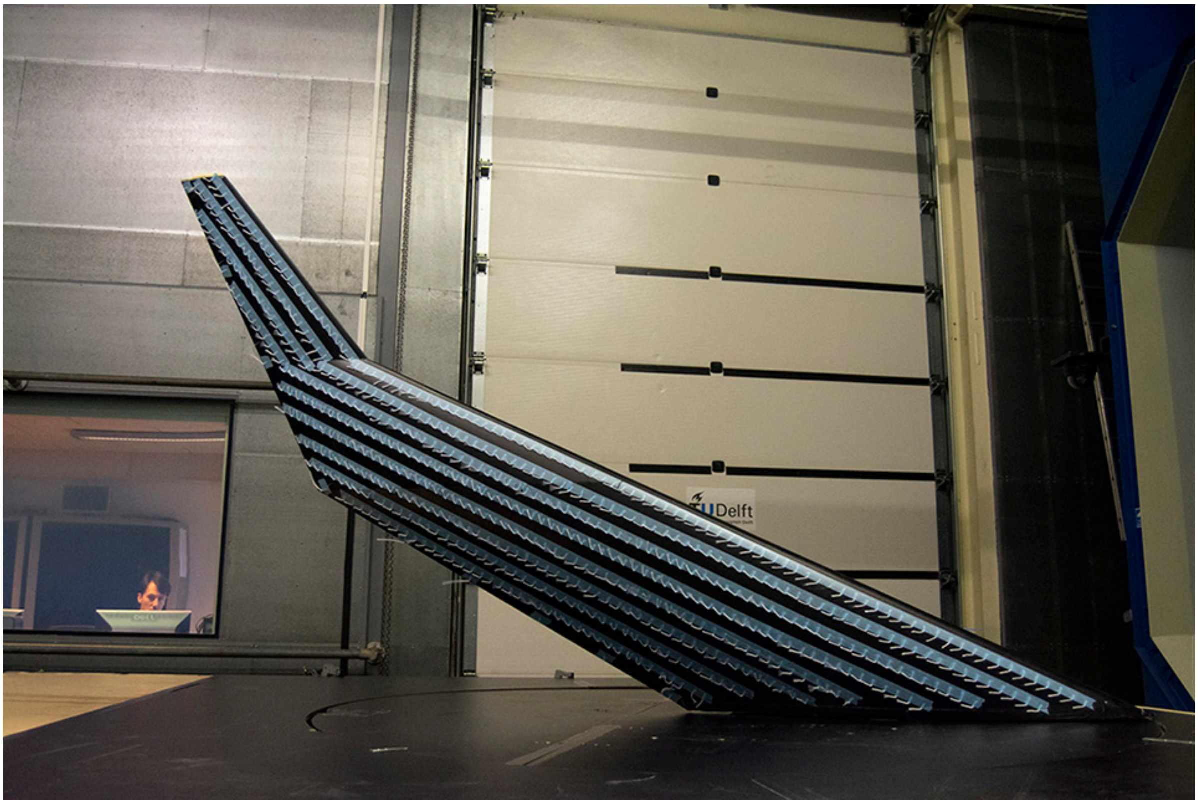

Figure A.48: Strip-on wing with vortilon 2 at $\alpha = 22^\circ$ and $V = 18.7$ m/s

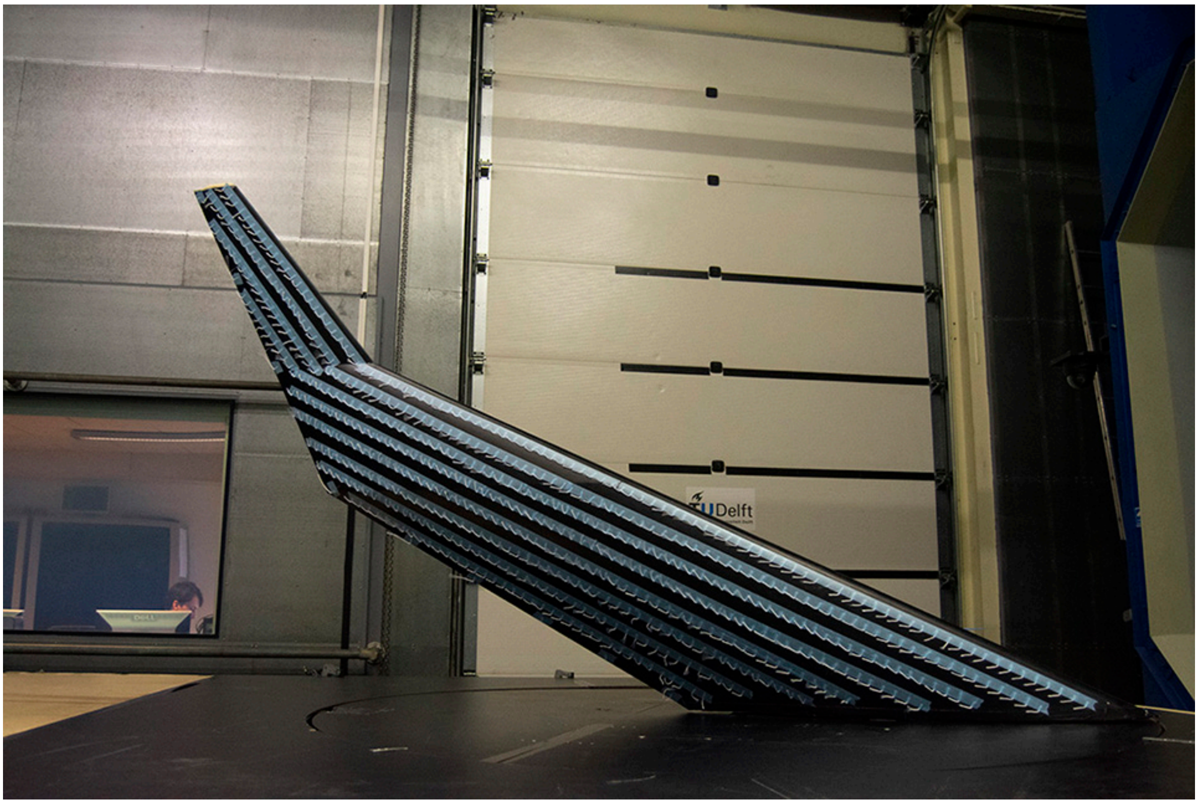

Figure A.49: Strip-on wing with vortilon 2 at $\alpha = 25^{\circ}$ and $V = 18.7$ m/s

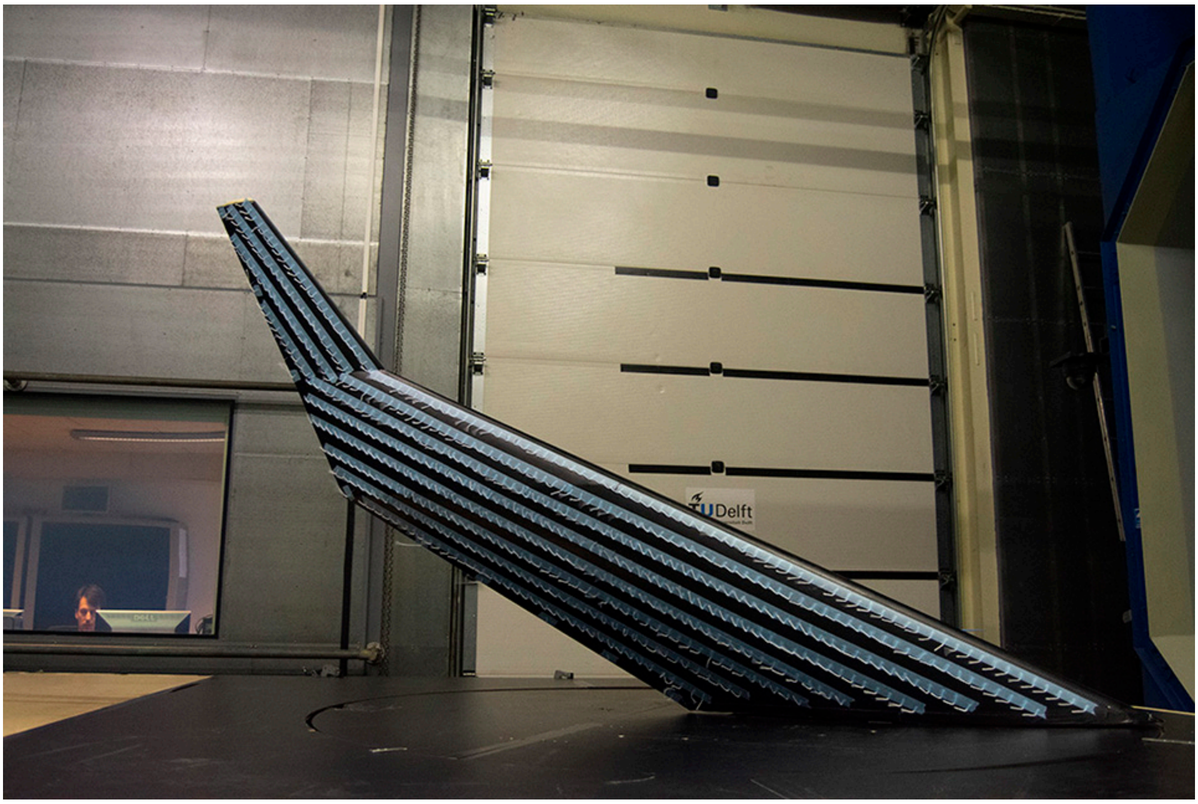

Figure A.50: Strip-on wing with vortilon 2 at $\alpha = 30^{\circ}$ and $V = 18.7$ m/s

A.8. Strip-on Wing + Vortilon 8

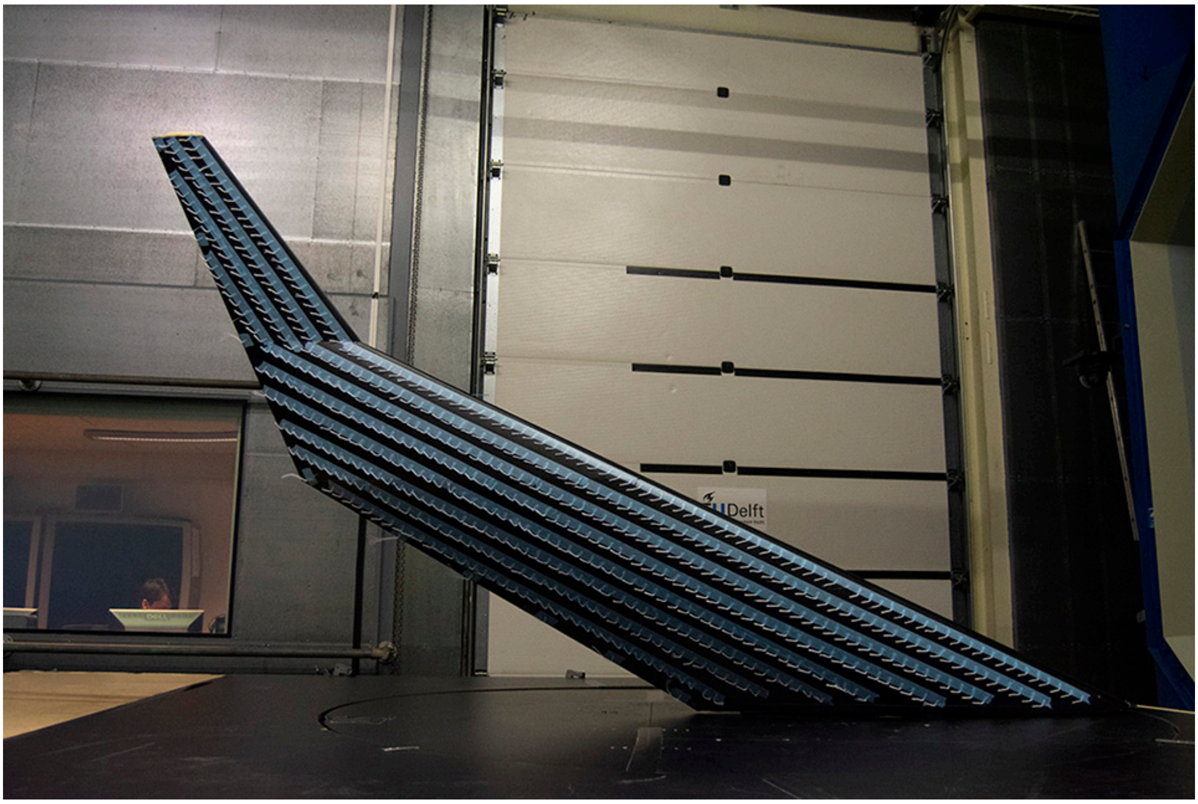

Figure A.51: Strip-on wing with vortilon 8 at $\alpha = 10^{\circ}$ and $V = 18.7$ m/s

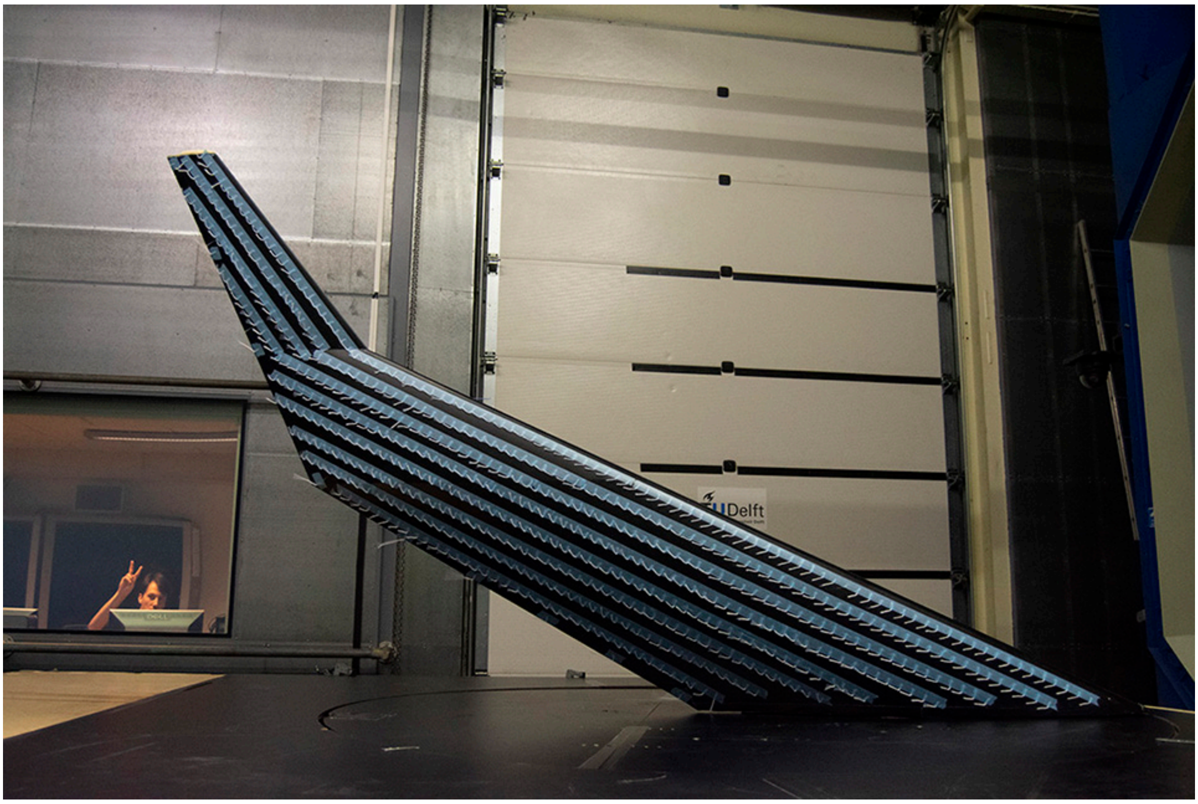

Figure A.52: Strip-on wing with vortilon 8 at $\alpha = 15^{\circ}$ and $V = 18.7$ m/s

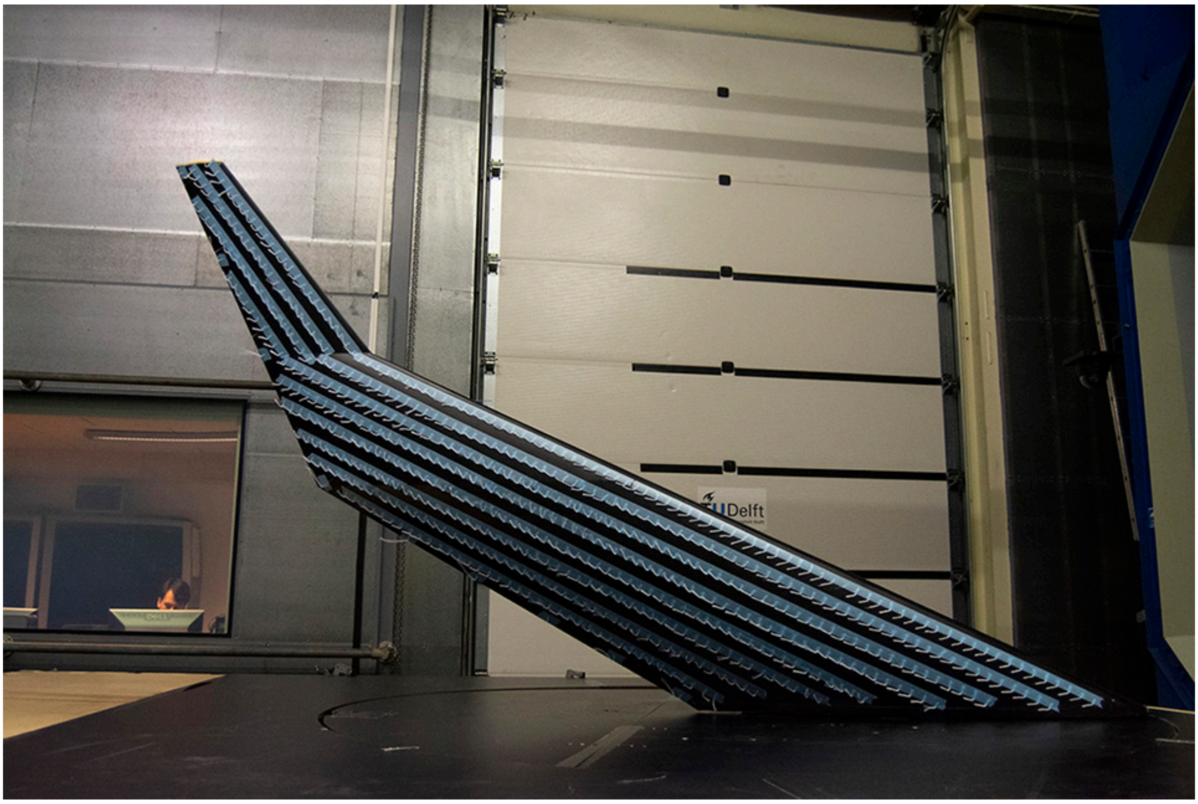

Figure A.53: Strip-on wing with vortilon 8 at $\alpha = 17.5^{\circ}$ and $V = 18.7$ m/s

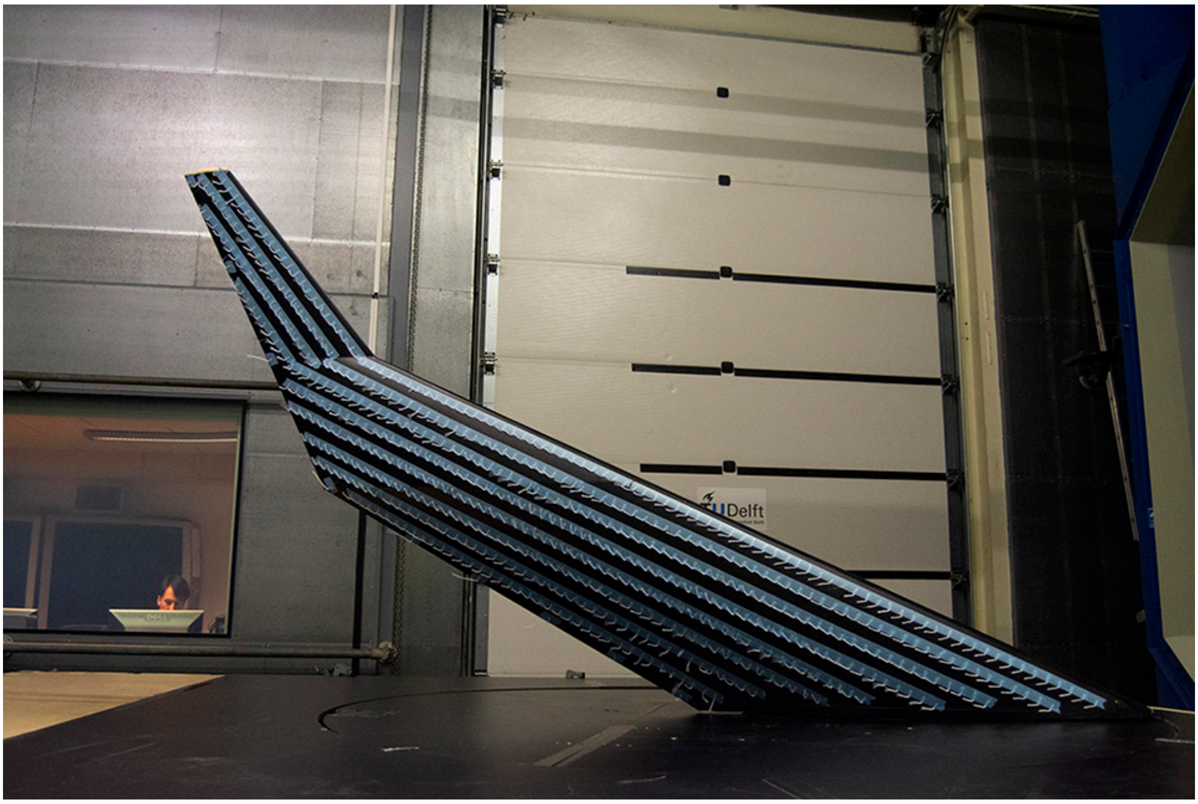

Figure A.54: Strip-on wing with vortilon 8 at $\alpha = 20^{\circ}$ and $V = 18.7$ m/s

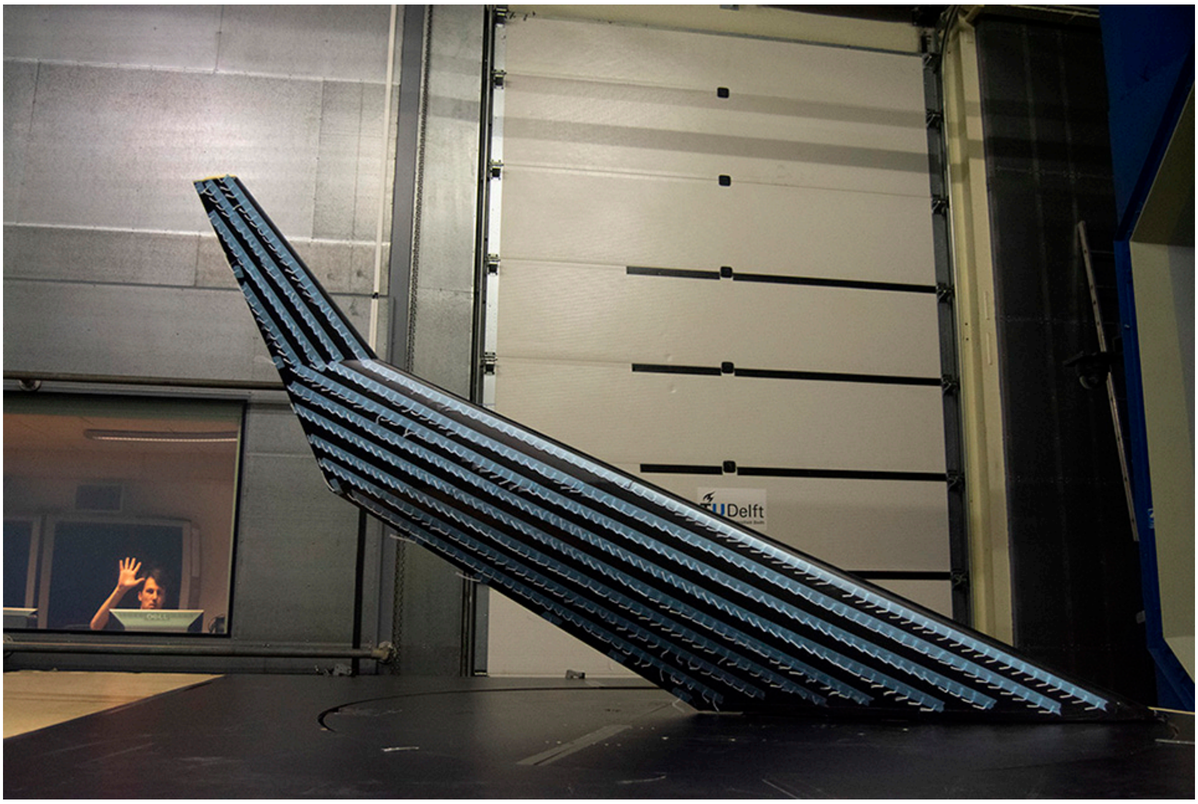

Figure A.55: Strip-on wing with vortilon 8 at $\alpha = 22^{\circ}$ and $V = 18.7$ m/s

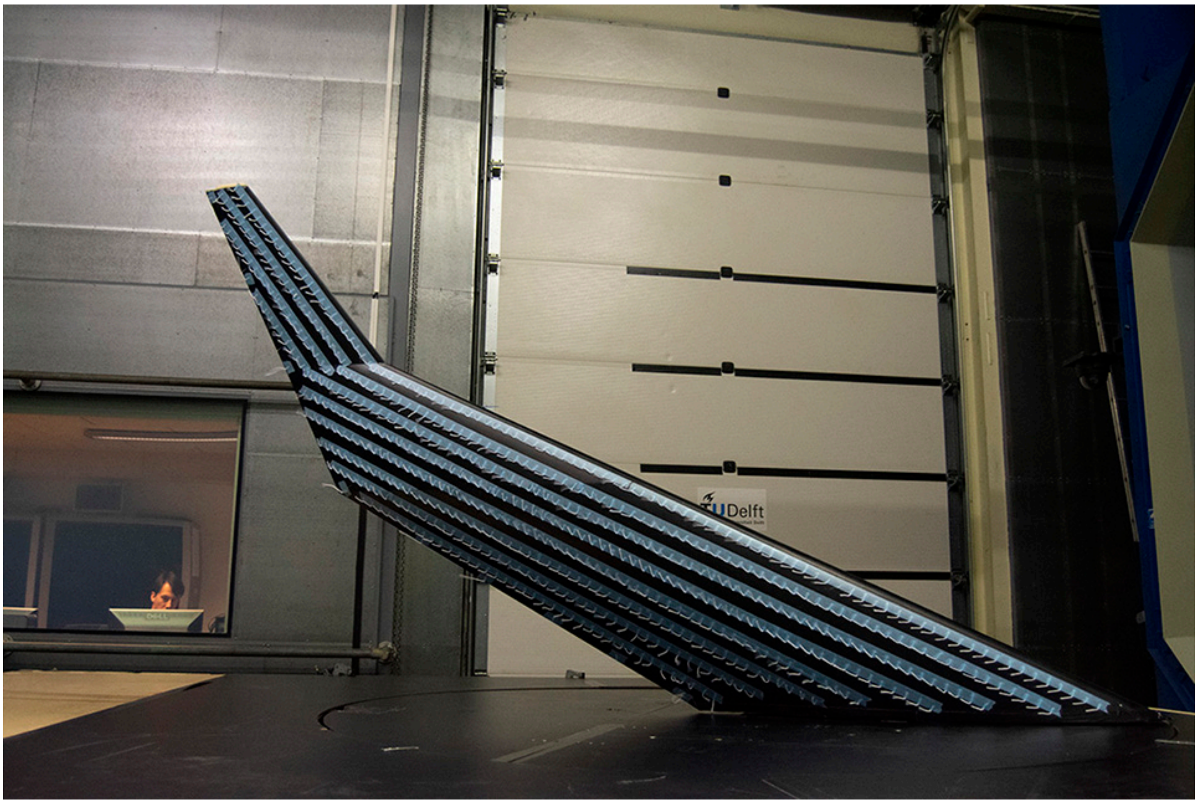

Figure A.56: Strip-on wing with vortilon 8 at $\alpha = 25^{\circ}$ and $V = 18.7$ m/s

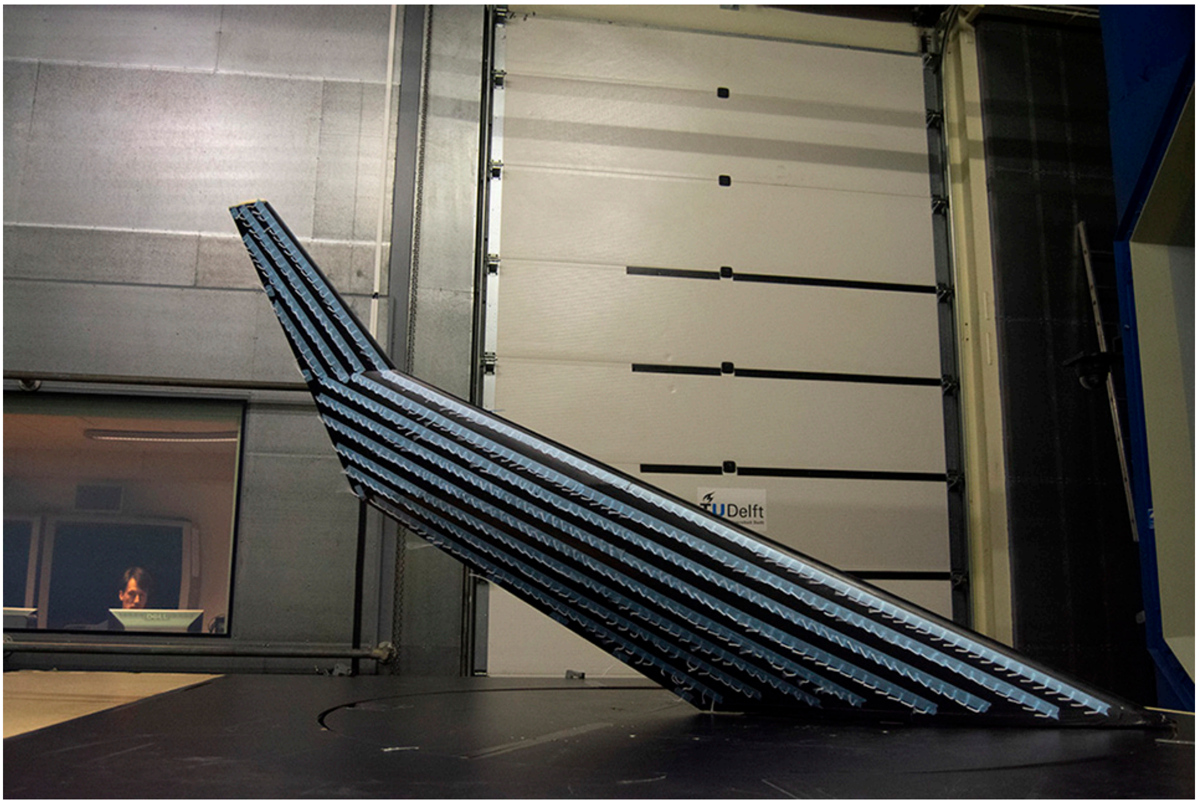

Figure A.57: Strip-on wing with vortilon 8 at $\alpha = 30^{\circ}$ and $V = 18.7$ m/s

A.9. Strip-on Wing + Vortilon 9

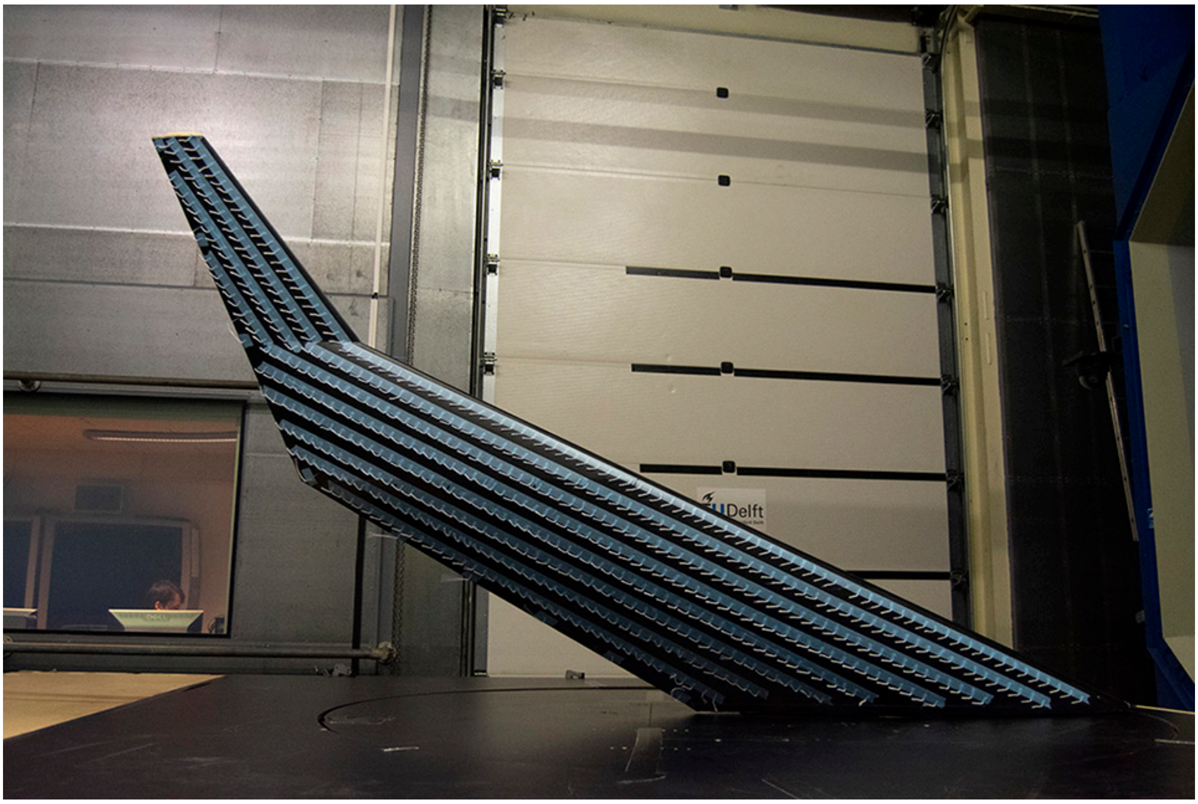

Figure A.58: Strip-on wing with vortilon 9 at $\alpha = 10^{\circ}$ and $V = 18.7$ m/s

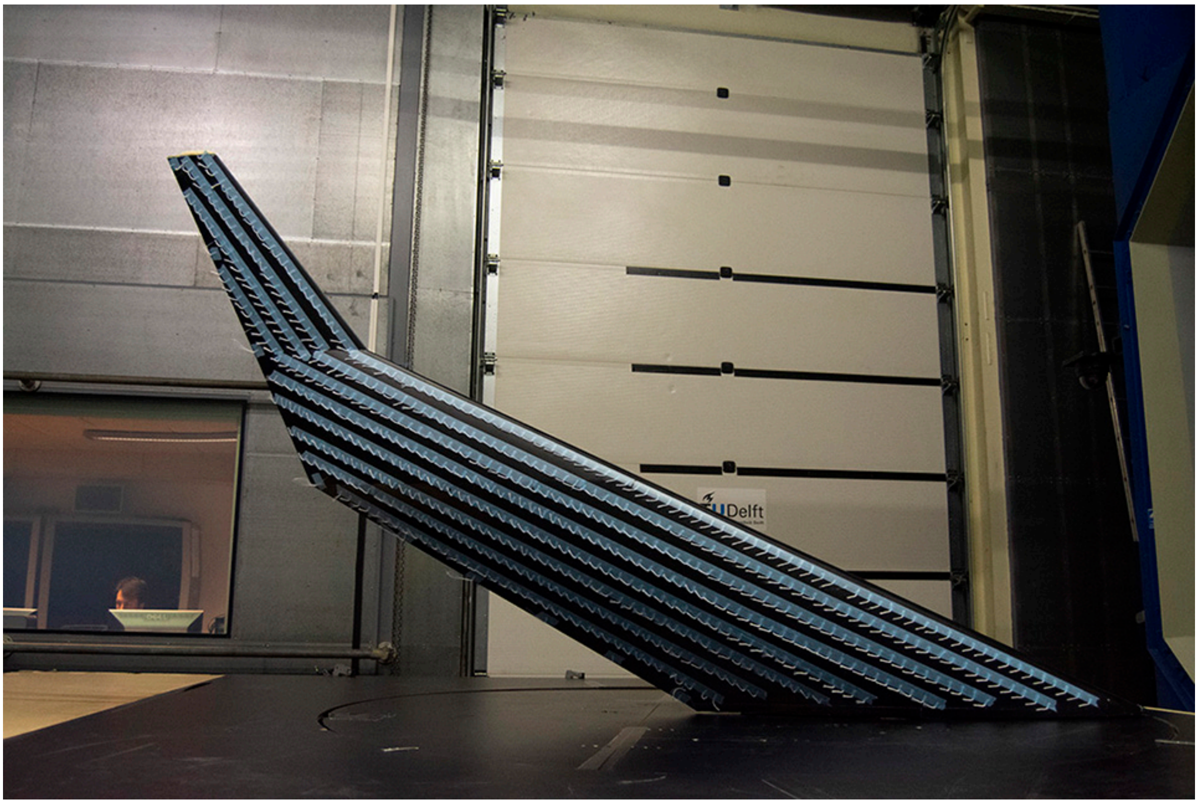

Figure A.59: Strip-on wing with vortilon 9 at $\alpha = 15°$ and $V = 18.7$ m/s

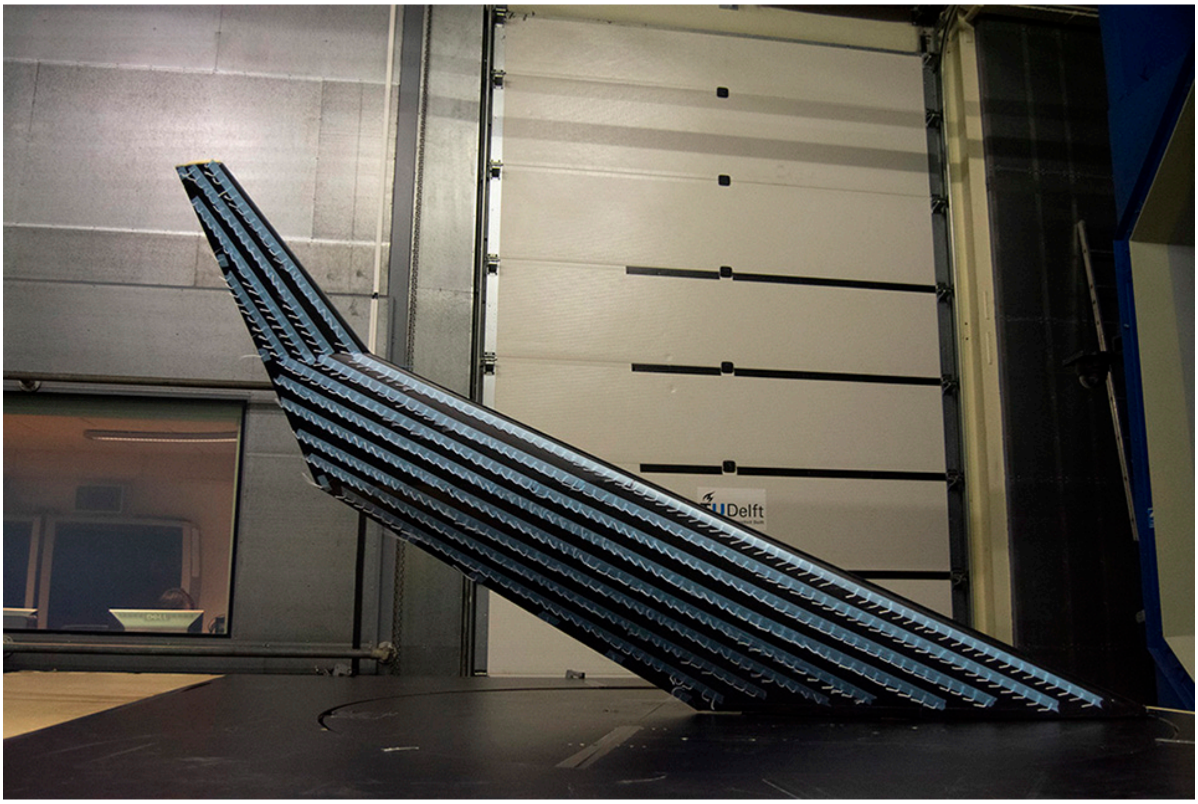

Figure A.60: Strip-on wing with vortilon 9 at $\alpha = 17.5°$ and $V = 18.7$ m/s

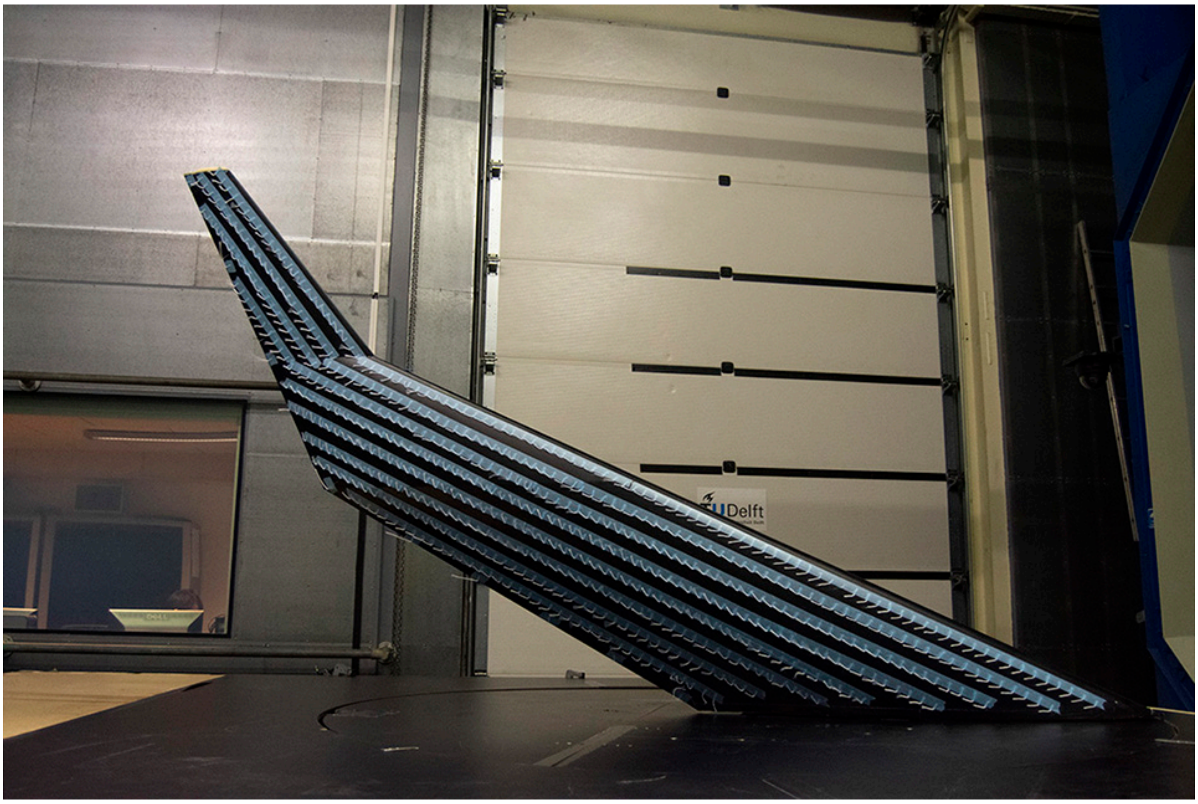

Figure A.61: Strip-on wing with vortilon 9 at $\alpha = 20^{\circ}$ and $V = 18.7$ m/s

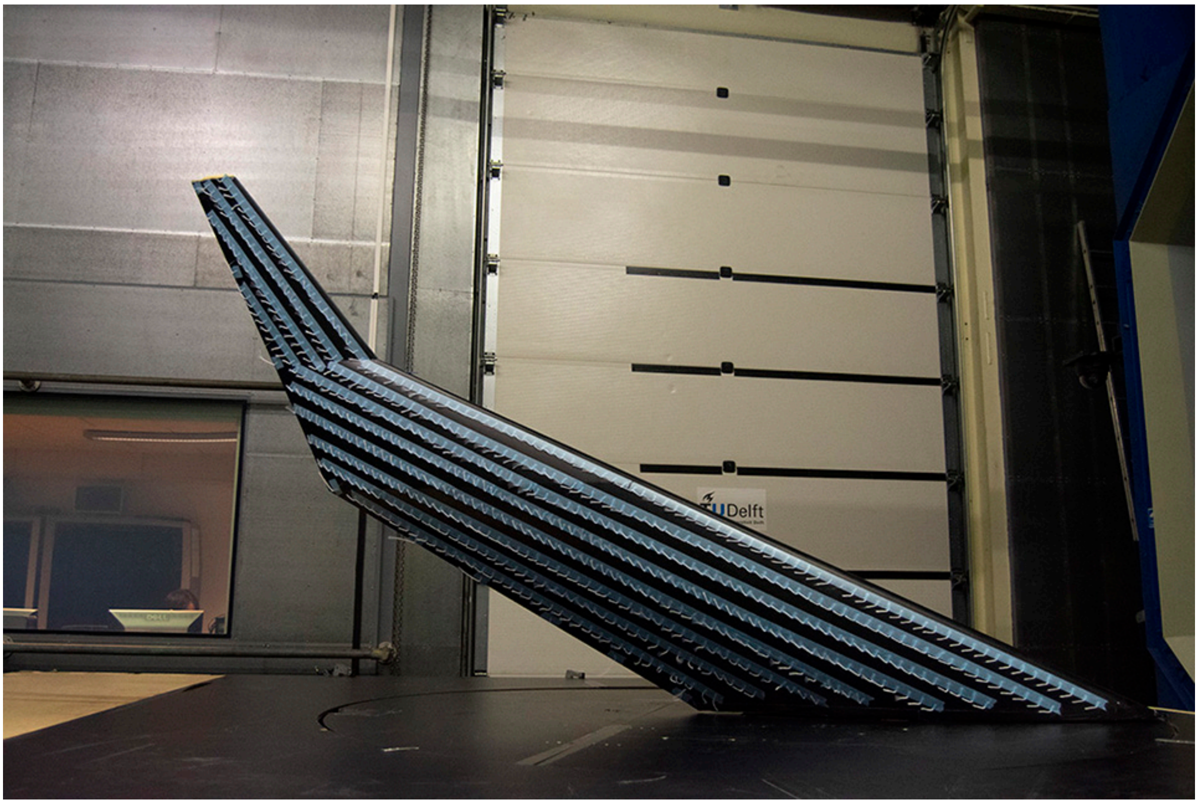

Figure A.62: Strip-on wing with vortilon 9 at $\alpha = 22^{\circ}$ and $V = 18.7$ m/s

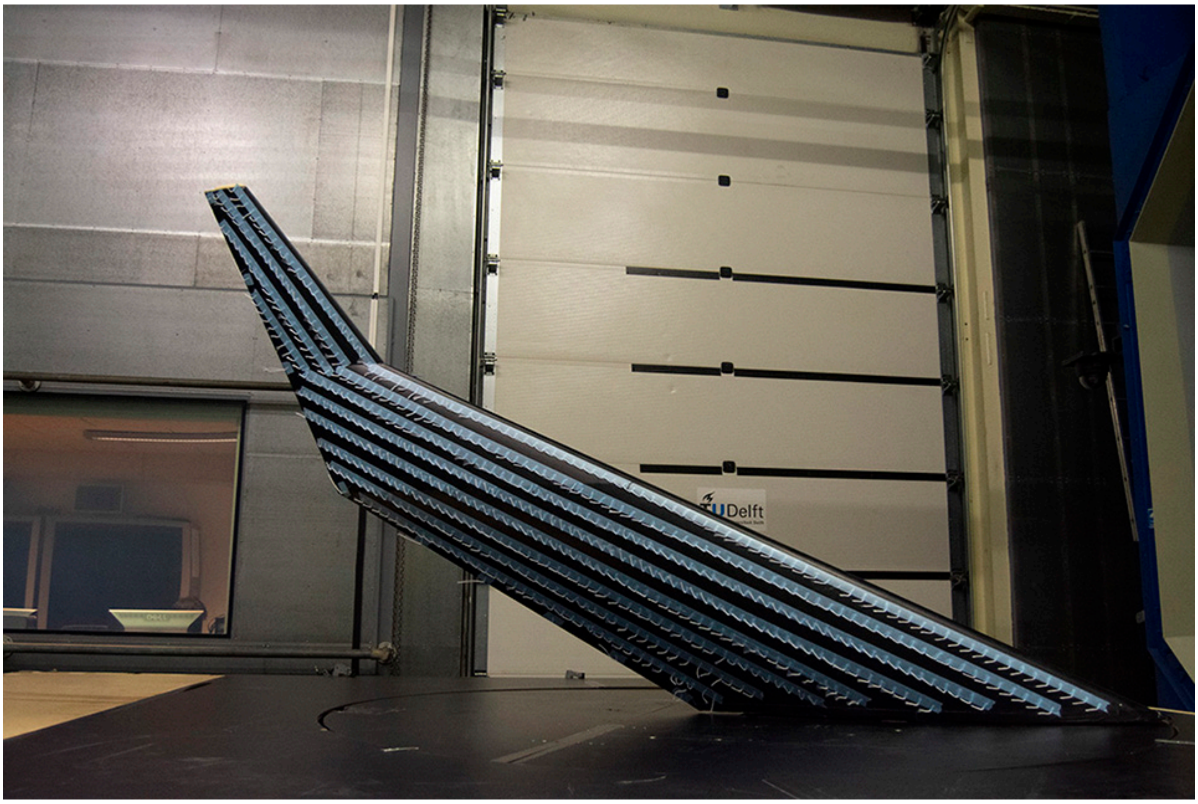

Figure A.63: Strip-on wing with vortilon 9 at $\alpha = 25°$ and $V = 18.7$ m/s

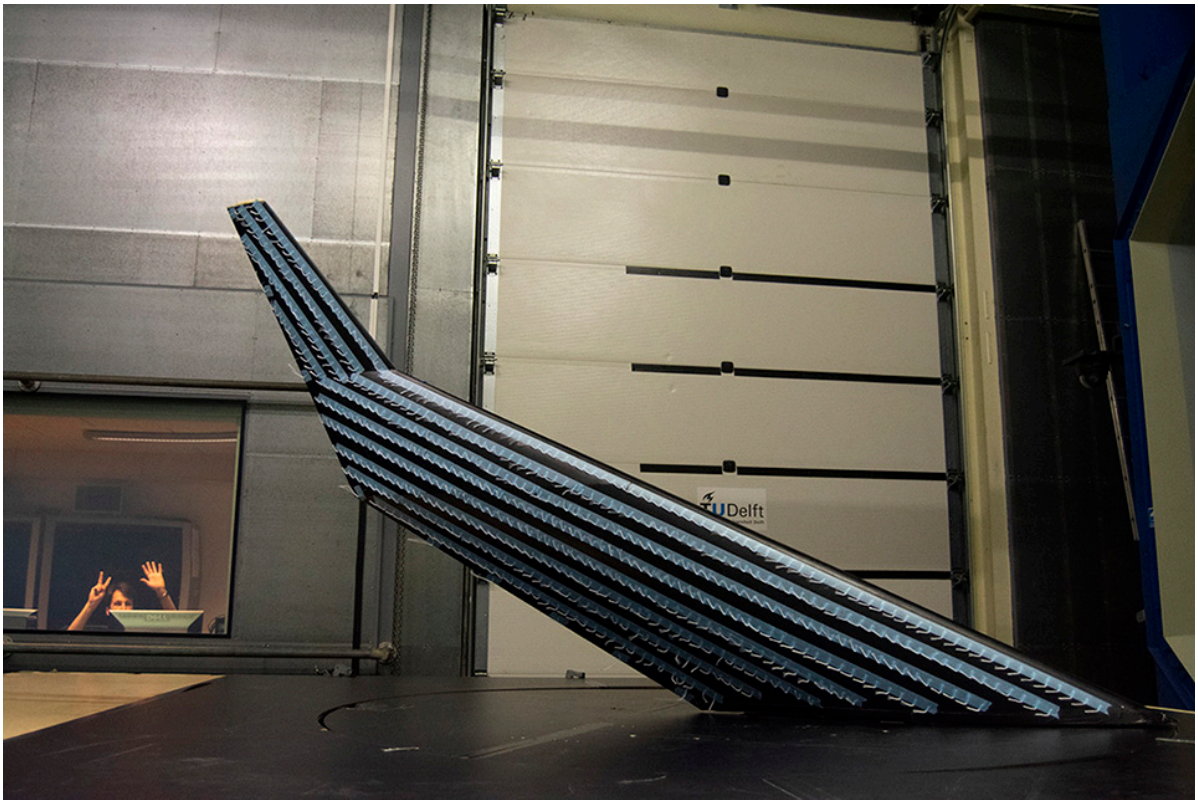

Figure A.64: Strip-on wing with vortilon 9 at $\alpha = 30°$ and $V = 18.7$ m/s

A.10. Strip-on Wing + Vortilon 2 and Vortilon 9

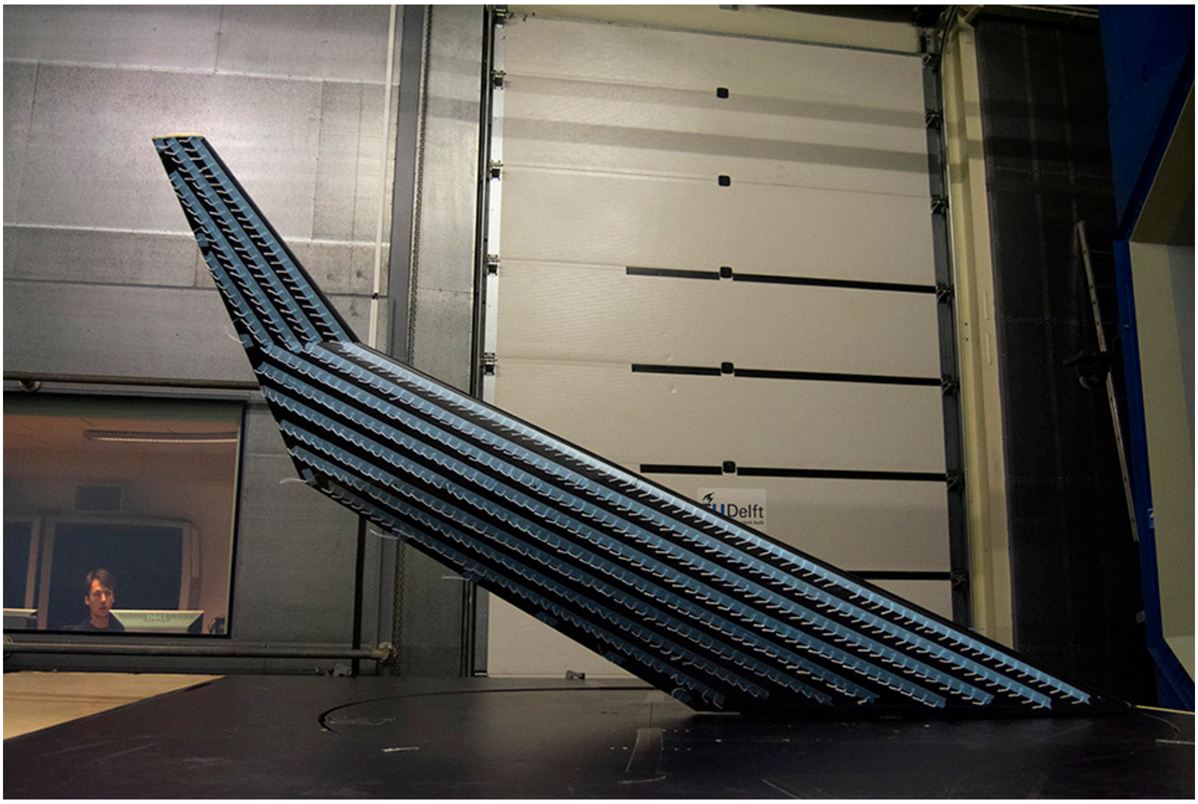

Figure A.65: Strip-on wing with vortilon 2 and vortilon 9 at $\alpha = 10^{\circ}$ and $V = 18.7$ m/s

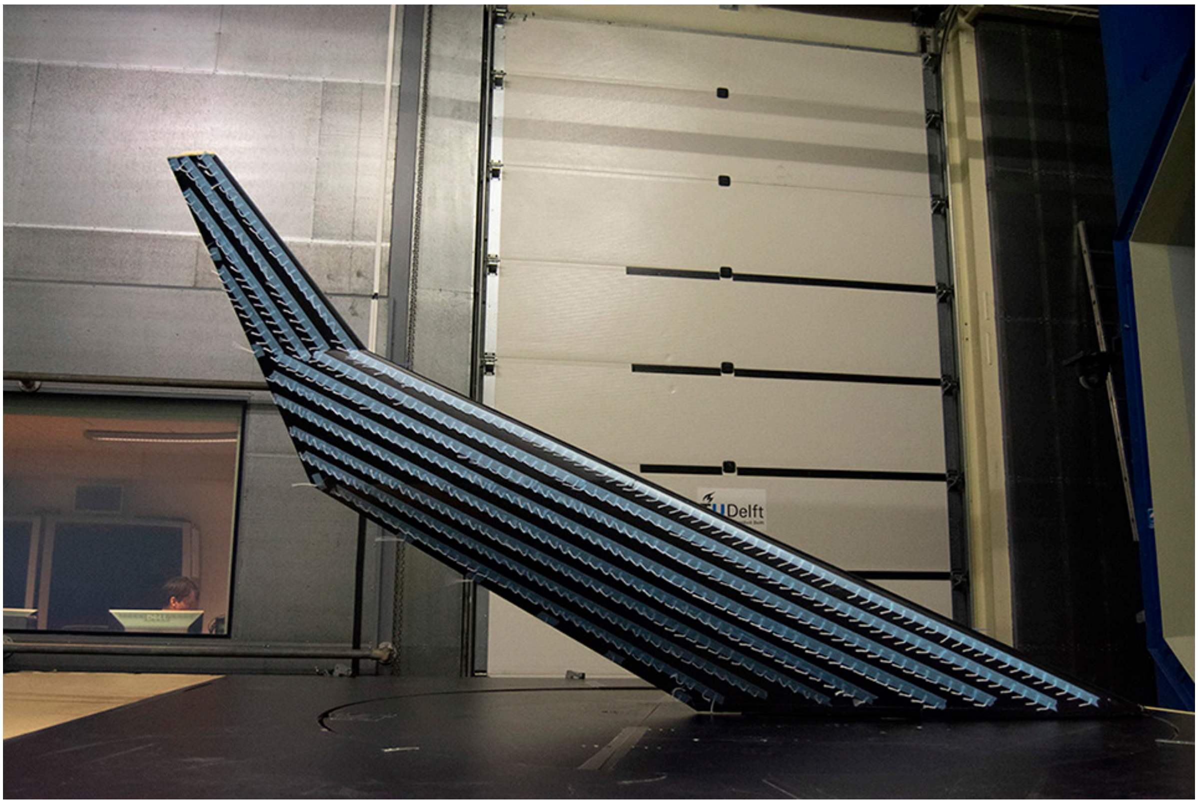

Figure A.66: Strip-on wing with vortilon 2 and vortilon 9 at $\alpha = 15^{\circ}$ and $V = 18.7$ m/s

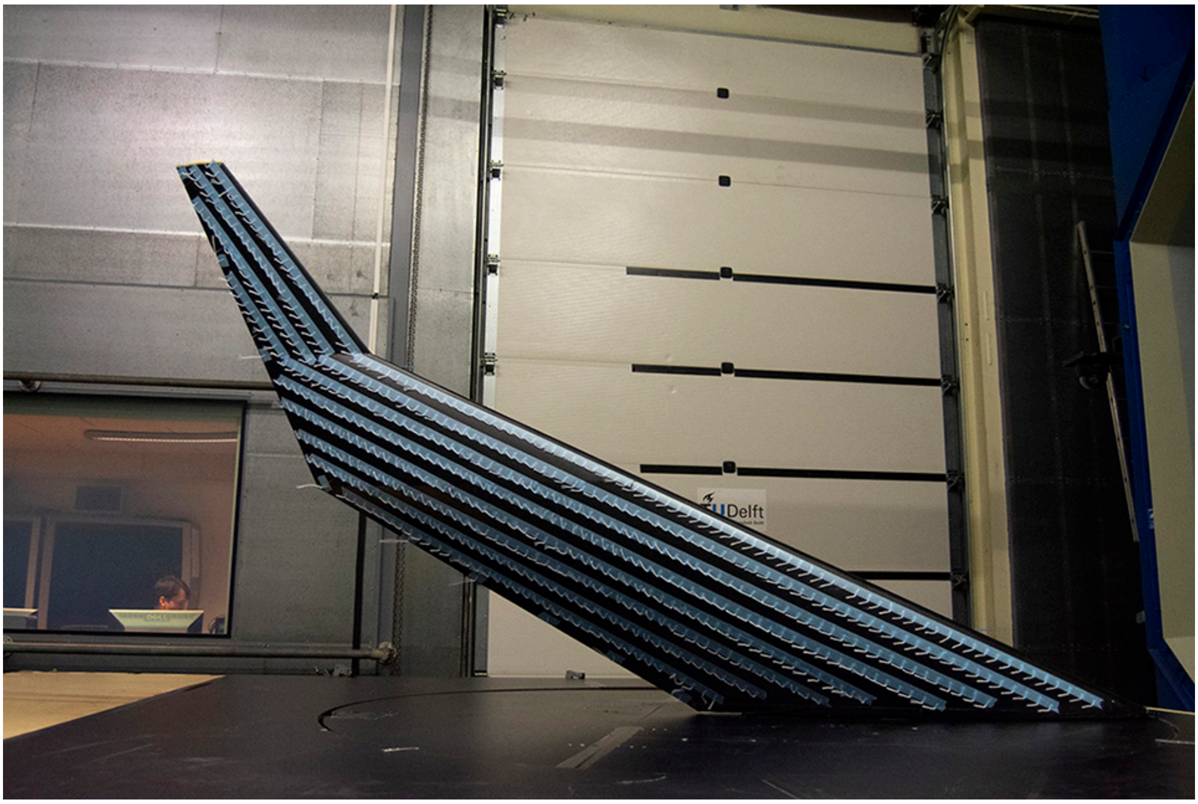

Figure A.67: Strip-on wing with vortilon 2 and vortilon 9 at $\alpha = 17.5^{\circ}$ and $V = 18.7$ m/s

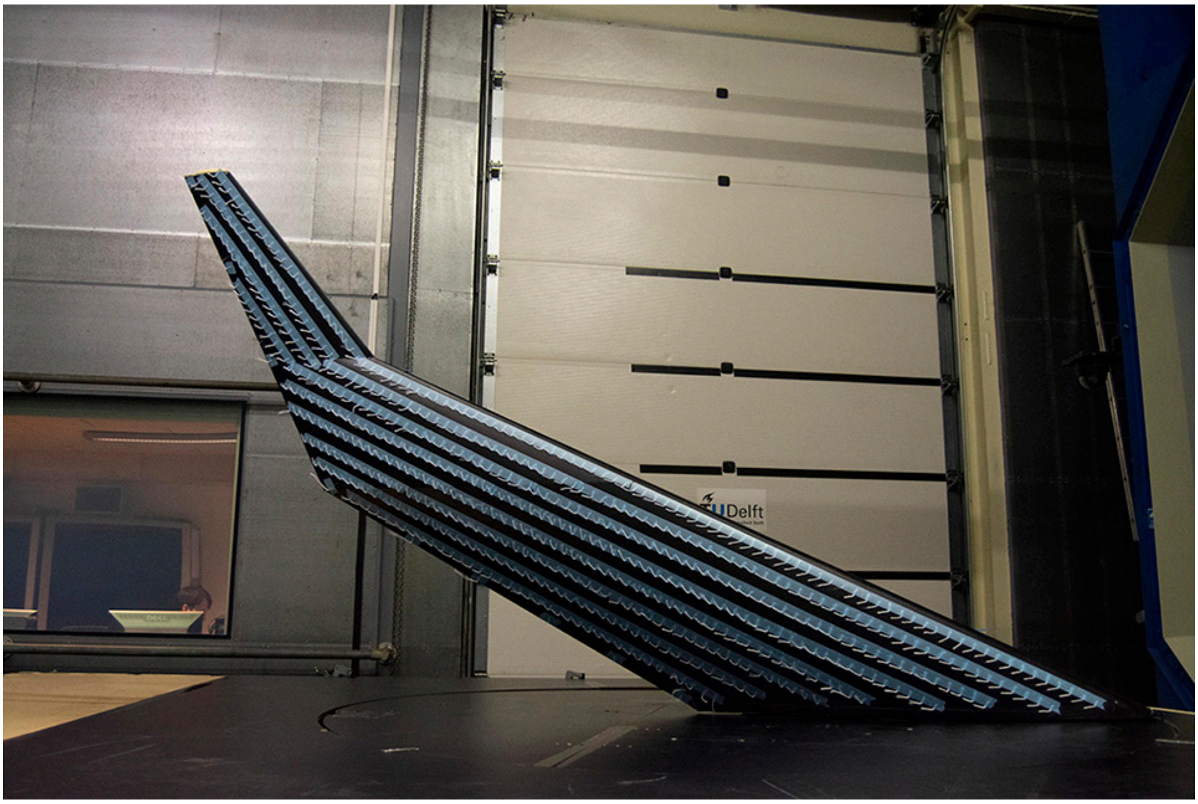

Figure A.68: Strip-on wing with vortilon 2 and vortilon 9 at $\alpha = 20^{\circ}$ and $V = 18.7$ m/s

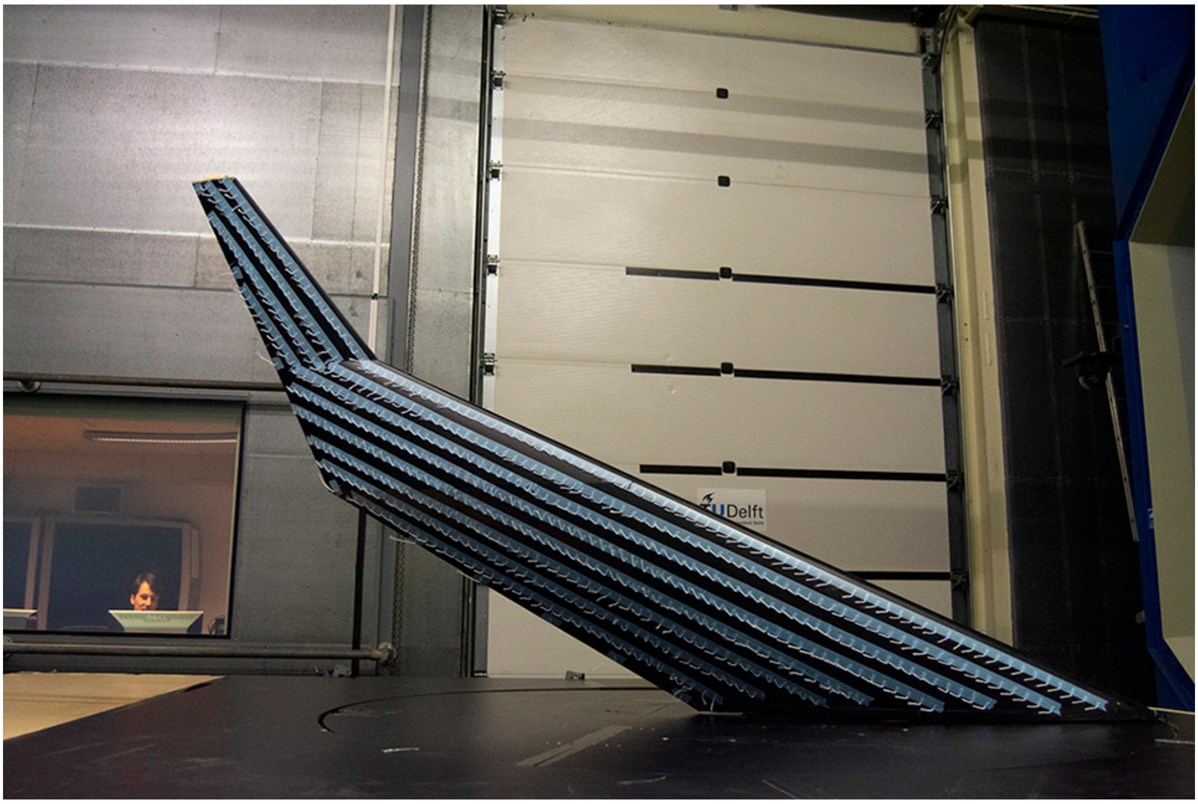

Figure A.69: Strip-on wing with vortilon 2 and vortilon 9 at $\alpha = 22^\circ$ and $V = 18.7$ m/s

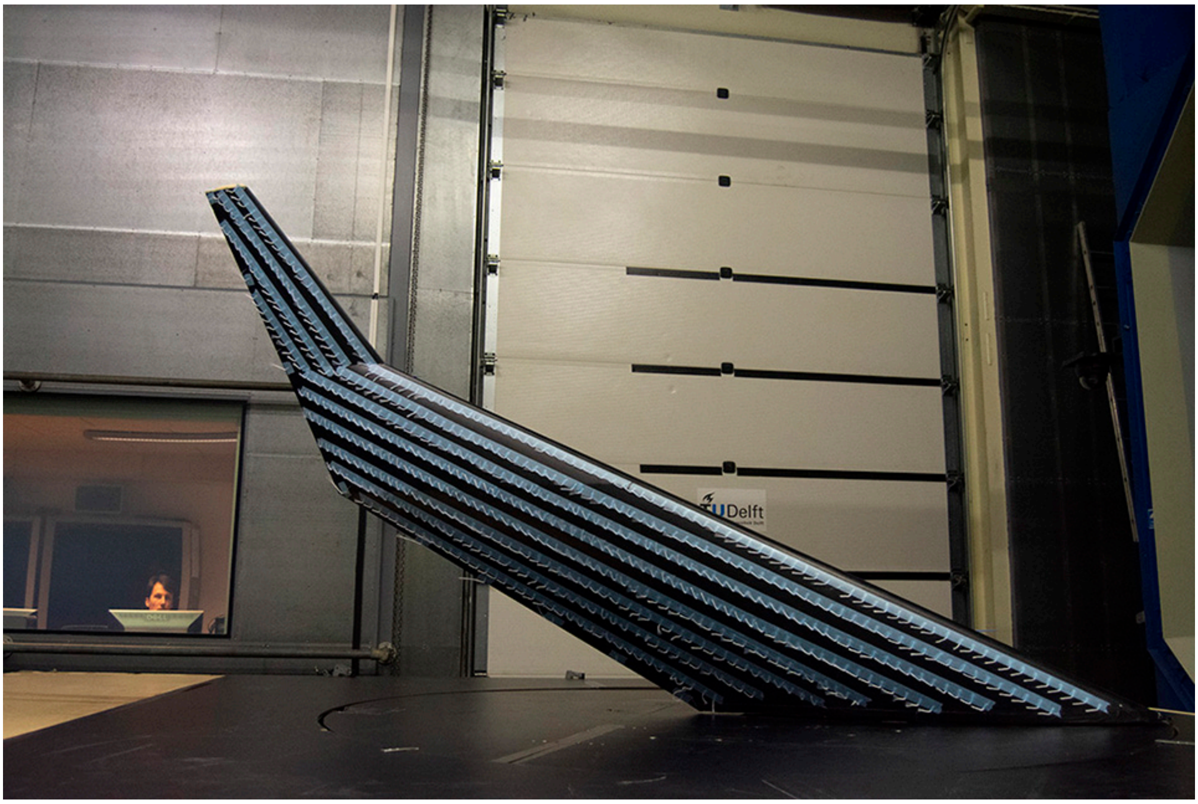

Figure A.70: Strip-on wing with vortilon 2 and vortilon 9 at $\alpha = 25^\circ$ and $V = 18.7$ m/s

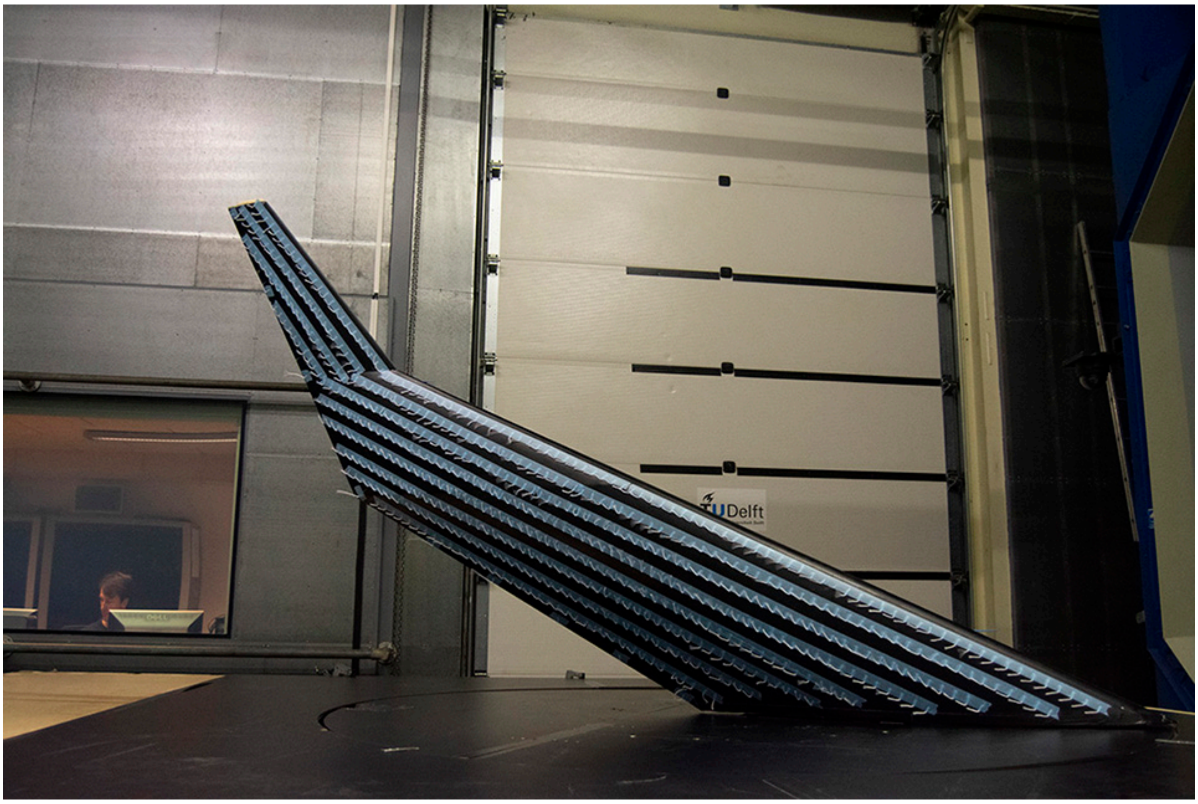

Figure A.71: Strip-on wing with vortilon 2 and vortilon 9 at $\alpha = 30^{\circ}$ and $V = 18.7$ m/s